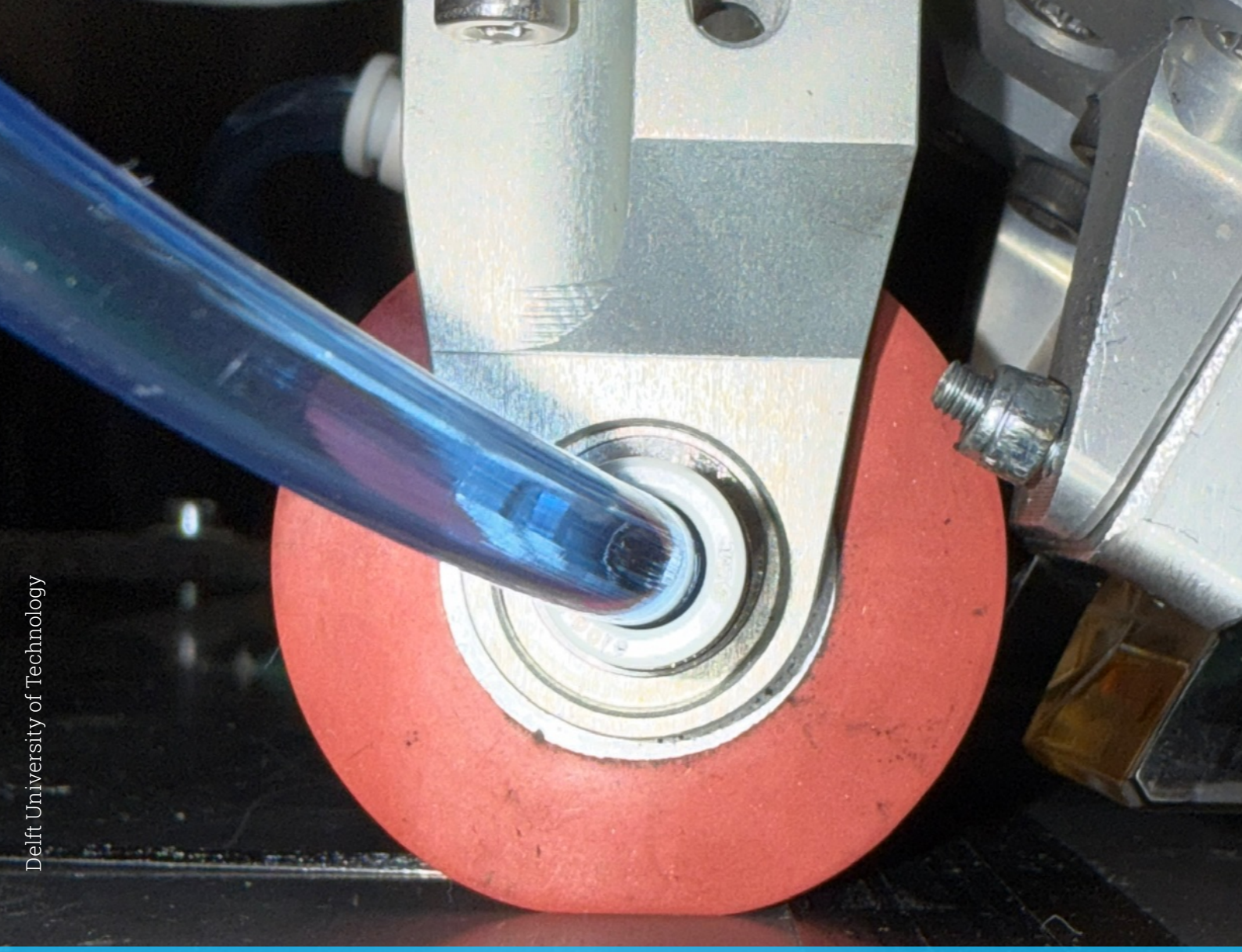

Delft University of Technology

Morphology of gaps and overlaps in ISC-AFP composites

Master Thesis

J. Öge

TU Delft

Morphology of gaps and overlaps in ISC-AFP composites

Master Thesis

by

J. Öge

Instructors:	Dr. D. Peeters and Ir. S. Pantoji
Project Duration:	November, 2024 - August, 2025
Faculty:	Faculty of Aerospace Engineering, Delft, The Netherlands

Cover: Silicon roller of ADDcomposites AFP head (SAMXL)

Acknowledgements

Finalising this thesis will be the end of my master's degree in aerospace engineering at TU Delft. The process of working on this thesis has been highly rewarding and would not have been possible without the support and guidance of several individuals.

Firstly, I am sincerely grateful to Siddharth Pantoji from TU Delft for his continuous support during this project. His willingness to meet weekly and to answer questions, even outside office hours, was truly appreciated. His detailed academic feedback and ability to provide precise explanations were fundamental for my development as a researcher. André Florindo from SAMXL aided significantly in the manufacturing process and showed the extensive insights it takes to convert a digital design to a valuable result. The patience he had and the time he took specifically to aid me are highly appreciated and were vital for this thesis. Daniël Peeters from TU Delft provided continual guidance on the academic direction of my thesis during weekly meetings. I am thankful for his critical insights and his extensive knowledge regarding the topic of this thesis, allowing me to always ask in-depth questions. His input shaped the methodological aspects of my work and shaped the direction of this thesis for which I am grateful. Lastly, I would like to thank my family and friends for their support throughout the course of this thesis.

Summary

Introduction and literature review: This thesis will start with a general introduction on the relevant topics regarding this work. It discusses what a composite material is, what the differences are between thermoplastic and thermoset materials, and finally how the automated fibre placement process works. This introduction will then be followed by a literature review which takes a deeper dive into the separate aspects underpinning the topic. It explores the different parameters for the manufacturing process to be used for this thesis and investigates the available heating method at SAMXL in detail. The review then moves on to the defects that can manifest during the process. Specifically, it discusses the gap and overlap defect types, as these will be the focus of this work. The consequences of gaps and overlaps are then discussed to provide a good understanding of why it is important to be able to describe gaps and overlaps accurately. To illustrate what type of research this thesis will be, several morphological approaches are discussed. Finally, from all literature discussed, the research gap could be identified and the research question could be formulated. To be able to provide answers to the research question, several experiments were designed, which are discussed in the next chapter.

Design of experiments: This chapter discusses the design for two experiments and their resulting samples. It takes into account the process parameters: layup velocity, consolidation pressure, and heater settings. With this in mind, two layups could be designed. The first layer was designed to have an embedded gap that increased in width. This allowed for the extraction of multiple samples with different gap widths from a singular gap. The second layup had several embedded gaps, three gap sizes, and three repetitions for every gap. This resulted in a total of nine gaps. Then the top layer tows were placed with different combinations of the previously mentioned process parameters to investigate their influence on the morphology of the gap. This thesis, however, focused on only one gap size for this experiment (including its repetitions), for the sake of time. With the design for the experiments finished, the manufacturing process could start. Hence, the next section discusses all steps necessary to extract samples from the designed experiments.

Sample manufacturing: The manufacturing process was done at SAMXL. Both experiments were manufactured with the same setup. The setup consisted of a large robotic arm, an AFP head end-effector, and the flashlamp heating system. To be able to analyse the results after manufacturing, the process was recorded by several types of equipment. Firstly, for both experiments, a laser line scanner was used to capture the top surface profile. For the second experiment, the setup was additionally equipped with an infrared camera and a force torque sensor. These allowed for the capture of the temperature and the force profile during the placement of the material. Next, the laminates had to be post-processed. This was done for both experiments by first cutting the laminates into samples. The samples were then embedded into an epoxy to be later polished. After polishing all samples, they were ready to be analysed with a microscope. The polishing losses for the samples from the first batch were thoroughly monitored as this influenced the gap width due to the singular gap that increased in size. With all this taken into account, the samples were ready to be analysed.

Sample analyses: The following chapter discusses the analyses of the samples. Once the polishing losses were taken into account, the laser line scanner data could be compared to the data obtained from the micrographs. Finally, the micrographs could be used to parametrise the gaps, from which three types of gap were identified. For the second experiment, firstly the data from the laser line scanner, the infrared camera, and the force torque sensor were analysed. From this, it became clear that excessive force was used. Following this, the gaps from the micrographs could be parametrised, confirming that the excessive force resulted in more closed gaps. Lastly, an ANOVA was performed to determine whether there were any underlying trends in the data that were difficult to spot by eye. This showed that no metrics for describing morphological features of the gap were influenced by their respective

process parameter combinations but rather on their repetition. The results for experiments one and two were then discussed further. This made it possible to draw certain conclusions and reflect on the process. From the first experiment, it was possible to assign quantitative metrics to different types of gaps, allowing for an accurate description of the gap's morphology. From the second experiment, it became evident that an overshoot in consolidation force and different substrate material had significantly influenced the gap morphologies.

Conclusion and recommendations: The conclusion chapter addressed the results of the experiments again but mainly focused on what the results mean for future work regarding ISC-TP AFP produced laminates. Lastly, recommendations for future work were made. These recommendations focused on the substrates used for both experiments and the force monitoring system. The substrates used for both experiments made the production possible, but both had significant downsides that if solved, would yield clearer results. The force monitoring system used for experiment two seemed robust during the production, but the data shows a large discrepancy from the intended used forces. Therefore, for future work, it is recommended to investigate this further and provide a foolproof system.

Contents

Nomenclature

Abbreviations

Abbreviation	Definition
AFP	Automated Fibre Placement
ANOVA	Analysis of Variance
CFRP	Carbon Fibre Reinforced Polymer
CF/LM-PAEK	Carbon Fibre/Low Melt Polyaryletherketone
DOF	Degrees of Freedom
FTS	Force Torque Sensor
HGT	Hot Gas Torch
ILSS	Interlaminar Shear Strength
IR	Infrared
ISC	In-Situ Consolidation
LAFP	Laser Assisted Fibre Placement
LLS	Laser Line Scanner
PEEK	Polyether Ether Ketone
PPS	Polyphenylene Sulfide

1

Introduction

In recent times, the aerospace industry has witnessed a significant shift towards the use of composite materials. This shift is mainly driven by their weight. Composite materials have a higher strength-to-weight ratio than the historically used metals for aircraft manufacture. This allows for aircraft with the same strength but a decreased weight. Lighter aircraft with the same strength as their metallic counterparts have the benefit of a considerably lower fuel consumption. A lower fuel consumption contributes not only to lower fuel cost, but also a decrease in carbon emissions. The combination of both a lower fuel consumption and lower harmful emissions to the environment makes the investigation into composite aircraft parts a key area of research in the field of aerospace engineering.

The definition of composite is: ”*made up of disparate or separate parts or elements; compound*” [1]. Hence, a composite material is a compound material consisting of two separate materials made into one. There are many different types of composite materials, but they mainly share the same working principle. One material serves as a matrix, and the other material functions as a reinforcement inside this matrix. Figure 1.1 shows an illustration of what a composite material can look like.

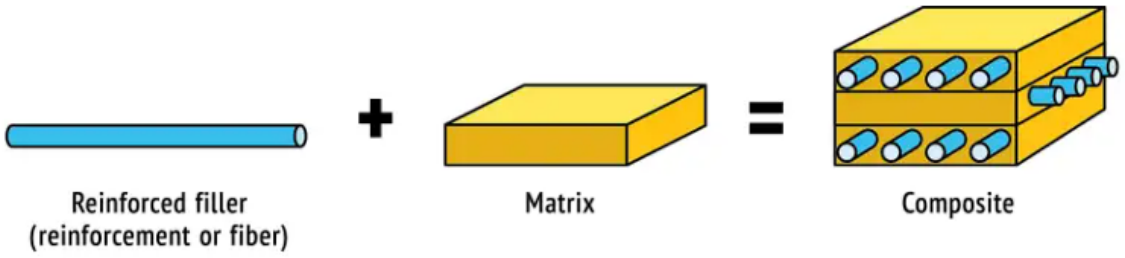

Figure 1.1: Composite material illustration [2]

The figure above illustrates an example of a composite material. It shows a matrix material that is reinforced by fibres. There are many different materials that are suitable as a good matrix material. A few examples are metals, polymers, and ceramics. Reinforcing the matrix material can also be done in several ways. The figure illustrates fibre-based reinforcement, which may consist of either continuous or discontinuous fibres. Alternatively, reinforcement can also be achieved using particles or platelet-shaped inclusions. Beyond those mentioned, various other matrix materials and reinforcement forms exist, each tailored to specific performance requirements. The main composite material for aircraft part production is carbon fibre reinforced polymers (CFRP). This material consists of a polymer matrix material with carbon material reinforcement in the form of continuous fibres. CFRP has properties well applicable for aircraft parts, such as desirable stiffness, fatigue and corrosion resistance, and it is suitable for the thermal range of aircraft parts.

Still, CFRP can be categorised further into two main types based on the matrix material: thermoset-based and thermoplastic-based composites. A thermoset polymer consists of long polymer chains with reactive groups. When curing, these groups form irreversible covalent bonds called cross-links. This results in a heavily linked 3D polymer network. Which is also why thermosets must be stored in freezers to slow down the curing, also meaning that they suffer from a limited shelf life. The bonds permanently lock the polymer chain in place and cannot be reversed by heating. However, these bonds do give the material high rigidity and thermal strength. Thermoplastic polymers also consist of long polymer chains, but these chains do not possess the previously mentioned reactive groups; therefore, these do not create irreversible bonds. The polymer chains in a thermoplastic material are held together by secondary intermolecular forces. At temperatures higher than the polymer's glass transition temperature, the intermolecular forces are overcome, resulting in the chains being able to slide past each other. Therefore, the structure of a thermoplastic polymer is reversible by means of heating, which is not possible for thermosets. As thermosets are not able to change in shape after being re-heated it becomes difficult to repair parts. Additionally, not being able to be re-heated also comes with recyclability challenges.

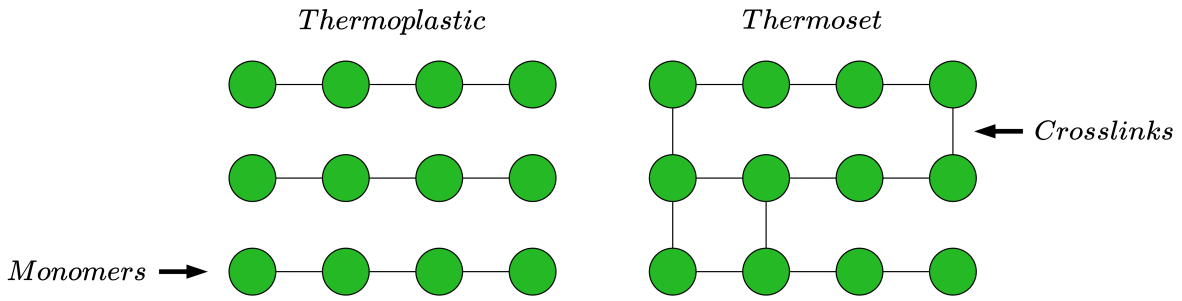

Figure 1.2: Simplified illustration regarding the difference between thermoplastics and thermosets

Figure 1.2 indicates a simplified schematic view of the difference in polymer structure between thermoplastic and thermoset matrix materials. Historically, thermosets were more developed as they had high-strength and high-heat applications, which made them attractive for weapon manufacturing during the Second World War. Therefore, thermosets could be processed using techniques that are already common in the industry, such as autoclave curing and vacuum bagging. As a result, the manufacture of CFRP aircraft parts is primarily dominated by thermoset matrix materials. Nevertheless, the processing techniques used to manufacture thermoset CFRP aircraft parts remained quite lengthy. For example, an autoclave is essentially a pressurised oven that runs cycles of varying temperatures and pressures for a specified duration. This time can be extensive and slows down the production line significantly.

From the previous discussion, it becomes evident that thermoset CFRP material has several significant drawbacks. These shortcomings are summarised below:

- **Irreversibility:** Once cured, thermoset materials cannot be remelted or reshaped in any way.
- **Long Production Times:** Thermosets require long curing cycles in an autoclave or oven, which slows down the manufacturing process.
- **Difficult Repairs:** Repairs are often complex and involve bonding or patching, which can be less reliable and time-consuming.
- **Strict Storage Conditions:** Thermoset prepregs need to be stored in freezers and come with a limited shelf life.

These shortcomings provided a strong motivation for researchers to investigate whether aircraft parts could instead be manufactured using thermoplastic CFRP. As a thermoplastic composite material can be repeatedly heated and changed in shape, this allows for reprocessing, while also making aircraft

parts easier to service and repair, as thermoplastic materials allow for welding-based repairs. Furthermore, thermoplastics are stable at room temperature, removing the need for difficulties regarding the storage of thermoset materials. Lastly, thermoplastic composites still currently also require a step involving heat and pressure but show potential in removing this step, which could significantly reduce the production time of parts.

Hence, producing aircraft parts from thermoplastic composites offers many benefits with respect to thermoset composites. Nevertheless, aircraft parts made from thermoplastic materials also come with their own challenges. The main challenges are related to the production process, as thermoplastic parts require significantly higher processing temperatures and consolidation pressures, which in turn demands specialised equipment. Furthermore, the removal of the autoclave does save a considerable amount of time. However, the autoclave process for thermoset materials lowers the viscosity of the matrix material, which results in an evacuation of voids that could have been formed during different parts of the production. Removing the autoclave from the process therefore reduces the production time but also eliminates the possibility for those imperfections to be healed by resin flow during curing. Hence, these imperfections will remain in the laminate and possibly weaken it.

A specific manufacturing process for thermoplastic composite aircraft parts is the in-situ consolidated thermoplastic automated fibre placement (ISC-TP AFP) process. In-situ consolidation means that the material that is being placed is also immediately bonded and compacted to the previous material. Therefore, merging the placement and consolidation into one process. This method is also utilised by the AFP process. This process is centred around a robotic system, usually a robotic arm, but different types of robotic configurations can work. This arm regulates the path, velocity, force exerted onto the material. The material is then rolled onto a tool or substrate, during which it is simultaneously heated by a heating system and pressed by the robot. Figure 1.3 illustrates the general AFP process with its main components.

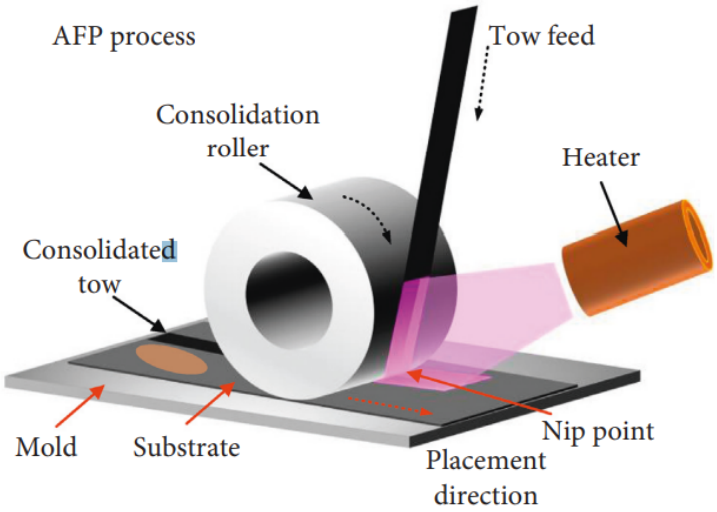

Figure 1.3: Automated fibre placement process (AFP) [3]

During the production of thermoplastic composites with the AFP process, the most common defects are gaps and overlaps [4], [5]. These defects occur when adjacent thermoplastic tows either leave a gap or overlap at their edges. Despite the extensive research into AFP and its shortcomings, most studies have either focused on avoiding gaps and overlaps overall or understanding their consequences on the mechanical properties of the resulting laminate. Although extensive research has been conducted on the formation and consequences of gaps in thermoplastic laminates produced via the AFP process, and some studies have investigated gap morphology in thermoset-based AFP, the morphological characterisation of such defects remains largely unexplored for in-situ consolidated thermoplastic AFP. Specifically, on how the processing parameters could have influenced the shape and size of these

defects. Understanding the morphology of these defects is essential to establishing predictive models and providing a universal language regarding gap shape and size.

Hence, this work aims to bridge that gap by investigating the morphology of gaps and overlaps in ISC-TP AFP laminates. This work was conducted through an experimental analysis. Exploring the formation and behaviour of gap morphology as a result of certain processing parameters, and quantifying metrics to allow for an accurate and repeatable procedure for identifying the morphological features of the defects. In doing so, it contributes to a more thorough understanding on defect formation and characterisation and aims to be of aid for future research regarding gap formation in ISC-TP AFP laminates.

2

Literature Review

This chapter will introduce the relevant topics and prior research. It will help this discussion by first elaborating on the general process of automated fibre placement processing. Then, the process parameters that play a role in this process will be touched upon. These parameters all have their unique influences on the process and the part quality. The process will result in inevitable defects that will be present in the finished part. These defects influence the part's strength, often resulting in a weaker part. Then specifically the gaps and overlaps defects will be discussed. After which several studies researching the same topic will be issued to gain an understanding of the models and experiments that have already been done. Lastly, morphological approaches will be discussed to showcase what such an approach entails.

2.1. AFP Parameters

From the introduction, it is already known that several parameters play a role during the AFP process and that varying them can result in changes in part quality [6], [7]. A schematic of the process can be seen in figure 2.1.

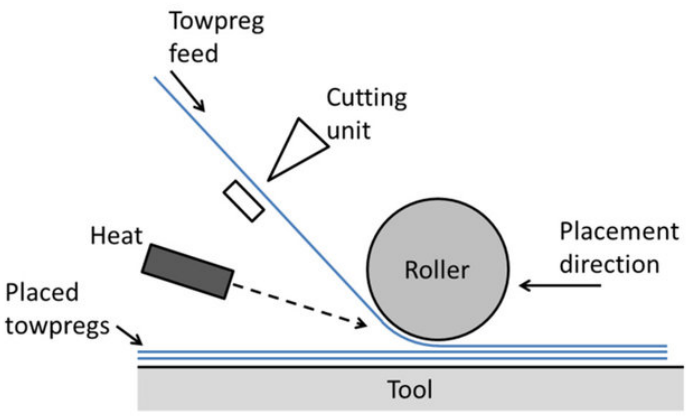

Figure 2.1: Schematic of the AFP process [8]

The layup path depends on the geometry of the desired path. A simple geometry, for example a flat square, does not require a complex layup path. However, a curved or even doubly-curved part adds several other aspects that need to be taken into account which will be explained in section 2.2.1. These additional considerations add complexity to the generation of the layup path.

The layup velocity of the process is the velocity with which the tow is placed along the layup path. This parameter is dictated by the material as it influences the amount of time heat can be deposited

into the material and the amount of time the material is subjected to pressure from the roller. Increasing this velocity, while keeping the other parameters constant, therefore gives the material less time to absorb heat. In other words it would reduce the consolidation time. Reducing the consolidation time results in a lower degree of bonding and potentially in a higher percentage of void content [6]. Which in turn creates a weaker part.

The compaction pressure in the process is the pressure with which the roller presses the tow onto the substrate or tool. The material of the roller can vary for different AFP processes. The roller can be made from a conformable material which increases the contact of the roller with the tow and substrate due to flattening of the bottom surface. A roller could also be made out of metal to increase the thermal conductivity of the roller. Changing this pressure, while keeping other parameters constant, affects the part. An increase of the compaction pressure results in a higher degree of bonding and a reduction in voids [6], [9], [10]. Better bonding and a reduction in voids increase the strength of the thermoplastic composite [11].

As this research will be conducted on in-situ consolidated thermoplastics instead of thermoset composites there is no need to investigate autoclave cycles. However, the in-situ aspect of this process does pose some challenges regarding the bonding of the thermoplastic composite tape to the substrate. In the autoclave process most imperfections and flaws created during the manufacturing process are erased as the resin can flow into the created imperfections in the laminate [12]–[14]. To ensure the amount and severity of these defects are minimised other process parameters such as the tool temperature and the heating method can be adjusted [6], [7], [15].

2.1.1. Heating Methods

There are several methods of heating the material in the AFP process. Some of them are Hot Gas Torches (HGT), lasers, infrared radiators, and flashlamp heating systems. Each method has its pros and cons. This section walks through the aspects of the previously mentioned heating options and concludes with the heating method that will be used for this research.

Different heating methods are suited to different material systems. Lasers and infrared heaters are typically used for thermoplastics, which require localized, high-intensity heating to melt and consolidate. HGTs can be applied to both thermoplastics and dry fiber tows, as they offer flexible heat control. For thermosets, heating often needs to be more uniform to ensure proper curing, making IR and flashlamp systems more suitable, especially when combined with post-curing methods.

HGTs emit a high-temperature inert gas onto the nip-point which results in heat transfer by forced convection [16]–[18]. The parameters influencing the heat transfer are the gas temperature, the gas flow rate, and the distance between the nozzle and the nip-point [18]. This allows the material to melt and fuse with the substrate or be laid on the tool. The HGT process is a relatively cheap option regarding the capital cost [19], [20]. However, since the gases used need to be inert, this requirement can significantly increase the operating costs [19], [20].

When a laser is used in the AFP process the process is often renamed as the Laser Assisted Fibre Placement process, or LAFP process. The LAFP process is a popular research topic. The lasers in this process can be characterised by their high radiation intensity. This allows for rapid heating of the material at a very controlled area called the nip-point [19], [20]. The downside of using lasers is that it requires an enclosed room and that the commonly used CO_2 lasers [21] can cause burning and oxidising on the surface of the prepreg tapes [20].

In the same line as the HGT method, the Infrared Radiators (IR) method is a relatively inexpensive heating method. This type of heater heats the material mainly by radiation. However, only the top layer of the tape is exposed to this radiation, which is why the rest of the heat must find its way into the material through conduction or convection [22]. Additionally, this heating method is generally used for thermoset materials as it cannot reach the required working temperatures for thermoplastics and generally stays between 32 and 50 C° [23]. This extends the processing time. IR heaters are also easy to operate and can be used to preheat the material, as a main heat source, or both. Compared to HGTs, IRs can deliver a more focused output achieving a higher heating efficiency [20], [24].

2.1.2. Humm3 Xenon flashlamp

This research will use another heating method called the humm3® developed by Heraeus Noblelight [25]. This is a flashlamp which makes use of pulsed light technology [25]. This works by emitting high intensity broadband infrared and ultraviolet radiation in the form of short high energy pulses from a Xenon-arc flashlamp [25]. Laser-based systems operate at a single wavelength, which can limit heating efficiency if the material does not strongly absorb at that wavelength. In contrast, flash heating systems like the humm3® emit a broad spectrum of light, increasing the likelihood of overlap with the absorption characteristics of various thermoplastic composites. This results in more efficient energy absorption, higher heating rates, and broader material compatibility [26].

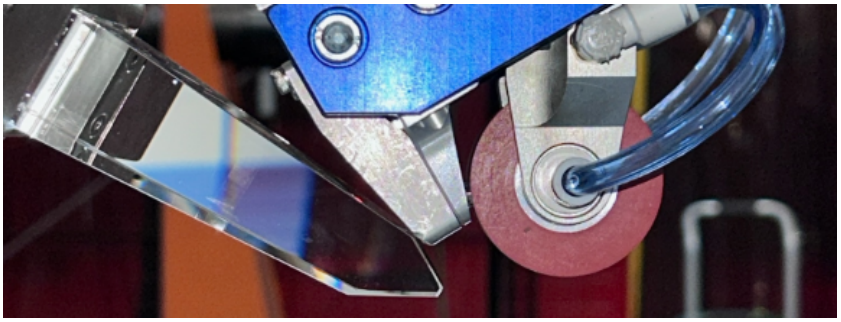

Figure 2.2: humm3® flashlamp pointed at nip point

The humm3® showcases similar heating capability to high-power lasers. One of the main advantages of this system, however, is its safety. There is no need for an enclosed environment, which makes it a safer option than the LAFP process. The humm3® head is also relatively small, which makes it optimal for mounting on an AFP head, as its smaller size allows for greater processing freedom [25], [27]. Compared to the LAFP process the flash lamp also shows greater control over its process capabilities and a decrease in system cost.

The radiative heat flux produced by the flash lamp is pointed at the nip point by means of a precisely cut quartz crystal. This crystal directs the light and delivers its concentrated energy pulses by using the internal reflections of the crystal. This can be seen in figure 2.2. The humm3® system has three parameters, as the name indicates. Energy, frequency, and duration.

The energy of the humm3® flashlamp refers to the total amount of power delivered by the flashlamp during each pulse. This determines the intensity of the pulse and influences how much heat is transferred to the material. The energy can be varied by adjusting the voltage to the flashlamp. This can be visualized as a variation in the amplitude of the power pulse delivered to the material, which can be represented by the following equation where A is the amplitude and f is the frequency:

$$A\sin(f\pi x) \tag{2.1}$$

For visualisation purposes A was increased from 0.5 V to 1 V. Figures 2.3 and 2.4 illustrate this change.

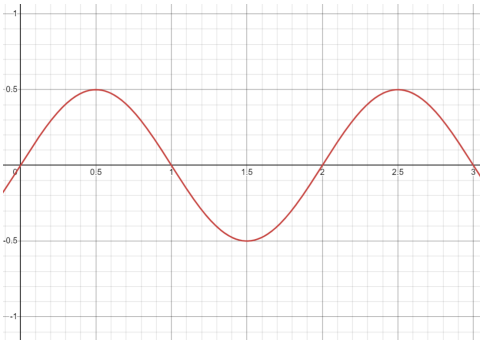

Figure 2.3: Pulse wave with predetermined input voltage (A) of 0.5 V

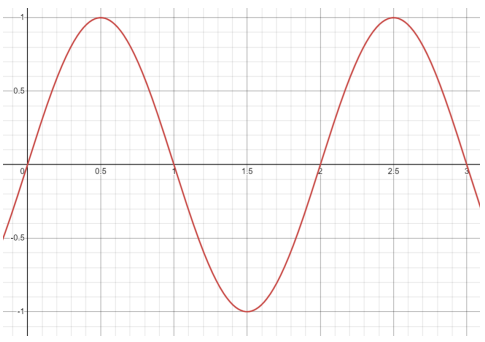

Figure 2.4: Pulse wave with increased input voltage (A) of 1 V

The frequency of the humm3® flashlamp describes how many of the previously mentioned pulses are delivered within a set time span, usually per second (Hz). Keeping other parameters constant, a higher frequency means more pulses giving the material less time to cool down between pulses. Using the same analogy of the pulse wave as for the variation energy a change in frequency can visualised as in figures 2.5 and 2.6.

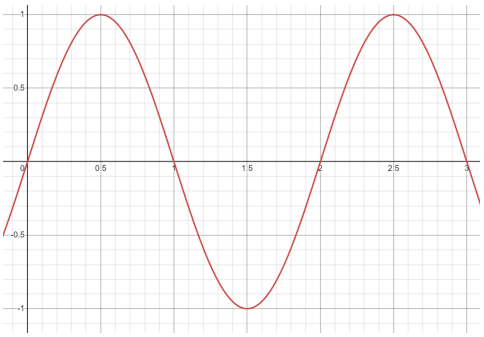

Figure 2.5: Pulse wave with predetermined input frequency (f) of 1 Hz

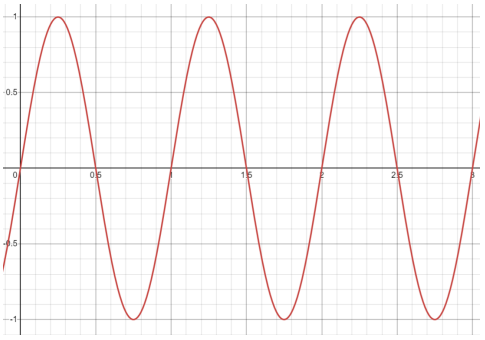

Figure 2.6: Pulse wave with increased input frequency (f) of 2 Hz

The duration parameter of the humm3® flashlamp refers to the duration of each individual pulse and be expressed as the following:

$$\text{Duration} = \frac{1}{\text{Frequency}}$$

Therefore, a lower frequency results in a longer duration. This influences how long the material is exposed to heat for each pulse. Longer pulses give the material more time to absorb the heat, which can be used to reduce the risk of overheating. The behaviour of the wave as a result of a change in duration is the same as for a change in frequency. Below, figures 2.7 and 2.8 indicate the change in wave behaviour due to an increase in duration.

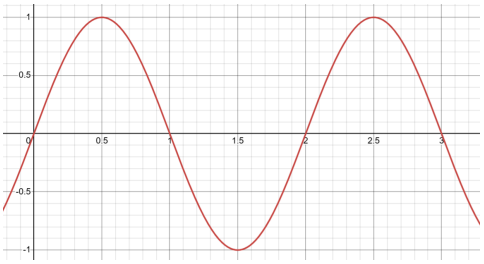

Figure 2.7: Pulse wave with predetermined input duration ($1/f$) of 1 1/Hz

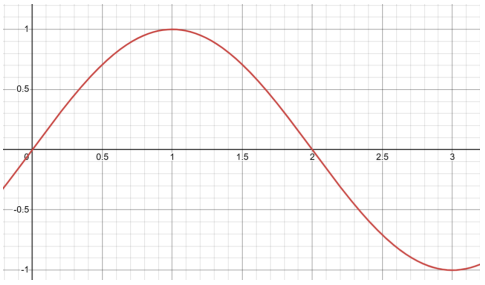

Figure 2.8: Pulse wave with increased input frequency ($1/f$) of 2 1/Hz

Therefore, adjusting these parameters influences the nip-point temperature in the process which influences the quality of the resulting laminate [28].

2.2. Defects

As previously mentioned the in-situ consolidation of thermoplastic composites AFP (IS TP AFP) can result in certain defects in the finished laminate and part. These defects in the laminate can be categorized into three orders of magnitude: micro, meso, and macro. The distinction between these scales is based on their size and the structural level at which they occur, ranging from individual fibres to entire laminate sections [29]–[31]. Figure 2.9 shows this distinction.

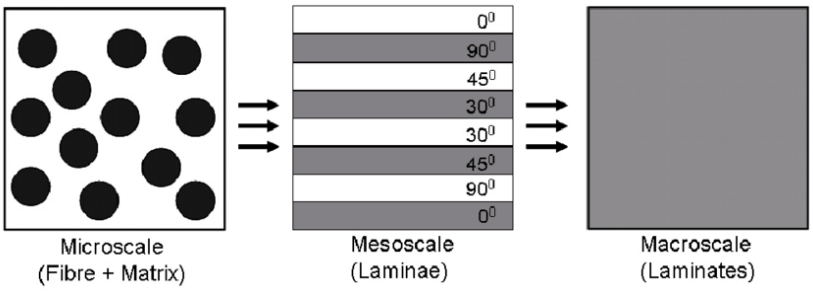

Figure 2.9: Micro, meso, and macro order of magnitude [29]

Micro-scale defects are defects that occur within a single tape. A single tape consists of fibres embedded in a resin. Within this tape defects such as an undesired fibre fraction, void content, or fibre misalignment can occur [12], [13], [30]. Figure 2.10 illustrates the void content within a single fibre. The voids can be recognised by their dark, almost black, colour.

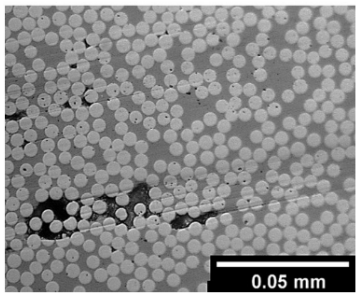

Figure 2.10: Micro-scale defect, fibre-resin separation [12]

Meso-scale defects are defects that occur between tows. Examples of such defects are tow misalignment, gaps, overlaps, twisted tows, and many other defects that could occur at this scale [32]. Illustrations of said gaps, overlaps, and twisted tows can be seen in figures 2.11 and 2.12.

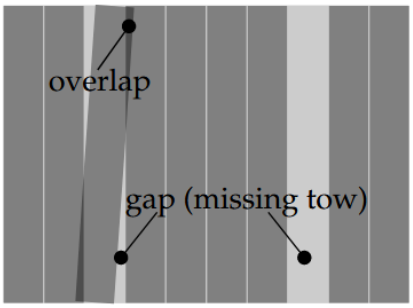

Figure 2.11: Meso-scale defects, gap and overlap [32]

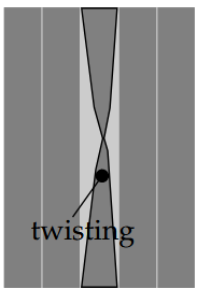

Figure 2.12: Meso-scale defect, twisted tow [32]

Macro-scale defects are larger structural imperfections, such as large delaminations or warping. Delamination could be considered as a meso-scale defect as it could also occur between tows. However, as mentioned before the distinction of the defects is based on its size and structural level. An example of a macro-scale defect can be seen in figure 2.13 where a wrinkle in a laminate is illustrated.

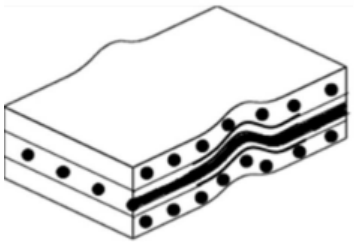

Figure 2.13: Macro-scale defect, wrinkle in laminate [31]

This work focuses on meso-scale defects, which arise from the interaction, or lack thereof, between the tapes. In an ideal scenario, tapes are perfectly straight and in full contact with adjacent tapes. However, real-world imperfections in raw materials, combined with deviations in the layup path, can introduce defects [32].

One example of such defects is fibre steering. In this process, the robot follows a layup path that requires a radial turn during the layup process. This can result in angle deviations and even a lack of contact with the substrate below at the inner radius [33], [34]. While a programmed robot can accurately repeat laying patterns, slight errors may still occur on the meso-scale level, leading to tow misalignment. This misalignment results in gaps or overlaps between tows, caused by the robot's errors [32].

If imperfections are already present in the laminate or if the to-be-laid structure is highly complex, fibre waviness can occur. This phenomenon can manifest as in-plane waviness between tows or out-of-plane waviness between layers which can be observed in figure 2.14 [32]–[34].

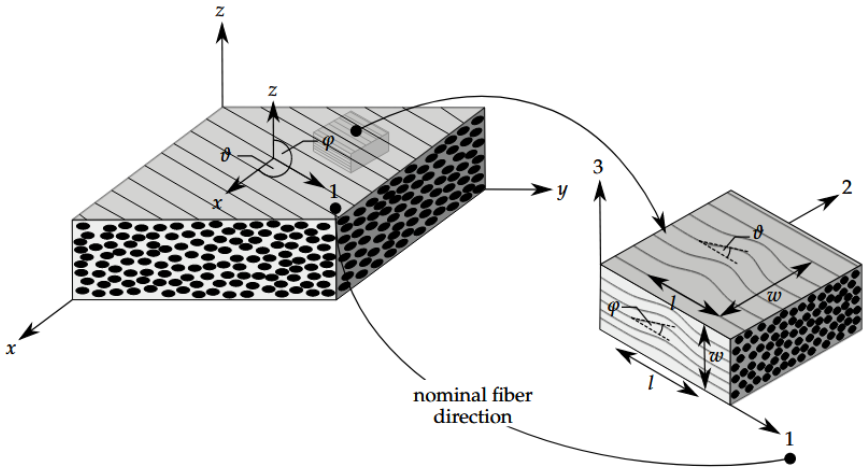

Figure 2.14: In-plane and out-of-plane waviness illustration by Heinecke et al. [32]

There is also a more obvious class of meso-size defects. Defects such as folds and wrinkles can occur during the process if the adhesion to the tool or substrate is not enough [32]. Also fitting this style of defects is the twisting of a tow [32]. Similarly, contaminations can create fuzz balls on a tow or layer. Still, there exist some additional defects. The work by Heinecke et al. and Harik et al. combined cover all the defects [32], [35].

2.2.1. Gaps and Overlaps

This work will focus on gaps and overlaps as it has been found that these defects most frequent during the AFP process [5], [36]. Gaps are defects that occur when there is a discontinuity between adjacent tows, preventing proper bonding, as is illustrated in figure 2.16. A gap can be defined as the region between adjacent tape edges when they do not meet during placement, as can be seen in the schematic illustration of figure 2.11. However, this definition may no longer hold once matrix flow occurs due to Darcy flow effects. Overlaps, on the contrary, are points where two tows are on top or below one another and therefore overlap one another. There are two main categories for the generation of gaps and overlaps, geometry related causes and manufacturing process variation causes. For the first category, the gaps and overlaps are an artefact of complex part geometries or tool paths. A tow path is often the result of shifting the path from the previous tow by one tow width to one side, however in the industry this distance is slightly increased as gaps are preferred over overlaps. Therefore, complex geometries can create spaces where the tows need to bend and shear to a certain amount or in other words the fibre angle continuously deviates from the desired fibre angle. This effect plays a large role when the geometry is to be manufactured on a flat plate but does require tow steering. The steering of the robot creates the fibre angle deviation. This effect can be observed in figure 2.15. It can also be a problem for doubly curved surfaces to be manufactured as it shares the same issues as a flat part that requires fibre steering.

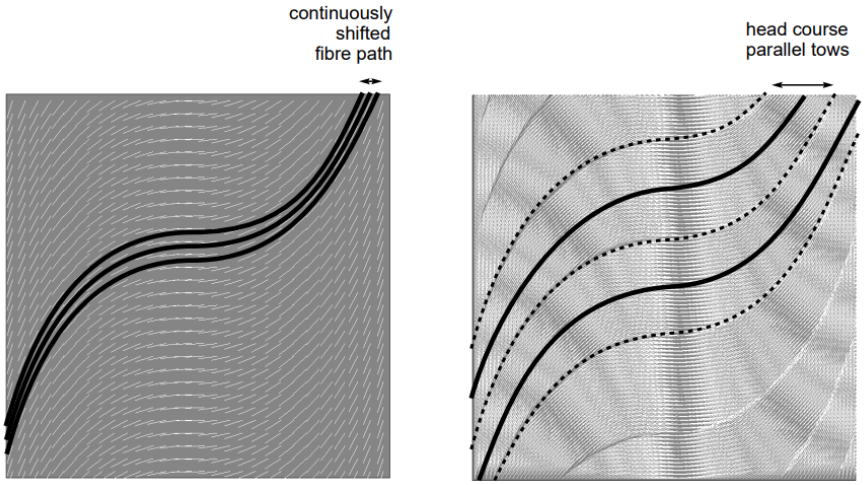

Figure 2.15: Fibre angle deviation by Lopes [37]

Figure 2.16 shows the different types of gap and overlap situations that can occur. It can be seen how the gaps and/or overlaps can be an artefact of fibre steering during the manufacturing process. Configuration (a) shows what it looks like to avoid overlaps, with gaps as a result of this. Configuration (b) shows what it looks like to completely avoid gaps, with overlaps as a consequence. The configuration in (c) indicates a middle ground that reduces the size of the gaps and overlaps but this means that both defects would be present. Configurations (a-c) are illustrations of what gaps and overlaps look like generated by the first category. The last configuration (d) is an illustration of gaps and overlaps can be created following the second category where gaps and overlaps can be created by variations in the width of the tape material. This category discusses the defects as a consequence of manufacturing process variations.

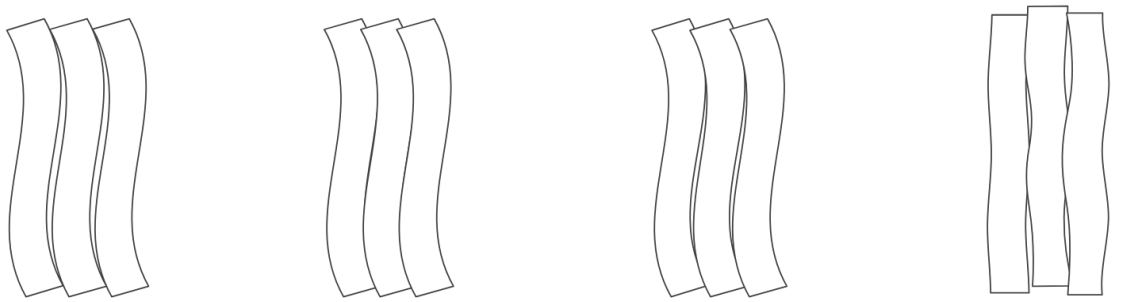

(a) Gaps (b) Overlaps (c) Gaps and overlaps (d) Gaps and overlaps

Figure 2.16: Gaps and overlaps situations [38]

In the second category, gaps and overlaps arise as a result of manufacturing process variations, which are caused by imperfections in the raw material or errors made during the process. An example can be seen in figure 2.16(d). By the raw materials, is meant the actual tow that was delivered by its manufacturer. The tows seem straight but in reality, still show irregularities at the edges. Therefore, by trying to lay the tows as closely as possible next to each other, one can create overlaps. On the other hand, to avoid overlaps one could introduce a small gap between the tows; however, this naturally results in gaps.

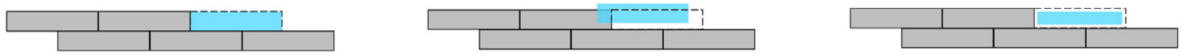

(a) Correct position and geometry (b) Position variation (c) Geometry variation

Figure 2.17: Category 2 gaps and overlaps [38]

Figure 2.17 indicates the two causes of a manufacturing process variation that can lead to gaps and overlaps. Figure 2.17(a) shows a perfectly placed tow without positional or geometrical variations. The position variation observed in 2.17(b) shows that the position of the manufactured tow could be placed incorrectly. The geometry variation observed in figure 2.17(c) illustrates that even if the tow is placed correctly its dimensions can still deviate from the desired dimensions. The process variation can have two causes. The first reason is that a process variation can be an artefact of robot inaccuracy. Even though robots are usually quite accurate, slight errors or deviations from their programmed path can still occur during the manufacturing process. These deviations from the programmed path could then create gaps and overlaps. The second reason the position can be varied during the process is if the tow would move laterally on the compaction roller [38]. During the process, the tow is subjected to several forces which can manifest as lateral forces trying to move the tow across the compaction roller. Naturally, this would create inaccuracies in the laminate or even gaps and overlaps.

The variation in geometry can also have two main causes. The first, as previously mentioned, was the variation in tow width which can be a result of manufacturing the raw material of the tow. The second variation in geometry can be caused by the compaction roller. The compaction roller, as its name suggests, compacts the tow. However, the compaction of a tow also results in the expansion of the tow in the lateral direction. This expansion at the sides of the tow can be uneven as a result of variations in the substrate or non-uniform pressure distribution [39]. If the sides of the tows are uneven while the programmed path is perfectly straight it could result in gaps and overlaps at the edges.

The presence of these defects creates irregularities in the final part and influences the integrity of the laminate, often resulting in a decrease in mechanical performance [4], [40]–[44]. As the ISC TP composite is considered a material of the future, research on defects in this material is a popular topic.

2.3. Consequences of Gaps and Overlaps

As briefly mentioned before, more gaps and overlaps in the final material will result in a material with lower strength than a part with fewer gaps and overlaps. This section will delve into this statement more thoroughly. A material can have multiple types of strength, and not all are affected in the same way by variations in the number of gaps and overlaps present

2.3.1. Tensile and compressive strength

A paper by Ju et al. [40] investigated the influence of gaps and overlaps on the mechanical properties of axial tensile and compressive strength. Ju et al. first assumed that as a result of gaps and overlaps, out-of-plane waviness would be present. They then characterised the out-of-plane waviness for gaps as a sine wave and overlaps as a sine-like wave, which can be seen in figure 2.18.

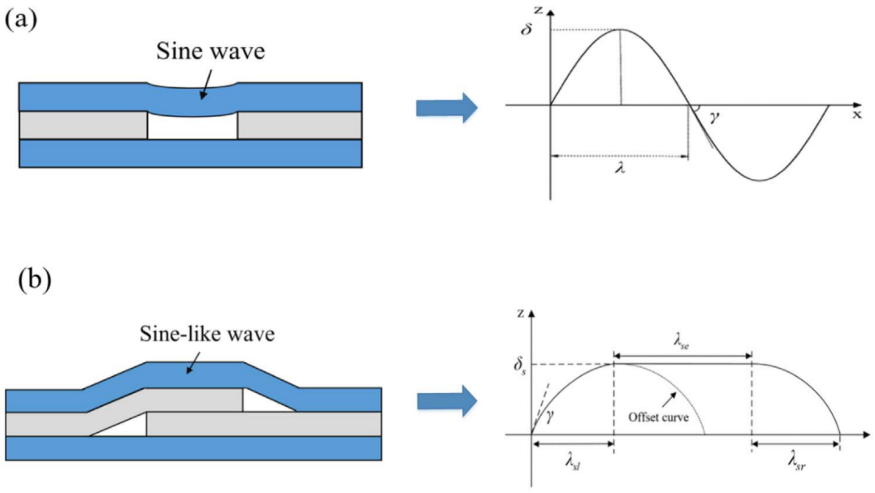

Figure 2.18: Description model of out-of-plane fiber waviness: sine wave (a), sine-like wave (b)[40]

An analytical model was made after which an experimental setup could be defined. Many different layup sequences with different types of gaps and overlaps were tested. For the axial tensile strength, it was found that for the sine wave and the sine-like wave, the tensile strength kept decreasing with an increase in fibre waviness. The measurements stopped after the reduction rates of 23.86% and 29.50% respectively [40]. For the axial compression strength testing the same approach was used and similar results were obtained. Again, the measurements ceased after both the sine wave and sine-like wave–induced waviness caused the compressive strength to drop by about 30%. “Therefore, it can be stated that an increase in the number of gaps and overlaps in a laminate significantly reduces its tensile and compressive strength [40].

2.3.2. Shear strength

To investigate the shear strength of a composite laminate, Lan et al. [41] performed several experiments. In this study, an autoclave is used but the behaviour can be assumed to be similar for ISC TP composite laminates. Lan et al. investigated two types of layups, [-45°,+45°] and [90°, 0°]. It was found that for both layups, a damage threshold was observed at a shear strain of approximately 0.15%, after which the modulus began to decline and the damage factor increased. This meant that the embedded gaps and overlaps did not exert a significant influence on the damage development. Therefore, it can be concluded that gaps and overlaps can slightly reduce the shear strength of the material, particularly in the presence of larger embedded gaps. Furthermore, Lan et al. also used the same set-up to investigate the influence of gaps and overlaps on the compressive strength of the laminate. For a small gap of 0.5 mm, there was little effect on the compressive strength. However, with gaps of 3.175 mm, the compressive strength decreased by 20% [41]. This is consistent with Ju et al. [40] which confirms the assumption of considering the effects of gaps and overlaps in autoclave cured laminates and ISC TP’s similar.

2.3.3. Stiffness

Diemar et al. [4] manufactured several laminates, each with different gaps and overlaps, and layup set-ups. After the manufacturing process, X-ray tomography was used to create a one-to-one model of the test sample. This model was used to compare experimental data with FEA data. From the experimental results, it could be concluded that the effective stiffness (E_{11}) in the loading direction was always negatively impacted by the presence of gaps and overlaps. The maximum decrease was found to be 3.3% [4]. Furthermore, this paper also investigated the effect of the gaps and overlaps on the overall effective strength of the material. Gaps and overlaps caused the laminate to decrease in strength with a maximum of 12.4%. This seems significantly lower than the results by Ju et al. and Lan et al. [40], [41]. This discrepancy is discussed by Diemar et al. and is concluded to be an effect of defect size, which was considerably lower than the other two papers.

2.3.4. Interlaminar properties

In addition to the effects of gaps and overlaps on the mechanical properties of composite laminates, the interlaminar properties can also be looked at. The interlaminar properties entail the properties of a laminate w.r.t. how the layers interact with each other and how well they are bonded [45]. The paper by Cartié et al. [42] has investigated this by doing several tests and experiments. Cartié et al. investigated the results on the interlaminar shear strength (ILSS) of gaps and overlaps in mode I and mode II. The tests in mode I concluded that by introducing gaps and overlaps the apparent crack resistance tended to increase. This resulted in the interaction with through-thickness defects, including resin cracking and debonding. The tests in mode II clearly indicated that the increase in gap size had a significant effect on the crack propagation behaviour. This was eventually followed by unstable crack growth. The effect with overlaps turned out to be less than with gaps, most likely due to large resin pockets, resisting mode II crack propagation [42].

To provide a short summary, the table below constructed by Croft et al. [44] is given. This table indicates the consequences of certain defects on the mechanical properties of the tested laminate according to Croft et al.

Figure 2.19: Performance comparison of different defect configurations [44]

		Gap	Overlap	Half Gap/Overlap	Twisted Tow
Tension		—	—	↘	↗
Compression		—	↗	—	—
In-Plane Shear	Length	—	—	↘	↘
	Width	↗	↘	↘	↘
OHT		—	—	—	
OHC	Length	↗	↗	↗	
	Width	↘	↘	↘	

↗ ≥ 3% increase (up to 13%)
— ±3% variation
↘ ≥ 3% decrease (up to 12%)

Table 2.19 contradicts the paper by Ju et al. The table does not indicate a significant variation in tensile strength, while Ju et al. report a variation of around 30%. The same difference is found for the compression strength between the two papers, as Ju et al. record a reduction of again around 30% while Croft et al. find an increase of the compression strength larger than 3%. Furthermore, the results in the table for in-plane shear in the length direction match the findings of Lan et al. They also found no significant influence on the in-plane shear strength as a result of embedded gaps and overlaps.

2.4. Morphological approach

From the previous sections, it has become known that defects are an unavoidable byproduct during the manufacturing process of AFP composites. It was discussed what defects can occur, how these defects occur, and what the consequences of these defects are on the material. From this, it was

concluded that the formation of gaps and overlaps was the most frequently occurring defect. Then the consequences of said gaps and overlaps were investigated to either confirm or deny the intuition that gaps and overlaps hurt the quality and/or strength of the part. The investigated works each had their specific research objectives but also shared similar findings [4], [40]–[42].

Most of the previously investigated works put their focus on the consequences of gaps and overlaps in the material. This makes sense but this also inherently sets aside the characteristics of the present defects. From section 2.3 it has become evident that the shape and size of a defect can greatly affect the influence said defect has on the material. Lan et al. [41] already confirmed this when their research showed a lower decrease in strength than other research. The conclusion was made that the research of Lan et al. used significantly smaller gaps and overlaps which resulted in a lower knock-down on the total effective strength. Furthermore, the size and shape of gaps and overlaps influence the waviness factor in the laminate. This waviness leads to a knock-down of the axial modulus [40], where a higher waviness results in a lower axial modulus. This emphasises the need to study the exact shape and size of gaps and overlaps as it can be crucial for the strength of the laminate.

This entails what a morphological approach is all about. Although the definition of morphology is often used to describe the shapes and sizes of biological structures, it can also be used to describe other structures. According to *dictionary.com* [1] one of the definitions for the word morphology is: ”The study of the form or structure of anything”. Considering this definition and referring it back to gaps and overlaps generated by the AFP process one can begin to imagine what a morphological approach regarding these defects can look like. To further explore this approach several research papers were investigated.

The first example of a morphological approach to the investigation of defects resulting from the AFP manufacturing process is a paper by Ravangard et al. [46]. This paper researches the morphology of gaps and overlaps manufactured in thermosets by the AFP process. This work looked at compression and deformation in two situations, one situation with a single tow gap which was only simulated and one situation with several gaps which were simulated and manufactured. The second situation is particularly valuable, as it allows the simulated findings to be compared with the actual samples This situation can be seen in figure 2.20.

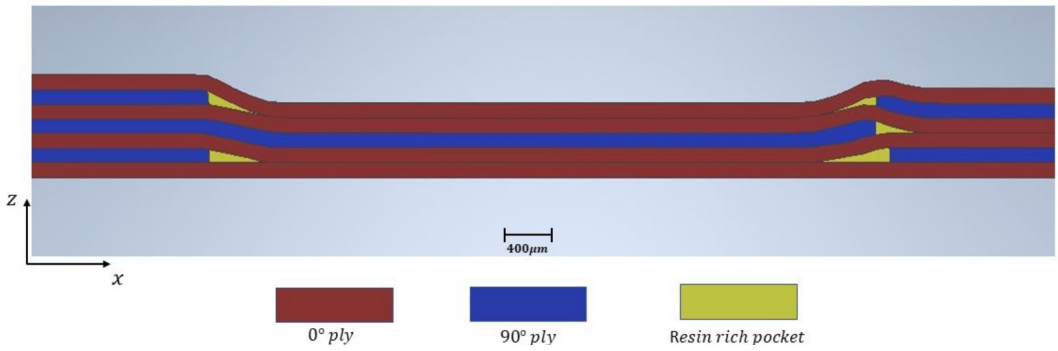

Figure 2.20: Sample morphology after compaction of a simulated model [46]

Figure 2.20 shows the layup of the to be manufactured sample by the AFP robot including the gaps. During the process, a compaction roller is applied on the tow to ensure good adhesion. This compaction force distorts the tows. This causes the layup to shift in shape. The shifted shape can be predicted by modeling the sample in FEM software and running a simulation that accurately reflects real-world conditions, as can be seen in figure 2.20. This does not give concrete answers but can be helpful to get an initial idea of what the shape is going to look like.

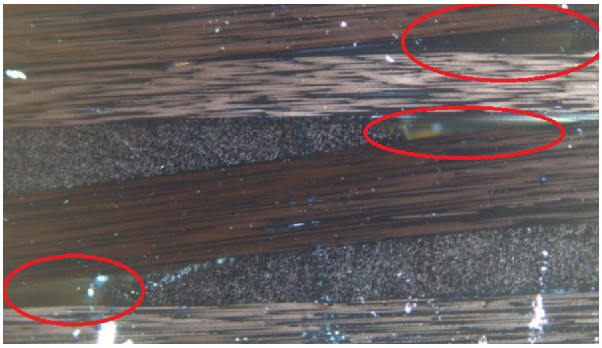

Figure 2.21: Manufactured sample with highlighted void: right side of the simulated laminate

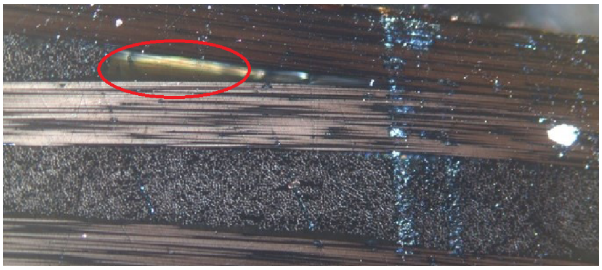

Figure 2.22: Manufactured sample with highlighted void: top left side gaps of figure 2.20

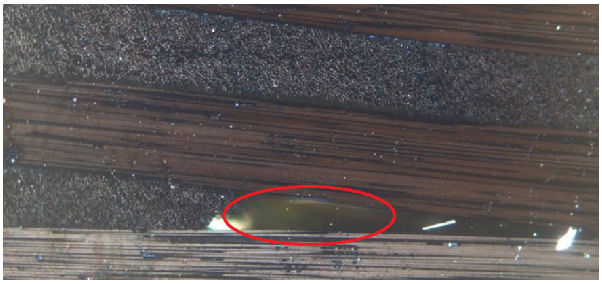

Figure 2.23: Manufactured sample with highlighted void: bottom left of figure 2.20

In figures 2.21 to 2.23, the first image corresponds to the right side of the simulated laminate, the second image to the top left side gaps, and the third image to the bottom left of figure 2.20. The gaps are visible, but they do not align exactly with the predicted locations from the simulation model. This difference emphasizes the importance of physically manufacturing the predicted models, as real-world conditions can lead to variations not captured in simulations.

The research is then followed by creating real samples. These samples are then cut and cross-sectional micrography is performed to inspect the samples. Afterwards, the real cross-sections can be compared to the cross-sections created by the FEM model. The real-life samples did confirm that the model showed an accurate representation of the expected results [46].

For this literature research, another paper showing a morphological approach to certain features of the AFP process was reviewed. This paper by Peeters et al. [47] investigated the influence of the roller direction and several different layups on the morphology of ply drops produced during the LAFP process. This research investigates a different phenomenon, namely ply drops instead of gaps and overlaps. It uses a different heating method, employing lasers instead of flashlamps. Nonetheless, it effectively demonstrates the type of approach that could be beneficial for the planned morphological research in this thesis. Its morphological approach consists of manufacturing the layups with ply drops and cutting the layup into samples. Then the surfaces of the samples are prepared and inspected under

a microscope. This results in clear images in which one can identify certain artefacts of the shape and size of the ply drops. In other words, this provides a clear morphological illustration of the ply drops. Such an image can be viewed in figure 2.24.

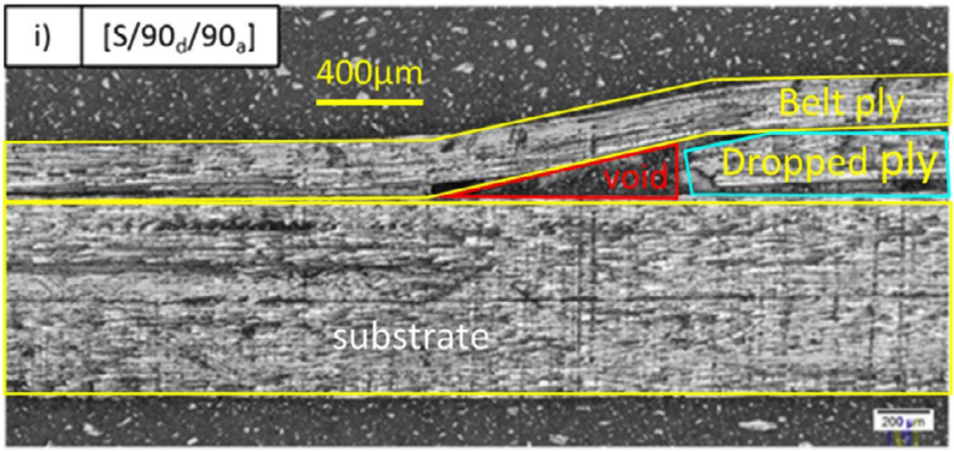

Figure 2.24: Morphological approach to ply drops [47]

This paper is seen as a good example of a morphological approach that would apply to this research. Peeters et al. can derive clear conclusions from the manufactured cross-sectional micrographs. This indicates that even though it could be possible to create 3D scans of a laminate, by for example using x-ray micro-computed tomography [4], one can still draw significant conclusions from 2D micrographs. The choice of methodology aligns well with readily available equipment. High-resolution microscopes used for 2D analysis are generally more widely available than 3D scanning techniques. Manufacturing 2D samples is significantly less time-consuming than producing 3D samples, as the latter requires a complete reconstruction of the sample volume, and therefore much more data. In this work, only a cross-sectional view is necessary, making 2D samples more than sufficient.

Even though a 2D approach for morphological research offers many benefits, it also has its limitations. For instance, it is not capable of detecting out-of-plane defects. This can mean that the identified features of the defect in the micrograph can differ if the cross-sectional cut was made at another place along the defect. To decrease the effect this can have on the final result one could take multiple samples along the defect. Therefore, if most of the samples made along the same defect display the same behaviour one can consider that the defect behaves the same along the whole out-of-plane length.

2.5. Research Gap

From the analysis and discussions in the prior sections, it is increasingly apparent that there exists a distinct research gap, indicating areas that warrant further exploration and investigation. Much research has been performed on the prediction and prevention of gaps and overlaps [6], [32], [38], [48]. These papers are all interested in the frequency of gaps and overlaps, or what parameters play which roles in creating them. This research is often done to be able to tweak the process parameters to create fewer defects in the resulting laminate.

Another class of papers regarding gaps and overlaps are the papers which investigate the consequences of gaps and overlaps. In contrast to the previous style of papers, these papers are not interested in how or why these defects form. These papers are predominately interested in what way the gaps and overlaps affect the properties of the final laminate. Properties of interest are for example tensile strength, compressive strength, and stiffness [4], [40], [41], [49], and the stiffness. Other properties that show a change due to gaps and overlaps can be interlaminar properties such as the interlaminar shear strength, and the interlaminar fracture toughness [42], [45], [50].

The last class of papers are the papers with a morphological approach to AFP-produced composite laminates. These papers aim to describe and quantify the shape and size of AFP-produced artefacts in the laminate. There are very few papers that investigate these artefacts with a morphological approach to the AFP process. The previously discussed papers were the only two found examples of a morphological approach of the AFP-produced defects. The paper by Ravangard et al. [46] nicely showed a morphological approach to investigate gaps and overlaps. However, this paper only researched this for thermoset materials and not for thermoplastics. The other example from Peeters et al. [47] did show a morphological approach to thermoplastics. This research, however; was focused on ply drops and not on gaps and overlaps.

Therefore, from the existing literature, it can be concluded that there is yet to exist a research paper on the morphology of the gaps and overlaps produced with the in-situ consolidated thermoplastic composites. This will therefore be the topic of this research.

With this in mind, the research question can be formulated:

What are the effects of the processing parameters in the in-situ consolidated thermoplastic automated fibre placement process on the morphology of gaps and overlaps?

To be able to construct the answer for the main research question, the question can be broken down into multiple subquestions. The answers to these subquestions combined then should form the complete answer to the main research question. These subquestions are:

1. *What metrics can be used to quantitatively describe the shape and size of gaps and overlaps?*
2. *What processing parameters have the greatest influence on the morphological features of gaps and overlaps?*
3. *How does the layup direction influence the described metrics of gaps and overlaps?*

As the main research question is now dissected into the three subquestions, hypotheses for all questions can be presented:

1. For the first subquestion, it is hypothesised that the actual width of the gap will influence the shape of the gap and hence the metrics to be used for quantifying the morphology. Furthermore, due to the applied heat and the investigated literature, it is expected that the edges of the gap will adhere to some sort of a curved shape. This can be a parabola, a circular arc, or a different curved geometry. For the top edge, it is expected to also show a curved profile if it does not close the gap. If it does close the gap, the top edges of the left and right voids are expected to be linear. This hypothesis is aided by a schematic visualisation below in figure 2.25.

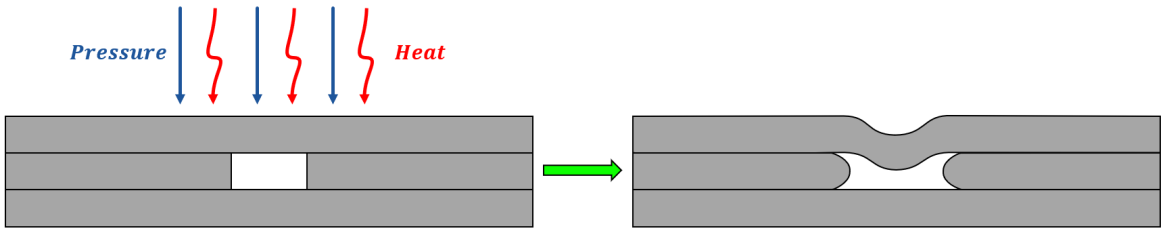

Figure 2.25: Schematic visualisation of first hypothesis

   These geometries can then be described by their corresponding metrics to fully define their shapes. For example, a circle could be parametrised by its radius and its centre point position.
2. For the second subquestion, it is hypothesised that the process parameters that have the greatest influence on the previously defined morphological features are the layup velocity, temperature, and consolidation pressure. It is expected that increasing the layup velocity will lead to a decreased degree of gap closure, as it exposes the material to less time under pressure and heat.

An increase in temperature is expected to result in more filled gaps, likely due to the decreased viscosity of the material at elevated temperatures. Furthermore, an increase in pressure is expected to press the material more and influence the extent to which the gaps remain open or closed.

3. Lastly, for the third research question. It is hypothesised that the layup direction largely influences the gap morphology. A different layup direction for the tows that form the side and top edges of the gap will dictate an entirely different geometry. It is expected that a change in the direction of gap edges will result in a possible shift in edge geometry from curved geometries, to edges with different shapes.

3

Design of experiments

With the research gap identified, a method can be developed to provide answers to the research questions. The main focus of this work will be the first two formulated research questions. The third research question will be investigated in a second part to this work. Furthermore, the focus was shifted more towards gap morphology, as overlapping behaviour can be partially inferred from the gaps themselves. This is because the top layer must climb the edges of the gap, inherently illustrating aspects of overlap behaviour. With this in mind, two experiments could be designed to each answer a research question.

3.1. Design of experiments: Trial One

It was decided to perform two experiments. This allowed the first experiment to be used not only to get answers to the research questions but also to become familiar with the general process. The parameter of interest for this experiment would be the gap size. With this experiment, the influence of the gap size on the shape of the gap can be determined. After that, metrics can be defined to quantitatively describe the morphology of the gaps. To be able to obtain these results from the experiment, a layup had to be designed from which these results could be extracted.

3.1.1. Design considerations

The material used for this experiment was chosen for its thermoplastic properties and availability at the TU Delft field lab where the layup was produced (SAMXL). The material is a tape made from CF/LM-PAEK (Carbon Fibre Low Melt PolyArylEtherKetone), a variant of thermoplastic PAEK that is well-suited for AFP processes because of its lower melting temperature and melt viscosity compared to standard PEEK, which enhances its workability. Figure 3.1 shows a cross-sectional micrograph of the tape material available.

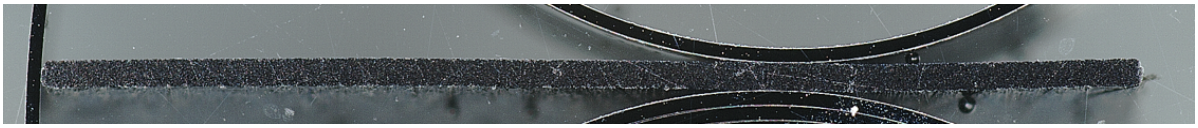

Figure 3.1: Raw material to be used for the experiments

As for this experiment, the gap size is the only parameter that changes. The other process parameters remain constant. These parameters include the layup velocity, the consolidation pressure, and the input parameters for the Humm3 flashlamp heater.

Layup velocity

The layup velocity for thermoplastics is slower than for thermosets as the material needs to be consolidated in-situ which limits the speed. Deden et al. showed that with a layup velocity of 50 mm/s good results could be achieved for the in-situ AFP process with CF/LM-PAEK. Therefore, it was decided to initially use this speed for the manufacture of this layup.

Consolidation pressure

As already explored in chapter 2, consolidation pressure is a critical parameter for the AFP process; however, in previous experiments at SAMXL, a consolidation force rather than pressure was used, and for a setup similar to the one intended in this work, a force of 250 N was measured and will therefore also be used in the first experiment.

Humm3 settings

The Humm3 settings are not predetermined, but are to be determined at SAMXL. Doing it like this allows for finding the right settings to ensure good consolidation for the tape being placed without burning it.

3.1.2. Layup configuration

Stacking sequence

For this experiment, the design choice was made to go for a stacking sequence of [Tool/0/90], as illustrated in figure 3.2. It was decided to go for this stacking sequence as this sequence is not over-complicated, making the production straightforward. However, this sequence will still result in a gap with distinct features later to be identified in the micrographs.

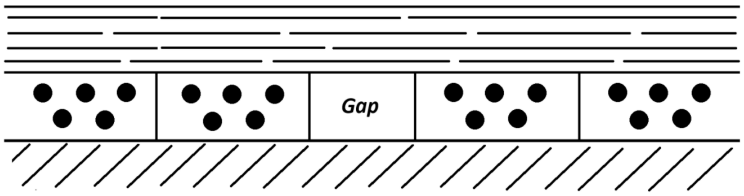

Figure 3.2: Stacking sequence experiment one, [Tool/0/90]

It is also important to note that figure 3.2 is only an illustration and is not to scale for the purpose of clarity. The width of a tow is 6.35 mm while its thickness is roughly 0.15 mm.

Boundary conditions

To ensure the gap mirrors a real-world scenario it has to satisfy several boundary conditions. In the real world, these gaps can often occur in the middle of a large layup. Therefore, in the 0-degree layer, there should be multiple tows at the left and right sides of the gap to mirror this situation as closely as possible. Furthermore, the time it takes the robot to reach the intended process layup velocity and the heating system to reach the desired temperature also needs to be taken into account.

Pantoji et al. [38] used the same setup as this work will use, and recorded the velocity profile over the layup length, which can be seen in figure 3.3.

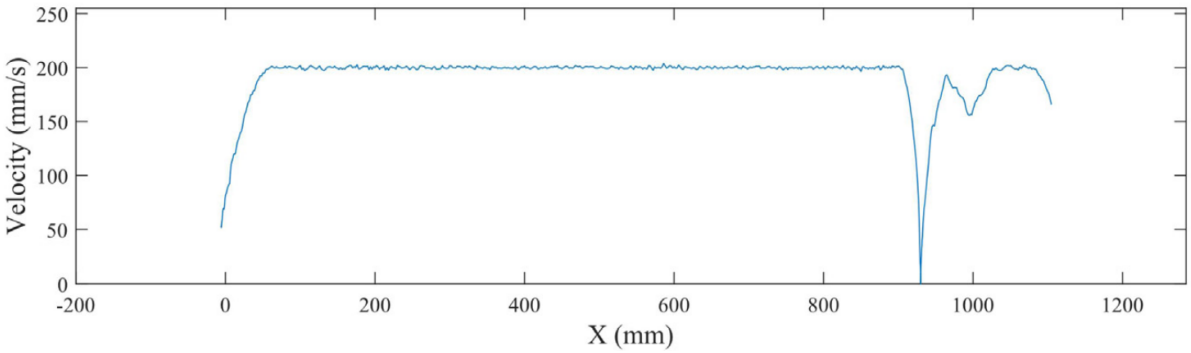

Figure 3.3: Layup position vs velocity graph by Pantoji et al. [38]

Assuming a constant linear acceleration, the time it takes to reach the desired speed of 200 mm/s can be computed as the following.

$$s = \iint a dt dt = \frac{1}{2}at^2 \quad \& \quad a = \frac{v}{t} \quad \rightarrow t = \frac{2s}{v} \tag{3.1}$$

From the image, the maximum velocity and the distance it takes to reach this can be extracted. Thus, by substituting $s = 62.61\ mm$ and $v = 200\ mm/s$ the time it takes to reach the desired speed can be computed as 0.63 s. Now that time (t) and velocity (v) are known, the acceleration (a) can be computed:

$$a = \frac{v}{t} = \frac{200\ mm/s}{0.63\ s} = 319.44\ \ mm/s^2 \tag{3.2}$$

In reality, the acceleration of the robot is not constant but reaches the desired speed quicker. Hence, this is an overestimation and the robot will likely have reached its desired speed quicker. As previously discussed, the layup for this experiment is to use a layup velocity of 50 mm/s. Assuming the same acceleration as Pantoji et al., as it is the same setup, the time and distance it takes to reach 50 mm/s can be computed:

$$t = \frac{v}{a} = \frac{50\ mm/s}{319.44\ mm/s^2} = 0.16\ \ s \quad \& \quad s = \frac{1}{2}at^2 = 0.5 * 319.44\ mm/s^2 * (0.16\ s)^2 = 3.91\ mm \tag{3.3}$$

Consequently, before reaching the gap there must be a minimal distance of 3.91 mm to achieve the desired constant speed at the gap. However, this distance seems quite short but the distance it takes to reach the right temperature also needs to be computed and could dictate the required distance.

The manufacturer of the Humm3 heating system claims that the system reaches the desired temperature in about a quarter of a second. This can be seen by the graph made by the manufacturer in figure 3.4

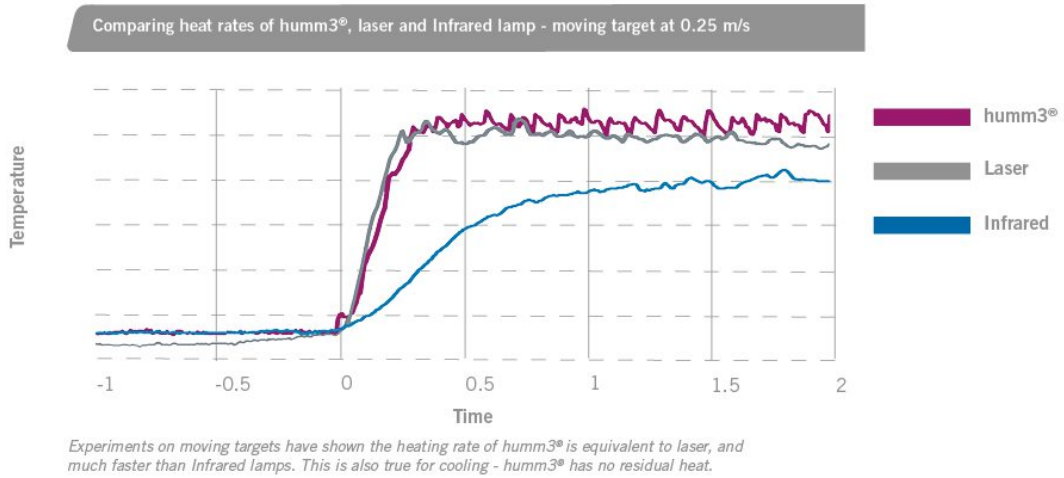

Figure 3.4: Humm3 heating time [51]

However, consulting another paper that used the Humm3 system from Danezis et al. [52] shows that the desired temperature was reached after half a second. For that reason it will be assumed that it will take 0.5 s for the Humm3 system to reach its desired temperature. Before the Humm3 is switched on the robot has already moved a distance. This distance is assumed to be larger than the distance it takes to reach constant velocity. Therefore, the following computation for distance, assuming constant velocity, can be used:

$$s = vt \quad \rightarrow \quad s = 50 * 0.5 = 25.0\ mm$$

Therefore, for reaching the desired temperature the layup demands an additional 25 mm of length away from the gap to ensure that the heating system reaches a constant temperature at the gap every time. As this distance is more than it takes the robot to reach the desired layup velocity, the additional length should be for now be governed by the added length for reaching this desired temperature.

In addition, the cut-off length of the AFP head is 70 mm. This means that 70 mm before the end of the layup, the robot stops and cuts the tape after which it accelerates again and places the remaining 70 mm of the tape. This could influence the morphology of the gap. Hence, the cut-off length needs to be added at the end of the layup to ensure that it does not affect the gap.

Heat affected region

As mentioned before, this work will use the Humm3 to heat the tows. Therefore, it is important to acknowledge that the crystal which is used to heat the tows is significantly wider than the width of the tow. Thus, the heated region will also be wider than just one tow width. From the literature review, it became evident that the number of times one heats the composite material has an influence on its quality. With this in mind, the 90-degree tows were designed to be spaced apart by the width of the crystal, which was 50 mm. This ensured that the 90-degree layer at every location was only heated once. This should reduce the influence of defects that could occur due to overheating close to the desired gap on the morphology of the gap.

Dimensional limitations

After contact with the automation engineer at SAMXL, who would later aid in the production of the layup. It became evident that the maximum length of the area on which the layup could be placed was 520 mm. To keep a safe margin at the bottom and top, the layup was designed to have a total length of 400 mm.

Tow compaction

The tows are expected to compress during the production of the laminate as a result of the combination of temperature and pressure. Spacing the tows (programmed shift) by exactly one tow width would certainly result in overlaps. As this does not account for the width expansion of the tows under compaction. Therefore, this compaction dictates the programmed shift. A paper by Agarwal et al. [21] shows an increase of a single tow width, 6.35 mm, to a width between 6.5 and 7.0 mm. These values were obtained for different pressure and temperature values. Therefore, this range was taken into account for the programmed shift.

Gap design

The main objective for the design of the layup is to include multiple gaps with varying sizes. This variation in gap size can be achieved in two ways: either by placing multiple gaps between tows, each with a different but constant width, or by designing a single gap that gradually increases in size along its length. In the latter case, the size of the gap depends on the position at which the cross-section is taken. Using a single, growing gap reduces the overall layup size, since the boundary conditions only need to be satisfied for one gap rather than multiple separate ones. Therefore, this approach was chosen for the current experiment. In a real-world scenario, the largest gaps that occur during the manufacturing process are around one tow width, 6.35 mm (or 1/4 inch). Thus, the gap that will be embedded in the layup for this experiment will grow from 0 mm to 6.35 mm.

This approach does require considering the effects of slightly over or under-shooting desired gap location during post-processing. To not overcomplicate the design of this gap, only one side will be under an angle. This means that the tow paths to be programmed for the robot only have to be under an angle at one side of the gap instead of two. This does mean that over- or undershooting the gap location results in a different gap size. If this angle is large the resulting gap can differ considerably from the designed gap size. To investigate this, the angle and the possible errors have to be determined.

From the heat-affected region, it became evident that this design will have five gap locations equally spaced apart by 50 mm. This means that the gaps will be located in the length direction of the design at 50 mm, 100 mm, 150 mm, and 200 mm. Additionally, since the final size, the number of gaps, and the increase in gap size follow a linear relationship, the angle of the sloped side can be determined accordingly.

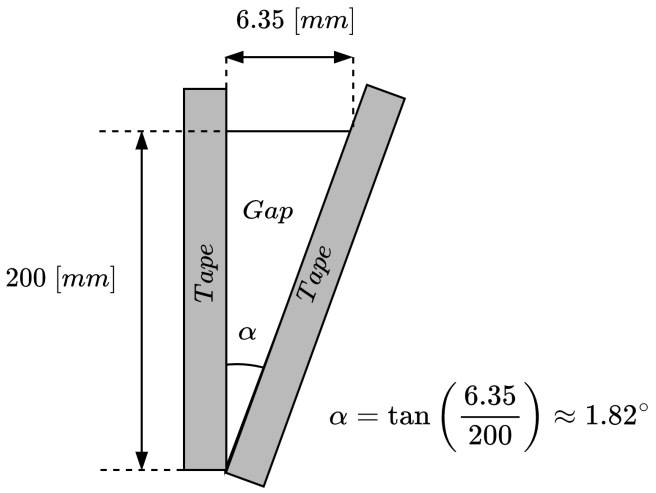

Figure 3.5: Designed gap geometry

With the angle known, the gap sizes at all locations can be determined accordingly:

$$\begin{bmatrix} w_4 \\ w_3 \\ w_2 \\ w_1 \end{bmatrix} = \begin{bmatrix} 200 \\ 150 \\ 100 \\ 50 \end{bmatrix} * \tan(\alpha) = \begin{bmatrix} 6.3500 \\ 4.7625 \\ 3.1750 \\ 1.5875 \end{bmatrix} mm \tag{3.4}$$

If the angle is known, the deviation of the gap size below a single 90-degree tow can also be determined. To compute this, the final gap with width w_4 was used as a reference. The computation is visually aided by figure 3.6. The figure shows the gap between a straight tow on the left edge and a sloped edge on the right side. The height is one tow width. Therefore, the illustration shows a top view of a location over which later a 90-degree tow will be placed.

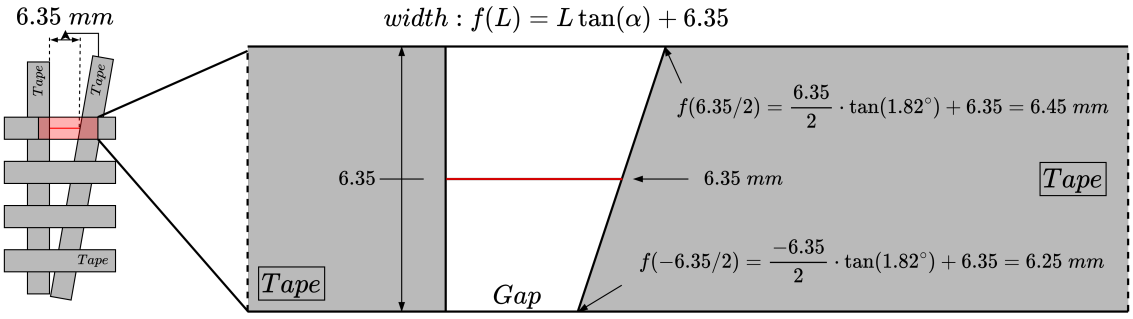

Figure 3.6: Gap size deviation below one 90-degree tow

This results in a maximum width deviation of $(6.45/6.35 - 1) * 100 = 1.59\%$. A difference of $\pm 1.59\%$ is considered small enough not to result in large changes in the morphology of the gaps. Therefore, it can be concluded that the angle applied to the right side of the gap is small enough and can be used to create several gaps within one layup.

3.1.3. Layup design for Trial One

Combining the material, design considerations, stacking sequence, boundary conditions, and the heat-affected region allows for the design of the layup for experiment one. The goal of this experiment was to manufacture multiple samples with varying gap sizes, enabling the investigation of how gap dimensions influence the laminate. The resulting designed layup is shown in Figure 3.7, and is expected to facilitate the extraction of such samples. Furthermore, the additional tape length added to ensure that the desired speed and temperature are reached was enlarged to be able to account for unforeseen process variations. Therefore, the minimal distance from both edges of the gap to the right and left ends of the 90-degree tape was set to be 100 mm. This would still be enough distance to account for the cut-off length in the case of an inverted layup direction with an additional error margin. The same reasoning is applied to the distance after the last gap and before the first gap.

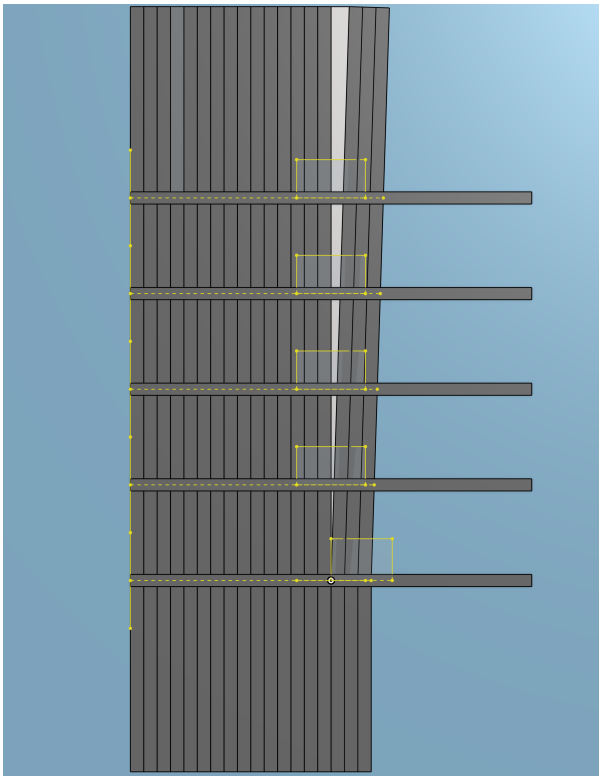

Figure 3.7: Design layup experiment one

The core point of this designed layup is to have several areas of interest in one layup. As previously explained, this could be achieved by having a single gap that expands in size, which can now be seen in figure 3.7. Accounting for the need to keep the 90-degree tows equidistant with no overlap in the heated zone, the run-up length required to reach stable process parameters, and the substrate's size constraints, it resulted in the layout in figure 3.7 with five 90-degree tows. These five 90-degree tows then finalise the areas of interest. These areas are indicated by yellow rectangles in figure 3.7, where the bottom edge of these rectangles are coincident with the desired resulting gaps. The 0 mm gap could be located anywhere below the bottom-most 90-degree layer, as long as there are two adjacent tows at that location. Therefore, it was decided to shift this area of interest to the right. This still encapsulates a 0 mm gap while also capturing the effect of a ply drop, which can be considered as additional information.

3.1.4. Production-driven design adjustments for Trial One

The section above explained in detail what decisions were made to eventually conceptualise the final design for Trial One. During production, it was found that several aspects of the design had to be altered slightly to make the production possible. This section discusses those aspects and elaborates on what changes had to be made and why, and how, if at all, they influenced the final samples to be

made after post-processing.

Tow compaction

The tow compaction for the design is already touched upon. However, it was merely a range from literature that was indicated. As this experiment was the first time at SAMXL that a laminate was produced using the LM-PAEK material in combination with the Humm3 flashlamp heating method, it meant that this range had to be confirmed. Through an initial test, it was confirmed that the tow width expanded from 6.35 mm to 7 mm. Hence, the shift was programmed to be 7 mm to ensure that there were no overlaps and minimal gaps between the tows in the 0-degree layer.

Substrate

The intention was to manufacture the layup onto the tool to have a straight bottom side of the gap. However, when setting up the experiment, it became quite evident that this brought several complications to the table. The tape was much more fragile than expected. This caused doubts if the laminate would be able to be removed after production. The chances of successfully removing the laminate without causing deformations to the areas of interest were considered slim. For this reason, it was decided to place the laminate on top of a pre-manufactured substrate. The substrate in question was a woven LM-PAEK laminate that was already present at SAMXL. This ensured that the substrate was made from the same material as the laminate that was to be produced, although in a different stacking sequence. The addition of this substrate ensured that the resulting laminate had enough rigidity to be confidently removed from the tool without altering the morphology of the embedded gaps. However, adding the substrate also had its downsides. Firstly, the substrate had limited dimensions which dictated the dimensions of the designed laminate and therefore influenced the number of 90-degree tows. Placing the laminate on top of this substrate also meant that the substrate was heated up multiple times. This resulted in significant warping of the bottom side of the embedded gaps. This phenomenon can be observed in figure 3.8, where there is a clear difference between the heated and non-heated parts of the substrate. Lastly, the substrate, even though well attached to the tool, showed some warping which later had to be corrected for in the LLS data.

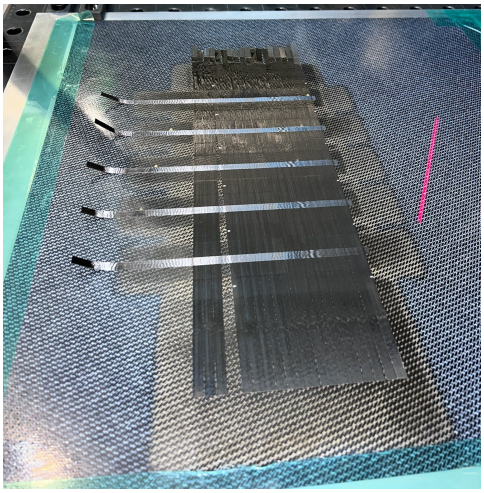

Figure 3.8: Manufactured layup placed on top of LM-PAEK substrate

Layup direction

After placing the 0-degree layer, as can be seen in figure 3.8, it became evident that the designed layup direction of the 90-degree layer was no longer possible. The 90-degree layer was designed to be placed from right to left in figure 3.8. However, the AFP-XS end effector on the robotic manipulator was too large and would run into the surrounding fence when the layer was to be placed in this fashion. Therefore, the decision was made to place the 90-degree tows from the left to the right (as seen in figure 3.8). Nevertheless, this did not have any influence on the laminate as such a process variation was already taken into account in the design. Enough length was added to both sides of the gap to reach the desired process parameters and take the cut-off length into account.

3.2. Design of experiments: Trial Two

3.2.1. Design considerations

The material used for this experiment is the same as in experiment one. The purpose of this experiment is to investigate the relation, if there is any, between the process parameters of the AFP ISC-TP production process and the morphology of the gaps that can occur during a layup. For this, the layup velocity and consolidation pressure were to be varied and measured. Additionally, from trial one, a suspicion was created that perhaps the direction of layup could also have an influence on the morphology of the gap. Only the mentioned variables will be varied. All other variables such as nip-point temperature and tape tension will be kept constant for this experiment. Furthermore, this three variables for layup velocity and consolidation pressure will be chosen to provide a low, intermediate, and high parameter setting. Additionally, two layup directions will be determined for the 90-degree layer.

3.2.2. Layup configuration

Stacking sequence

From the results of experiment two it became evident that using a pre-manufactured substrate could lead to a convoluted micrograph. Which meant that the attention was drawn away from the main focus, the gap. To prevent this the designed layup for this experiment was altered slightly from the design for experiment one. Figure 3.2 shows the tool and a 0-degree layer and a 90-degree layer. Experiment two will be designed to have an additional 0-degree layer between the tool and the other 0-degree layer containing the gaps.

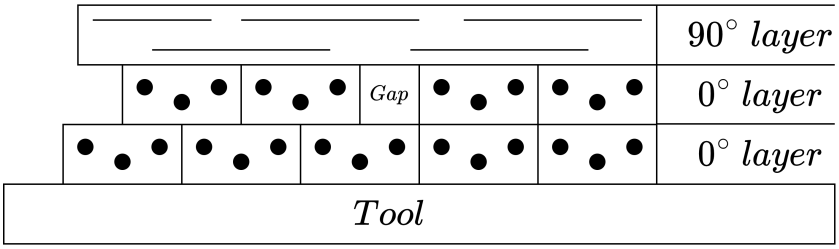

Figure 3.9: Stacking sequence experiment two, [0/0/90]

Figure 3.9 shows the stacking sequence for the second experiment. The figure also shows an effect that could happen between the two 0-degree layers. The right edge of the gap coincides with an edge of a tow of the bottom 0-degree layer. This could also show in the micrographs and one should be aware of this, as it can influence the resulting morphology of the gaps.

Boundary conditions

The boundary conditions for this layup remain the same as for the experiment one discussed in 3.1.2. Although the same boundary conditions applied as in trial one, a slightly adjusted heat-affected region was used due to the renewed availability of the smaller Humm3 crystal, allowing the heat-affected region to be reduced from 50 mm to 25 mm.

Tow compaction

For the design of experiment one a tow width expansion from 6.35 to between 6.5 and 6.6 mm was taken into account. However, later it became evident that the tows actually expand to 7 mm. Therefore, for this experiment, the tow width expansion and therefore distance between midlines of 7 mm was taken into account.

Gap design

From the analysis, parametrisation, and discussion of the first experiment it became evident that the second gap size of size 3.175 mm was the most interesting. The gap width for the second gap seemed to be just enough for the 90-degree layer to touch the bottom of the gap. This raised the question that if speed and pressure were altered if this would still result in a closed gap or that it would remain open,

similar to the first gap. What is meant by this is that it raised the question if a gap with the morphology of (1) in figure 3.10 would morph into a shape more similar to (2) or (3) when exposed to different speeds and pressures.

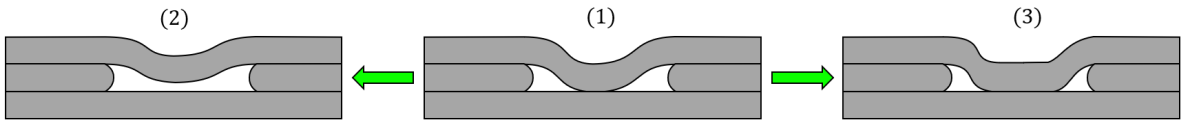

Figure 3.10: Possible gap morphology shift

To be able to answer these questions the width of the second gap in experiment one was chosen for this experiment. As this gap width could be a tipping point for the gap morphology it would also be interesting to see what would happen when these process parameters are varied on a gap that is slightly smaller or slightly larger than 3.175 mm. Therefore, two additional gap sizes were considered. The gap sizes that will be implemented in the layup will be:

1. Gap size one = 3.175 mm
2. Gap size two = 0.75 * Gap one = 2.381 mm
3. Gap size three = 1.25 * Gap one = 3.969 mm

Layup velocity

This experiment will investigate the influence of the process parameters on the morphology of the gaps. One of them is the layup velocity. Altering the layup velocity however can also influence other variables in the production process. For example, the speed of placing the tape has a large influence on the consolidation of the tape. A faster speed could mean that the tape does not consolidate and could peel off. A slower speed could mean that the tape is exposed to too much heat and could burn. Therefore, if one wants to adjust the speed for the AFP ISC-TP process it is important to monitor the temperature. Keeping the temperature constant at the nip-point across the speed variations would mean that the tape is still able to consolidate appropriately. The temperature is mainly a result of the combination between two variables in this process, the layup velocity and the voltage applied to the Humm3 flashlamp. As aforementioned, this experiment will investigate the effect of three different speeds on the morphology of the gaps. The layup velocity of experiment one was 40 mm/s, which was already close to the maximum voltage of the Humm3. Therefore, it was decided to take this as a maximum velocity and add two lower velocities. The velocities that will be used for this experiment are:

1. v_1 = 40 mm/s
2. v_2 = 30 mm/s
3. v_3 = 20 mm/s

the other input is determined such as to make sure the same temperature is reached at the nip point.

Consolidation pressure

Determining the consolidation pressure was more challenging than determining the layup velocities, as for trial one the consolidation pressure was not recorded. Additionally, it was decided to proceed with variations of the force applied on the substrate instead of pressure variations as the setup allowed for a straightforward force measurement with regard to a more complicated pressure measurement. Hence, the force measurements were taken with the average pressure values. This allowed for a force measurement which did not have to be converted to the right pressure profile for this roller. The force applied on the layup at SAMXL is primarily determined by two factors. Firstly, the air pressure applied in the pneumatic cylinder that presses the roller onto the laminate. Secondly, the vertical position of the robotic arm, which influences how much the cylinder is compressed and thus indirectly affects the resulting compaction force, even though the robot itself does not apply any force. This was tackled by first fixing the roller strain by the robotic arm and then altering the air pressure in the chamber that acts upon the piston and presses down the roller. This air pressure could be adjusted from 0.1 MPa to 0.5 MPa. From this, it became evident that the increase in pressure did not correlate to a linear force

increase on the laminate but rather a non-linear relation was present. As in practice an increase of higher than 0.3 MPa showed little increase in force, while varying the air pressure between 0.15 MPa - 0.20 MPa the force exerted varied drastically. Hence, a somewhat constant region of the non-linear profile was targeted, and the following three air pressures were selected to extract the forces from:

1. 0.19 MPa $\approx$ 15 kg
2. 0.225 MPa $\approx$ 20 kg
3. 0.26 MPa $\approx$ 25 kg

These pressures resulted in three different forces with an equivalent constant mass increase of 5 kg. The forces were measured by a force torque sensor (FTS) manufactured by ATI Industrial Automation. This FTS has six outputs, three force components (Fx,Fy,Fz) and three torque components (Tx,Ty,Tz). The XY-plane was parallel to the laminate, resulting in the only component which was used from the FTS, the Fz component. This force could then be divided by the gravitational constant of 9.81 m/s^2 to convert Newtons into kilogrammes. The masses mentioned before were measured statically, but the force will also be monitored during the placement of 90-degree tows to observe if there is a difference with respect to the static cases.

Full factorial approach

Now that the three layup velocities, three pressures, three gap sizes, and two directions are decided, all possible combinations can be constructed. However, in order to better evaluate the results, each combination of parameters must be repeated three times. This repetition ensures that any anomalies or outliers can be distinguished from the actual underlying trends or behavioural patterns in the data. This then in turn triples the amount of samples that have to be produced. Resulting in the following full factorial approach:

- Number of gaps = 3
- Number of layup velocities = 3
- Number of applied forces = 3
- Number of layup directions = 2
- Number of repetitions = 3
- Total number of samples = $N_{gaps} * N_{velocities} * N_{forces} * N_{directions} * N_{repetitions} = 3*3*3*2*3 = 162$

This results in a total of 162 samples to be produced in a single layup. As the actual placement of the layup does not take a long time, this is actually doable. However, the post-processing and analysis of the samples are quite time-consuming. In the interest of time, a selection had to be made.

Selection of samples

To make a selection, one first has to think about what results are desired. Firstly, it is hypothesised that the change of direction for the placement of the 90-degree layer only has a small influence on the morphology of the gap and does not provide any new information about the behaviour of the gap. Investigating only one direction of 90-degree tows already halves the amount of samples, but this still results in 81 samples.

Additionally, as aforementioned, from the analysis of the first experiment, it was evident that the second gap width of 3.175 mm was the most interesting to investigate. For this reason, it was decided that the analysis of the second experiment would focus only on gaps of this size. This reduces the number of samples by a factor of three, resulting in a total of 27 samples.

Finally, in the interest of time the amount of samples had to be reduced even further. Therefore, a selection has to be made which data points to investigate. As the crux of this experiment is to investigate the influence of a range of velocities and forces on the morphology of a gap, it was decided to select the full range of velocities at F_2, and the full range of forces at S_2. This then results in five unique combinations, repeating them three times finally results in 15 samples to be analysed. A visualisation of this selection of combinations can be viewed in figure 3.11 below.

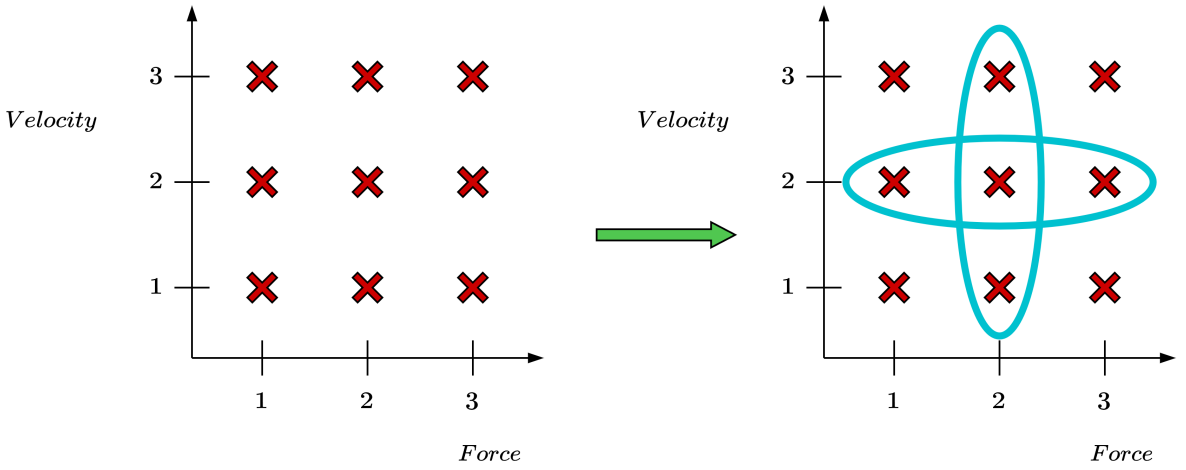

Figure 3.11: Final selection of data points to be later analysed

These five data points correspond to the following five combinations of velocities and forces:

1. v_1F_2
2. v_2F_1
3. v_2F_2
4. v_2F_3
5. v_3F_2

Although, for this research, only the above five data points and their repetitions will be investigated, all data was collected for all samples. This way, in the future, someone else has the ability to continue this research and has access to all data.

The data that will be collected during the production of this process will be Laser Line Scanner data of all 9 gaps along the length of the layup, an infrared video of every 90-degree pass, and a force torque recording of every 90-degree pass.

3.2.3. Layup design for Trial Two

Combining the design considerations, the stacking sequence, the boundary conditions, the heat affected region, the gaps, the velocity range, the force range, and the two layup directions, the final design could be made.

The second 0-degree layer has three different size gaps that are all repeated three times. Three gaps with three repetitions dictate that in this layer there will be nine gaps. From the boundary conditions in experiment one it is known that at the edge of the gap is good to have at least three tows to mirror real-life situations. Therefore, this results in $(9 + 1) * 3 = 30$ tows. The +1 comes from the fact that the last gap must also have three tows on both sides.

The first 0-degree layer will have no gaps but is preferably slightly larger than the second 0-degree layer to simulate a real-life large laminate upon which the second 0-degree layer is placed with the embedded gaps. By making this layer slightly larger, one also avoids strange edge effects that can occur when the width of both layers is the same. Therefore, it was decided to make the bottom 0-degree layer three tows wider than the second 0-degree layer on both sides. This resulted in 40 tows.

As seen in figure 3.11, there are a total of nine possible combinations between the layup velocity and force. For each combination of velocities and forces, a 90-degree tow has to be placed to investigate the effects of the different combinations. Nine combinations and two different directions mean that the 90-degree layer consists of 18 tows,

Now that for every layer the amount of tows and the boundary conditions are known, the final design can be constructed. The decision was made to extend the cut-off distance from 70 mm to 100 mm to add an additional margin for unexpected error cases. Furthermore, it was decided to make the layup completely symmetrical. For the 90-degree direction, this was already necessary as this was to be placed with two different directions. However, the layup is also made symmetrical in the length direction. This was done such that the 0-degree layer would also be able to be placed from the opposite direction. This gives slightly more freedom for the layup direction of the robot.

Combing all information above allows for the following design of layup two:

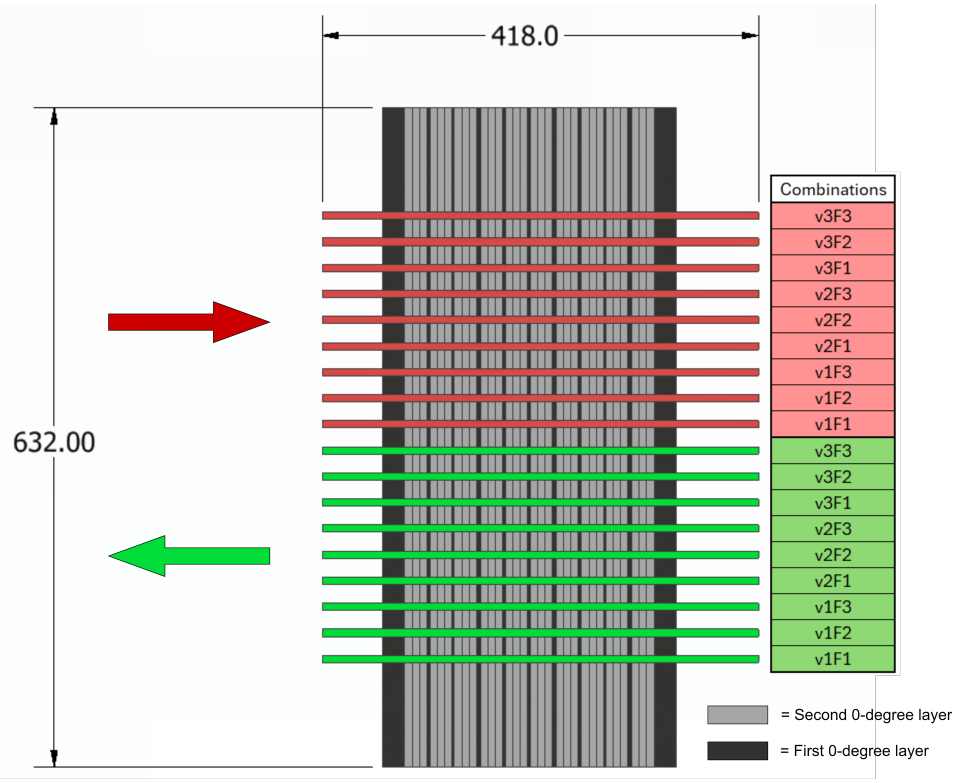

Figure 3.12: Layup design for Trial two

Figure 3.12 illustrates the 100 mm at the top, bottom, left, and right of the gap. Additionally, the green colour indicates the tows that are to be placed from right to left (+90), and the red colour indicates the tows that are to be placed from left to right (-90). One can also see the bottom 0-degree layer as the darker grey and the second 0-degree layer by the light grey tows, including the different sizes of gaps embedded in that layer. Every location where a 90-degree tow goes over a gap in the 0-degree layer can be seen as a sample. As mentioned before, this work will focus on 5 combinations of layup velocity and force for one direction, repeated three times, which results in 15 samples.

3.2.4. Production-driven design adjustments for Trial Two

The section above explained in detail what decisions were made to eventually conceptualise the final design for Trial Two. During production, it was found that several aspects of the design had to be altered slightly to make the production possible. This section discusses those aspects and elaborates on what changes had to be made and why, and how, if at all, they influenced the final samples to be made after post-processing.

Substrate

The intention as illustrated in figure 3.9 was to incorporate a complete 0-degree layer below the 0-degree layer that has the embedded gaps to act as a previously placed laminate. However, producing this layer on top of the aluminium tool turned out to be a challenge. Several methods were incorporated

to make the layer stick to the tool. Such as placing several 90-degree tows at the bottom and top of the 0-degree layer for the tows to stick to during the placement. However, after exploring several approaches to this method, it did not prove to be successful. The 0-degree tows bulged during the placement, which caused the tows to get closer to the flashlamp and burn.

Another method that was tested was to place the first 0-degree layer on a sheet of only the matrix material of LM/PAEK. This would also produce clear micrographs and had the ability to stick well to the tows placed. However, again due to the applied heat and pressure this sheet deformed and started to bulge. Again suffering the same problem as the previous method. Figure 3.13 shows the waviness of the matrix sheet after only placing two of the 40 tows.

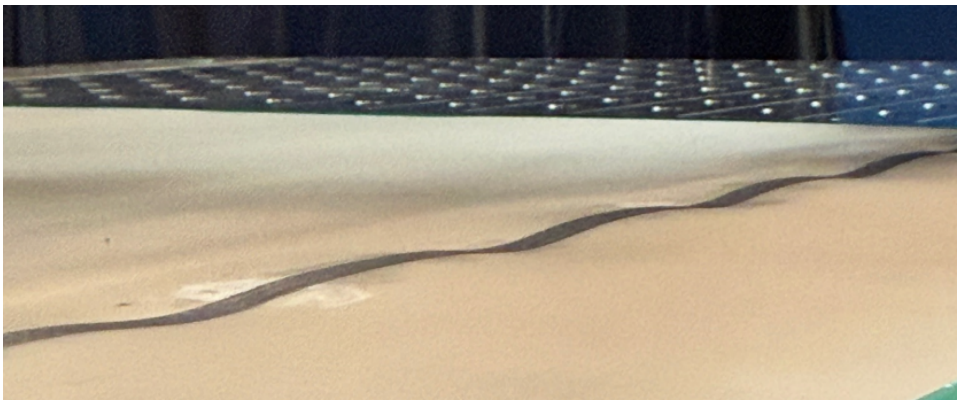

Figure 3.13: Matrix sheet waviness

As can be clearly seen from figure 3.13, the waviness was much too extreme to continue with this method.

The only solution seemed to again use a rigid substrate plate to which the tows could stick to. For experiment one an LM/PAEK substrate was used with a woven pattern. Although this did work quite nicely, it also created slightly distorted micrographs which are desired to avoid. This time a different substrate was used. The substrate used for this experiment was a PPS substrate. This substrate was chosen as its top layer already consisted of a complete 0-degree layer, voiding the need for the additional complete 0-degree layer designed for experiment two. However, a concern raised by using two different materials is the mismatch in working temperatures. PPS has a lower working temperature than LM/PAEK at 230-260 C°, around 100 C° lower than LM/PAEK [53]. Nevertheless, the temperature used during the process did not seem to burn the PPS, with some minor spots as exceptions. Therefore, it was decided to continue with this substrate.

Tow length

This new substrate showed one downside, its dimensions. In section 3.2 it was determined to increase the added length from the cut-off length (70 mm) to 100 mm. Due to symmetry, the distance to the gap was made 100 mm from all sides of the gap, also giving more room for unexpected errors. However, by switching to the PPS substrate, the original dimensions of the laminate were no longer possible. Therefore, it had to be determined how much of these distances were actually necessary to produce good results.

Firstly, the 0-degree layer required a reduction from 632 mm to 532 mm, so 100 mm had to be removed from the 0-degree layer in the length direction. From section 3.1.2 it became known that the robot requires at least 25 mm at the start to reach its desired velocity and temperature for the Humm3. Therefore, the bottom distance was reduced from 100 mm to 30 mm. This was still enough to provide constant conditions at the gap but reduced the total length of the 0-degree layer by 70 mm. Additionally, at the end of the 0-degree layer the cut-off distance was again reduced to 70 mm from 100 mm. Resulting in a total length loss of the 0-degree by 100 mm, which can be seen in figure 3.14 where the reductions are indicated by the red arrows.

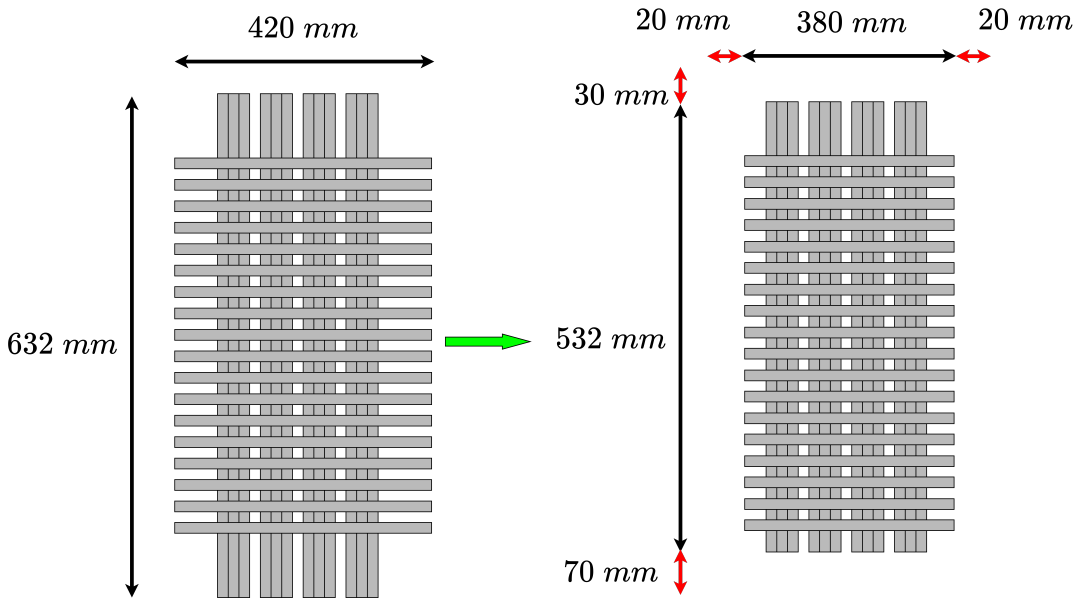

Figure 3.14: Simplified layup schematic for trial two to indicate Length and width reduction

Secondly, the 90-degree layer had to be reduced from 420 mm to 380 mm to fit the substrate. However, both sides of the 90-degree layer still had to maintain a minimum distance of 70 mm to the gap as the direction of placing the layup would be reversed after 9 tows, so both sides still required the cut-off length. Hence, both sides of the 90-degree tows were trimmed from 100 mm to the gap to 80 mm to the gap. Doing it on both sides resulted in a 40 mm reduction which brought the total length from 420 mm to 380 mm. This can again be seen in figure 3.14.

Both reductions in length still conform to all demands made to ensure constant conditions at the gap, while also causing the layup to fit on the substrate.

4

Specimen Manufacturing

The previous chapter was about designing a layup to be manufactured that encapsulates the behaviour and effects of an increasing gap size or a difference in processing parameter settings on the morphology of the gaps. This chapter will be about manufacturing the previously designed layups and all aspects involved in realising these layups.

4.1. Manufacturing Trial One

This section will specifically focus on the aspects that played a role in the manufacturing of the first designed layup.

4.1.1. Manufacturing system

The AFP system present at SAMXL consists of an AFP head and a robot manipulator. Furthermore, to accurately measure the dimensions of the layup and gap sizes, the AFP head was fitted with a Laser Line Scanner (LLS).

AFP head

The AFP head is made by ADD composites and is called the AFP-XS end effector. This system can lay down tape of dimensions 6.35 mm (1/4”), 12.7 mm (1/2”), and 25.4 mm (1”) and it is a single tow placing system. This end-effector can be observed below in figure 4.1.

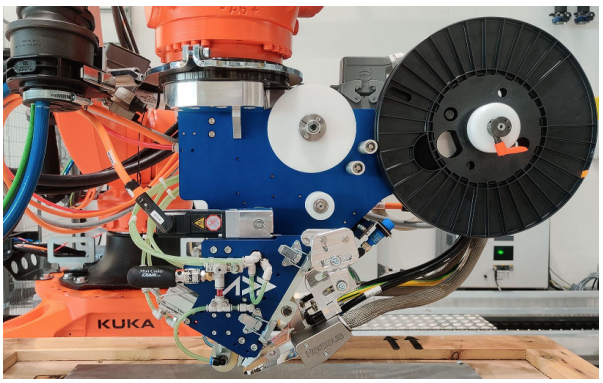

Figure 4.1: AFP end-effector, AFP-XS by ADDcomposites [54]

Robotic manipulator

The robot manipulator is a KUKA KR 210 R2700. This is a robotic arm with six degrees of freedom (DOF). However, the arm was mounted on a rail system, adding one DOF, making it effectively a seven DOF robotic manipulator [55]. This robotic arm can be viewed in figure 4.2.

Figure 4.2: KUKA KR 210 R2700 [55]

Roller

The roller used for this process is made of silicon and has a width of 30 mm and a diameter of 40 mm. This roller can be seen in figure 4.3.

Humm3 flashlamp

The Humm3 setup was photographed at SAMXL and can be seen in figure 4.3.

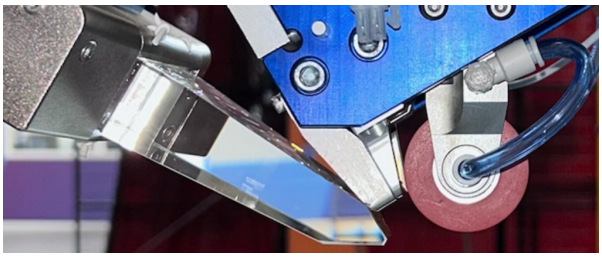

Figure 4.3: Humm3 setup at SAMXL

The working principle of the Humm3 flashlamp has previously been explained in chapter 2. The settings for the Humm3 were previously tuned for this material at SAMXL. The same settings were used for this particular layup. The settings in question are:

Table 4.1: Settings of the Humm3 flashlamp during production

Parameter	Value	units
Frequency	60	Hz
Pulse width	3	ms
Voltage	180	V

Laser Line Scanner

The 3010-25 LLS by MicroEpsilon was used during the manufacturing of the layup. The LLS was attached directly to the AFP head. LLSs are useful as they can create high-resolution 2D profiles of surfaces. A LLS works by projecting a laser line onto a surface, which is then reflected. Triangulation is then used to convert this reflection into a measurement of the surface. This triangulation results in a trapezoidal measurement window. The LLS unit and measurement window can be observed in figure 4.4.

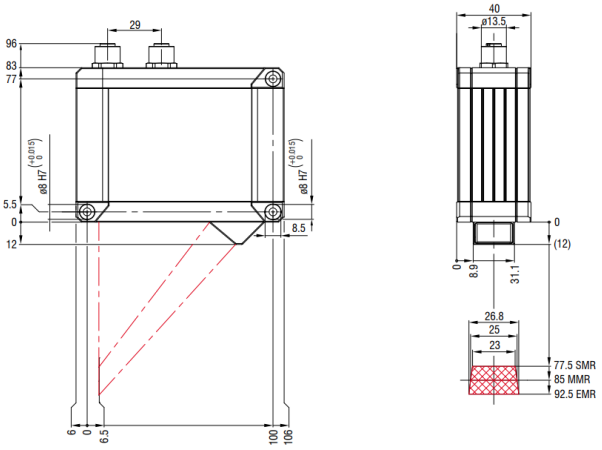

Figure 4.4: Dimensional drawing of the LLS measurement unit and -window [56]

The output provided by the LLS in the corresponding software is given in X and Z coordinates mm. Z is the height dimension of the profile, and X is the dimension corresponding to the length of the laser line. This specific LLS has an X range of around 25 mm when mounted at the correct Z position. This specific model dictates a Z position ranging from 77.5 mm to 92.5 mm in the Z direction. The LLS has to be positioned in this range to provide a high-resolution image and to get the right X dimension. For this setup, the LLS was mounted at 80 mm which showed a laser line on the composite surface of 25 mm. The LLS has 2048 measurement points along the profile [56]. Accordingly, the resolution in the X direction is 12.2 μm.

$$\text{Resolution} = \frac{X_{length}}{N_{points}} = \frac{25\ mm}{2048} = 12.2\ \mu m$$

The resolution in the Z direction is given by the scanCONTROL datasheet by MicroEpsilon to be 1.5 μm [56]. These fine resolutions allow for the LLS to accurately capture the gap's dimensions. The full scan was made after completing the 0-degree layer. The gap was embedded in this layer and not yet covered by the 90-degree layers. The path of the robot that was programmed for making the scan was the same as the path for the fourth tow to the right side of the 0-degree layer. This tow can be seen in figure 3.7. This tow also forms the left edge of the gap along the entire length of the layup. Following this path ensured that during the complete scan, the gap would always be close to the centre, but slightly shifted to the right. Initially, the scan was taken at the same speed as the layup velocity, 40 mm/s. However, after inspecting the scan, it turned out that this did not produce a valuable scan. Therefore, the scan speed was halved to 20 mm/s. This produced a readable and interpretable scan of the entire gap. An example of a profile that can be produced by the LLS is displayed in figure 4.5.

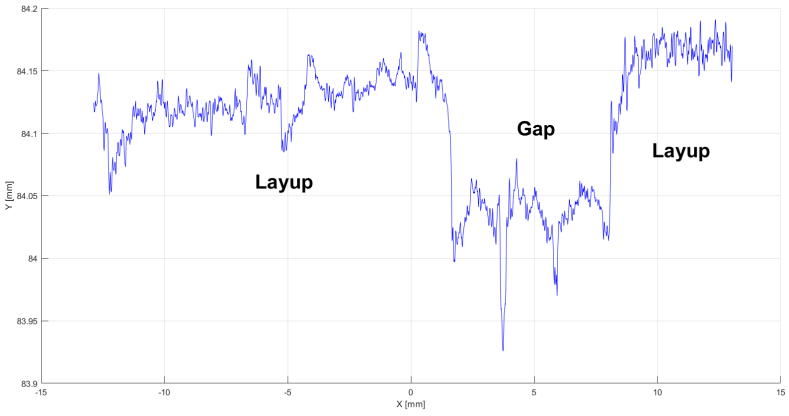

Figure 4.5: Laser Line Scanner exemplary profile

Figure 4.5 shows an example of a profile made by the LLS at a certain position along the laminate length. This is done by extracting a single frame from the complete scan. The LLS was first used to make one complete scan of the gap. Secondly, the programmed LLS path was altered such that it would stop at the exact locations of the intended gap sizes. Therefore, this path stopped at 50, 100, 150, and 200 mm. At these locations, the exact gap width was read from the corresponding software, which displayed the live data. This way, the gap widths in the real scenario could be compared to the designed gap widths.

4.1.2. Reference markers

To be able to track the positions where the desired gap sizes are located, a method had to be developed. This method consisted of placing reference markers exactly in between the gap locations on the already placed 0-degree layer. This was done with a silver permanent marker. For example, the indicator between the gaps designed to be at 50 mm and 100 mm was put at 75 mm. This meant that the reference markers would always be placed exactly 25 mm away from the gap. As these markers would not be covered by the 90-degree tows, they could function as reference points to track the intended gap locations after manufacturing. Additionally, to ensure that every gap location could be measured from two reference markers, an indicator was placed 25 mm below the first gap and above the last gap. The top edge of the 0-degree layer was taken as the origin for the dimensions of the reference markers, as this edge was consistently straight. The last gap was designed to be located 100 mm before the top edge of the 0-degree layer. Therefore, the first indicator was placed 75 mm before the top edge. Hereafter, the next reference markers were all placed 50 mm apart. This resulted in reference markers placed at 75, 125, 175, 225, 275, and 325 mm (from the top edge in figure 3.7), or as indicated below in figure 4.6.

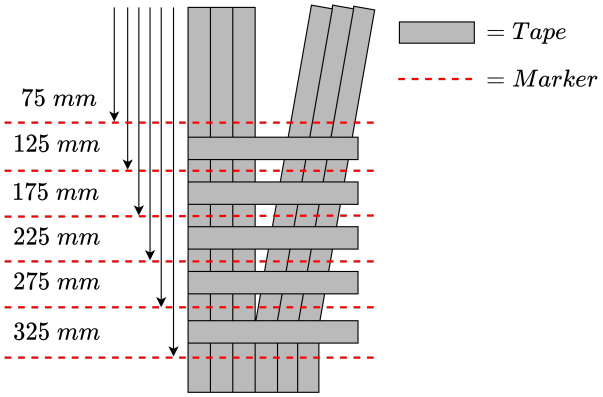

Figure 4.6: Reference marker visualisation

Lastly, one has to be aware of the thickness of the marker used to place the reference markers. The thickness of the tip was 0.7 mm, but when placed the indicator was 1 mm wide. This was taken into account by placing the markers such that the left edge always coincided with the desired measurement. Therefore, everything was measured from the left sides of the markers which ensured consistent and accurate measurements. With the reference markers correctly placed, the 90-degree layer could be placed. After placing the 90-degree layer, one could come back and place the reference markers on the gap locations on top of the 90-degree tows exactly 25 mm above or below the previously placed in-between reference markers. The markers should then be placed exactly at half the width of the 90-degree tows, ensuring that the exact locations of the planes of interest are visually indicated and documented.

With the locations for the reference markers in mind, all information necessary for the production of the laminate is known and can therefore be produced. Figure 4.7 shows the produced laminate.

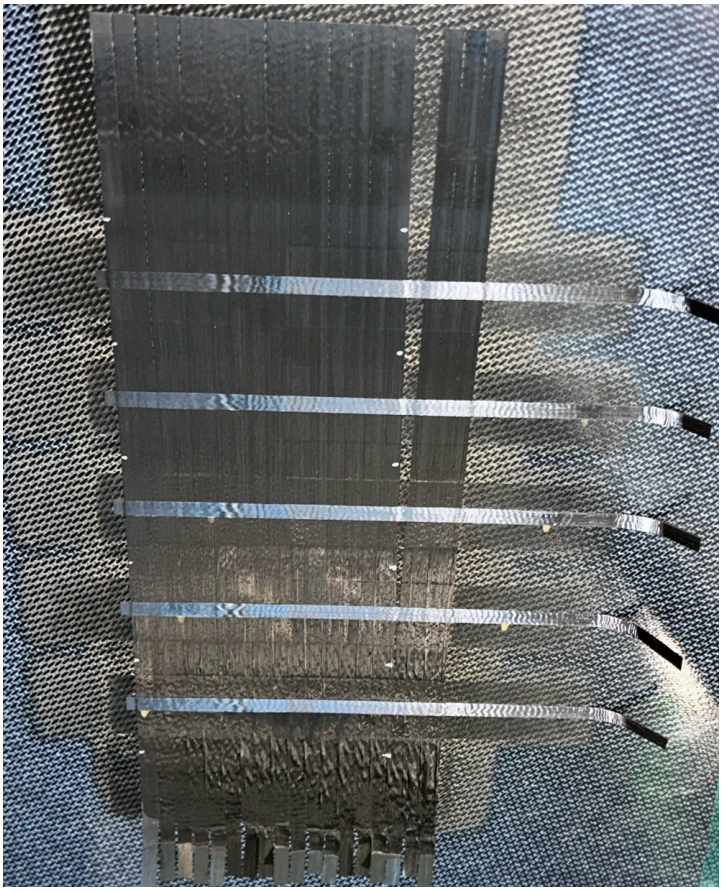

Figure 4.7: Produced laminate for Trial One

Path deviation

From the produced laminate, seen in figure 4.7, a suspicion arose that the 90-degree tows had shifted slightly. The path for the robotic manipulator for the 90-degree tows was programmed so that the midlines of the tows would exactly be placed at 0, 50, 100, 150, and 200 mm. However, after placing the 90-degree layer and using the markers previously made as references, it became clear that an error had occurred. All 90-degree tows were shifted up by exactly 1.175 mm. This was not a critical error as the error was still smaller than half a tow width (3.175 mm). Therefore, the plane of interest remained to be placed under a 90-degree tow. However, the error must be taken into account later to reach the desired plane of interest. This shift of the plane of interest can be seen in figure 4.8. Where the plane of interest is indicated by the red plane and the shift in its position by the dimensions on the left side. For demonstration purposes, the fourth gap was used at 200 mm.

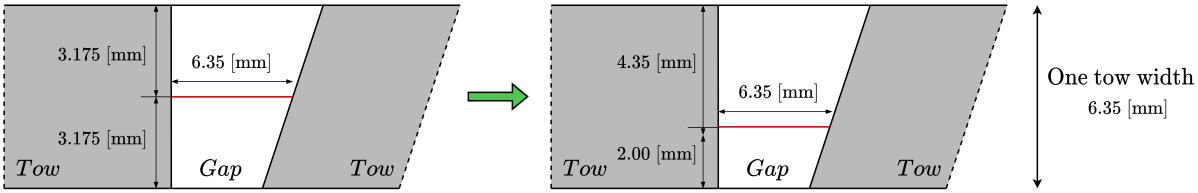

Figure 4.8: Shift in the plane of interest by 1.175 mm

Now that the path deviation is known, the production process for Trial One is complete and ready for post-processing.

4.2. Manufacturing Trial Two

4.2.1. Setup Trial Two

This section will be about manufacturing the layup designed for experiment two in section 3.2. It uses the same setup as mentioned for experiment one. However, slight additions have been made to allow more data to be collected. The first addition is an infrared (IR) camera to monitor the live temperature during the placement of the 90-degree tows. The second addition is a force torque sensor which was already briefly mentioned before.

The IR camera recorded a video but also monitored the temperature of every pixel at every frame. In the corresponding software, areas of interest could be indicated, which would then output a mean temperature over this marked area over the complete duration of the video. For the purpose of this research, two areas were marked. One area on the hottest part of the tape, and one area at the hottest part of the substrate just below the Humm3 crystal. Mean temperature values from the selected areas were plotted across the video duration to illustrate the thermal profile of the tape and substrate throughout the process. Figure 4.9 shows an example of a frame recorded by the IR camera. This particular frame was extracted from a IR video made for the third 90-degree tow

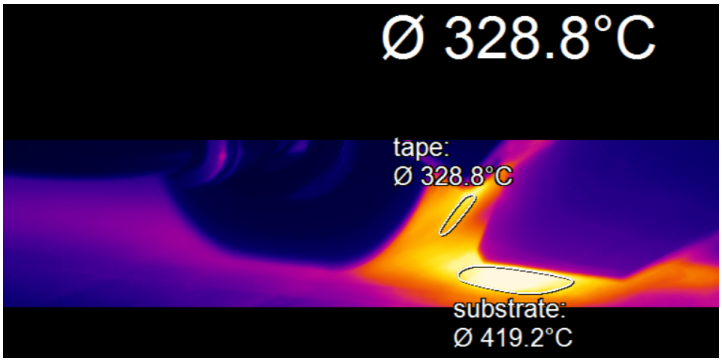

Figure 4.9: Frame of IR video of tow 3

The software then records the mean temperatures of these areas over the whole length of the video, and for the third tow such a profile looks like figure 4.10:

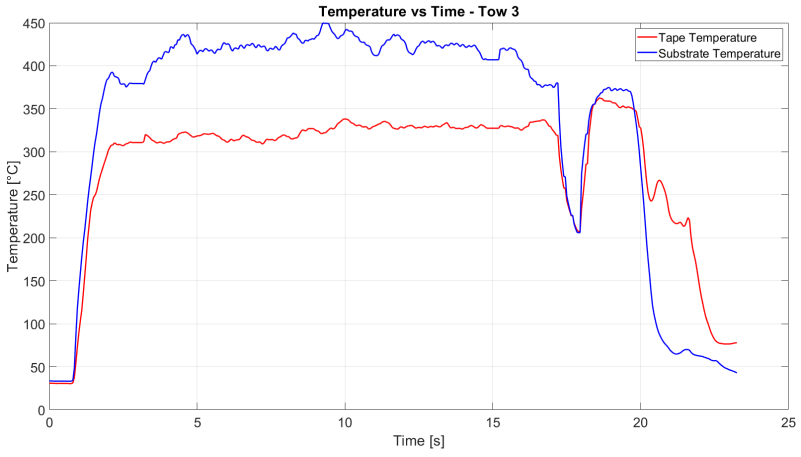

Figure 4.10: Temperature profile for the tape and substrate of tow 3 during placement

The FTS records the forces and torques in all three directions many times a second. The particular FTS used for this setup was set to a measuring frequency of 2333 Hz. This meant that the sensor

measured the forces and torques 2333 times per second. This resulted in large raw data files that had to be converted to useful information about the force used during the layup of the 90-degree tows.

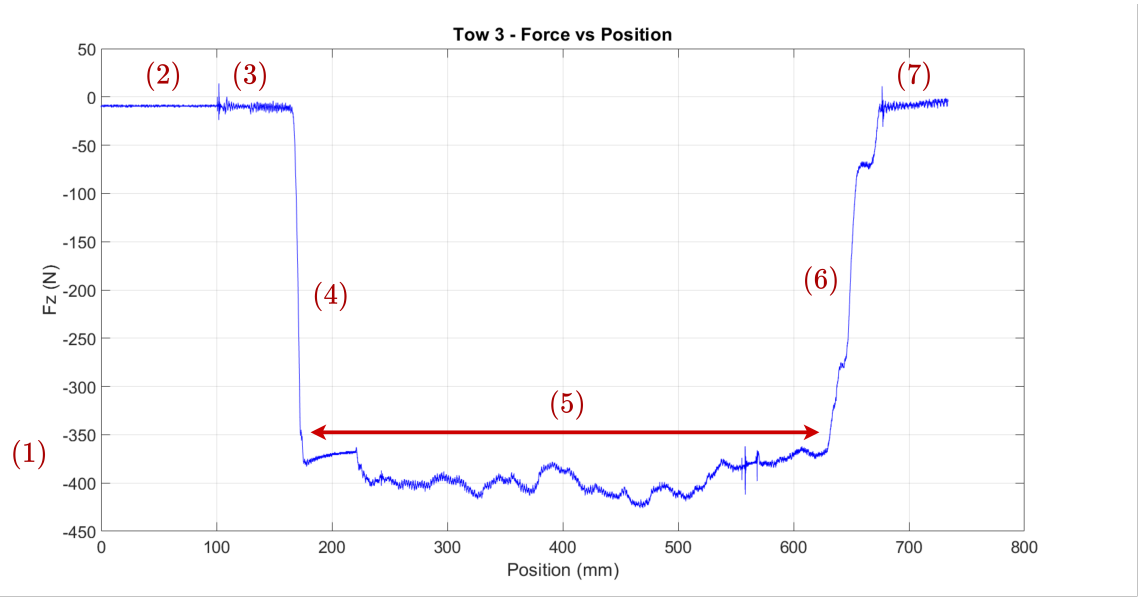

Figure 4.11: Vertical force component of robot during the placement of the third 90-degree tow

Figure 4.11 illustrates an example of what the FTS data looks like for the placement of a tow. Firstly, as indicated by point (1), the vertical force component is plotted as a negative force. This is because the tool pushes back on the roller in the opposite direction of how the robot arm pushes the roller into the tool, thus resulting in a negative vertical force component.
Secondly, as indicated by point (2), at the start the vertical force is not exactly zero but is quite low. This is due to the fact that at this point the roller is still suspended in the air and has not been placed upon the tool yet. The slight force component that is still seen in the figure occurs most likely because of the gravitational force acting upon the system.
Additionally, point (3) indicates that as the roller nears contact with the tool, more noise is introduced into the previously flat vertical force signal. This noise occurs because the roller is not yet in contact while the system is already moving toward the tool. This causes the robotic arm's cables to shift, thus creating slight vertical force fluctuations in the system
When the roller is pressed on the substrate one can clearly see the force increase, indicated by the steep force increase at point (4).
Furthermore, the development of the vertical force along the length of placement can be seen in the figure annotated by point (5). From which, in the analysis, the mean of this force range can be taken to get a clearer idea of what the general average force was.
At the end, one can again observe the same behaviour that was perceived before the roller touched the laminate. Hence, point (6) annotates the same behaviour as point (4), similarly point (7) annotates the same behaviour as point (3)

Furthermore, the same setup for the LLS scanner was used as for experiment one. However, a slight improvement was achieved in the ability to accurately match the location and size to the corresponding frames in the LLS data. This was done by placing physical landmarks on the laminate after placing the 0-degree layer with the embedded gaps before the scan was made. The landmarks were placed at the positions where the 6th, 12th, and 18th tow were to be placed. These are indicated by the three red squares in figure 4.12. These landmarks consisted of a thin slice of plastic positioned at the right location with masking tape which was barely sticky to reduce the chance of leaving a residue behind on the laminate. A zoomed-in view of this can be seen in figure 4.12.

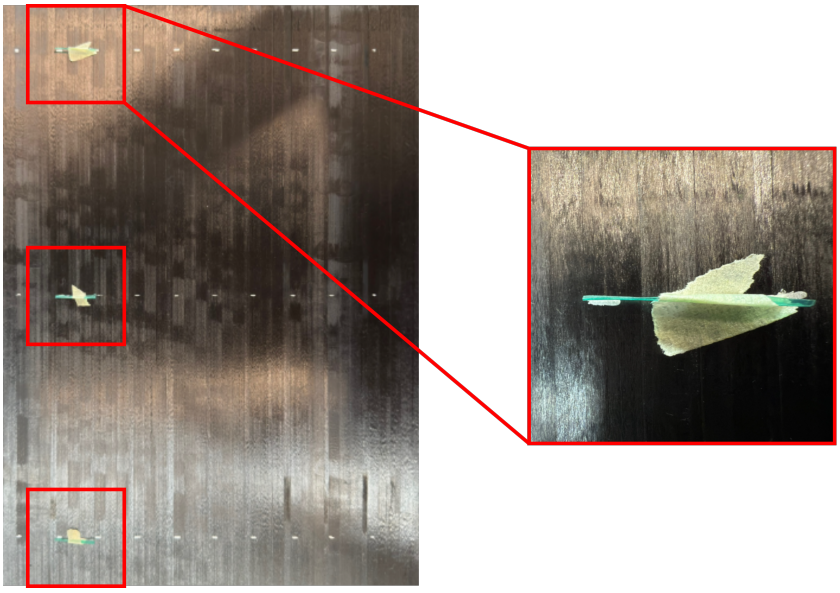

Figure 4.12: Landmarks placed on 0-degree layer, with zoomed in view

Spacing these landmarks equally and assuming a constant moving speed of the LLS of 20 mm/s one can accurately determine the location of all the gaps along the length of the laminate, and therefore also their corresponding sizes. This reduced the need for stopping the scanner at all 18 gap locations along nine gap lengths. Therefore, streamlining the process while also making it more accurate.

4.2.2. Settings used for Trial Two

Settings used for the 0-degree layer

The purpose of the 0-degree layer was to have embedded gaps and not to observe a change in behaviour due to a change in parameter values. Therefore, this whole layer was placed with constant process parameter settings:

Table 4.2: Settings used during production of the 0-degree layer

Parameter	Value	units
General settings		
Velocity	40	mm/s
Air pressure	0.26	MPa
Humm3 settings		
Frequency	60	Hz
Pulse widths	3	ms
Voltage	180	V

From previous testing, it is known that an air pressure of 0.26 MPa is equivalent to 25 kg of exerted force on the substrate. These settings resulted in a well-consolidated first layer and provided a suitable base for the subsequent 90-degree layer.

Settings used for the second layer

Although most settings for the second layer have already been discussed in the chapter about the design of experiment two 3.2. The Humm3 settings to reach the constant nip-point temperature while changing the velocity and force have not yet been touched upon. As already mentioned, to be able to change the velocity and force and still consolidate and not burn the material, some tweaking of the Humm3 settings to keep a constant nip-point temperature of around 350 C° was required. This temperature was chosen as the material performs well with this temperature and lies within its optimal

processing temperature range. The Humm3 setting that plays the largest role in determining the nip-point temperature is the applied voltage. Increasing the voltage, while keeping the velocity constant, also increases the temperature. Therefore, the velocity was set to a value later to be used for the placement of a 90-degree tow, and the voltage was varied until a temperature was reached that resulted in good consolidation. After some testing, the following voltages were found to reliably reach this temperature:

Table 4.3: Velocities and corresponding voltage inputs

Velocity	Voltage	Temperature
40 mm/s	175 V	352 $C°$
30 mm/s	167 V	352 $C°$
20 mm/s	159 V	350 $C°$

Produced Laminate for Trial Two

The section above finalises all the settings necessary for the production of Trial Two. With these settings as input for the process, the final laminate could be produced. The produced laminate for Trial Two can be seen in figure 4.13.

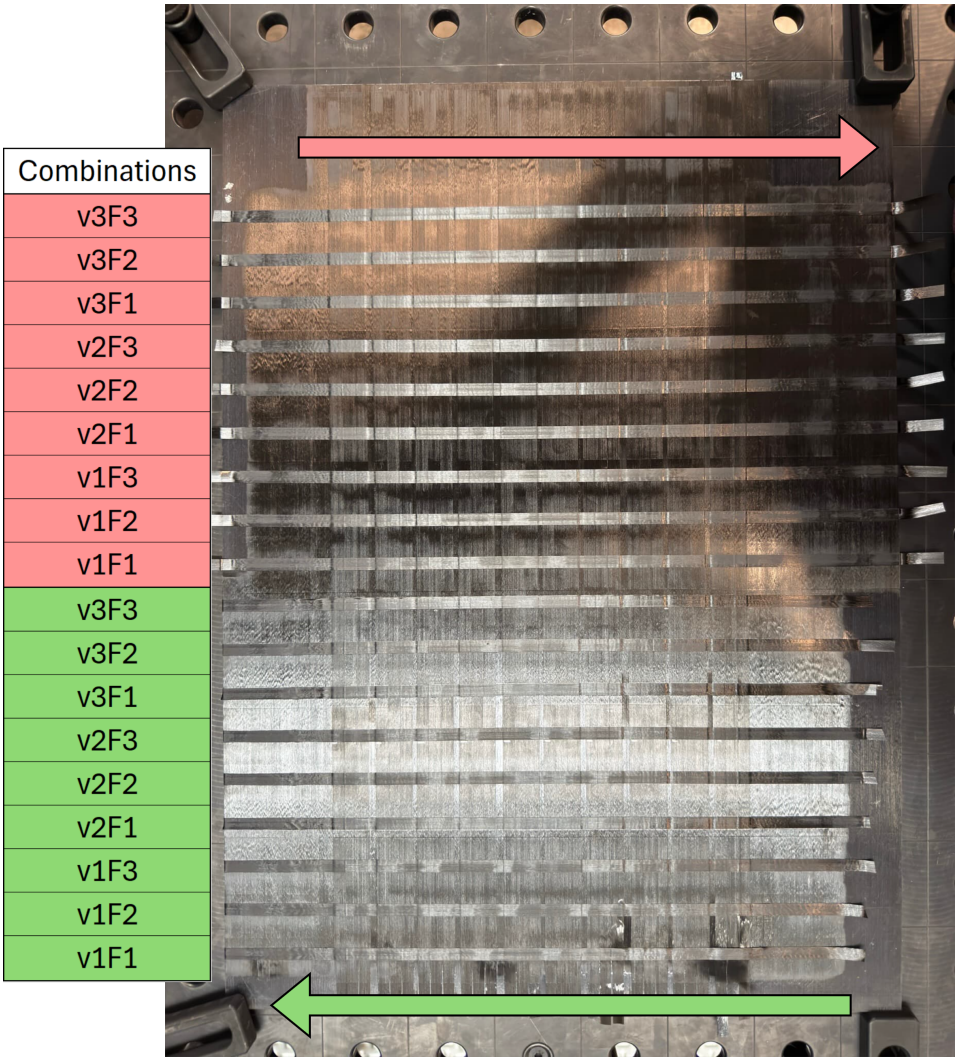

Figure 4.13: Produced laminate after implementing all changes with respect to the initial design

In figure 4.13 at the bottom right side one can see slight burning compared to the bottom left side. The

0-degree layer was placed from right to left. A setting from the robot that had to be tweaked was the initial velocity for the first 10 mm after reaching contact with the substrate. At the first few tows, this velocity was too low resulting in slight burning. However, after a few tows this velocity was tweaked and the material did not burn, as can be seen in figure 4.13.

From this laminate, the 15 samples (5 combinations repeated 3 times) could then be extracted in the post-processing of the experiment, which will be discussed in the next chapter. This concludes the manufacturing of both experiments.

4.3. Post processing of Trials

After concluding the production of experiment one, the next step could begin. To be able to produce the desired 2D micrographs later, the manufactured layup needed post-processing. This post-processing included cutting out the areas of interest. These areas of interest, which were shown in figure 3.7, share their bottom edge with the desired gaps. Extracting these areas of interest included cutting the composite laminate, grinding, and polishing to be able to create high-quality 2D micrographs.

Cutting

Cutting composite laminates suffers from several challenges. The thicknesses of the substrates were 1.5 mm and 4 mm, which is thin enough for multiple cutting methods. However, many cutting methods such as laser cutting or regular saw cutting suffer from an extensive generation of heat. The generation of heat could cause the morphology of the gaps to change. Therefore, this had to be avoided. An alternative was the compcut ACS 600. ACS is an abbreviation for advanced composite blade saw. The main advantage of this cutting machine is that the blade is watercooled which avoids heating the laminate. The working area of the cutting machine is 600x600 mm which could just fit the substrate which was 520x520 mm. The main advantage of this machine is coincidentally its disadvantage. The watercooled blade operates by continuously depositing a stream of water onto the blade. This inherently means that the composite laminate is also exposed to water. This can result in water being trapped inside delaminations and voids. This is especially relevant to keep in mind as this work will investigate the shape of voids. Therefore, the micrographs could show signs of water entrapment. The influence of moisture on this work is not crucial but Legenstein et al. [28] showed that moisture in a laminate can have a significant effect on the bonding strength. After cutting, only the areas of interest were left. These could then be prepared for the grinding and polishing process.

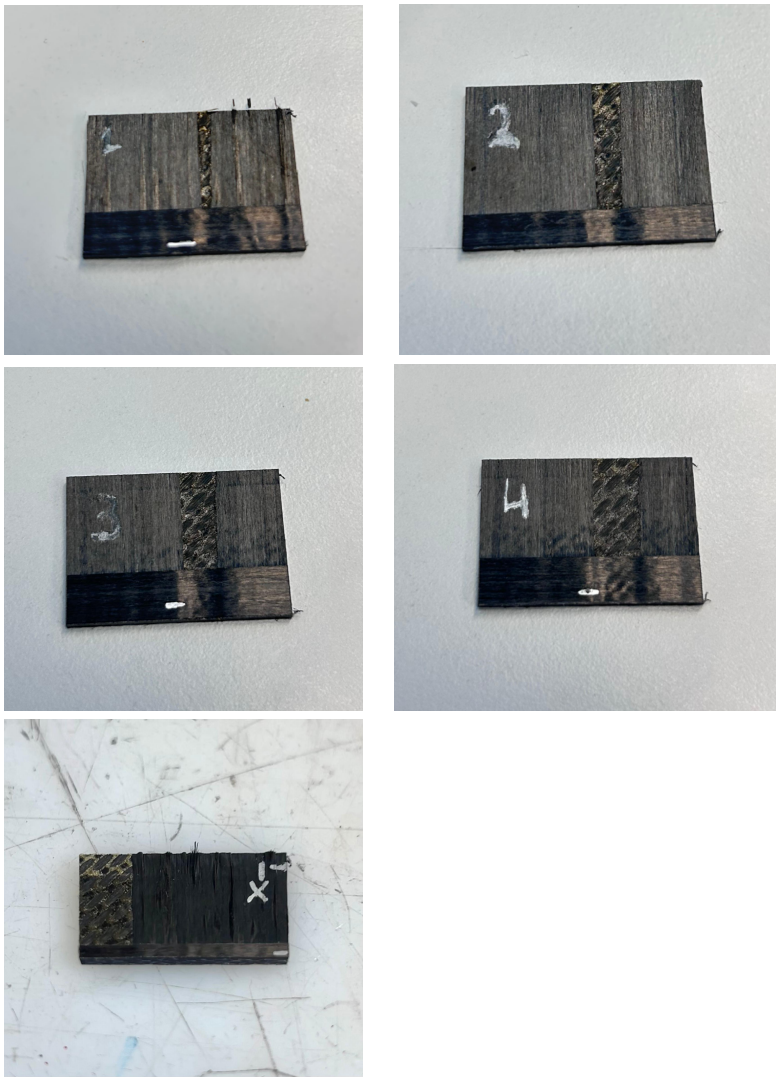

Figure 4.14: Samples one through four and the ply drop sample, produced by cutting the composite laminate

Figure 4.14 shows the samples from one through four and the 0 mm gap including the ply drop. One can quite clearly see the increasing gap size throughout the pictures. Furthermore, the silver horizontal indicator can be seen on samples one, three, four, and the ply drop sample. These are the indicators that were left from the manufacturing process. The distance from the indicator to the edge of the sample should be 1.8 mm. This information was obtained by firstly grinding and polishing the ply drop sample. For this sample, it did not matter how much material was removed by grinding and polishing as long as the complete 90-degree tow was not removed, as the gap size remains 0 mm below the whole 90-degree tow. Measuring the removed material at every step during the grinding and polishing process resulted in a total removal of 1.8 mm. Therefore, this distance was added to the length at the bottom of the sample. After the complete polishing process of the samples, one should then reach the planes of interest. However, one can see in figure 4.14 that sample 2 does not show a silver indicator. This is the cause of the cutting error where the additional 1.8 mm was not added. Hence, the bottom side of sample 2 is already coincident with the plane of interest. However, the sample still needs to be ground and polished. Therefore, the plane of interest will be slightly overshot which will need to be accounted for. Furthermore, the other samples might also show slight deviations concerning the added material for the polishing losses, as it turned out to be a challenge to get it exactly right. These deviations will not cause problems but will need to be taken into account when analysing them.

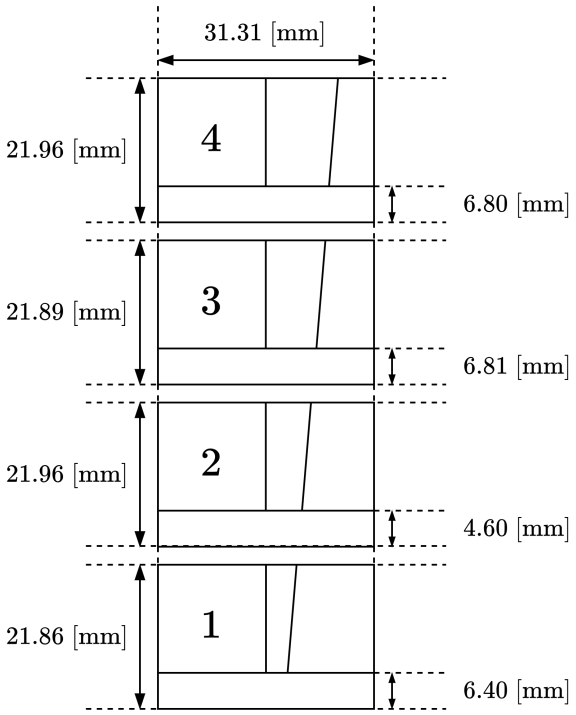

Figure 4.15: Schematic of the sample's dimensions after the cutting process.

Figure 4.15 shows a schematic of the resulting dimensions of the first four samples. The ply drop sample is excluded as its dimensions had little relevance as aforementioned. The widths of the samples are equal and had to be smaller than 40 mm for the next post-processing step. The heights of the samples do differ but do not influence the process. The heights had to be around 20 mm for the next post-processing step. Therefore, the widths and the heights are conforming for the next step.

For the second trial these post processing steps remained largely the same compared to the processes mentioned for the first trial. A slight adjustment was made to the cutting process, firstly, the same cutting machine was used as for experiment one. However, this machine was only used to cut the laminate into small enough pieces to later be cut by a different machine, which could manually be adjusted much more accurately and had a much thinner cutting blade. This resulted in more accurate cuts and therefore better samples. The cutting machine in question is the Secotom 60 by Struers [57].

Figure 4.16: Example of a sample from the laminate from experiment two

Figure 4.16 shows a single sample cut from the laminate shown in 4.13. The other samples are not shown, but all look similar to this example. Furthermore, during the post-processing of the first trial,

it was important to keep track of the material lost during the polishing steps, as this would result in a different gap size that was seen in the micrographs. This experiment incorporated gaps of constant widths; therefore, it did not matter much, as the gap should be the same size regardless of the polishing loss. Minor deviations can occur due to slight geometry or process variations, but these variations are not expected to be large.

Resin moulds

The extracted samples could then be mounted in cups to embed them in epoxy. This was a necessary step to be able to provide a good surface finish to the samples. The exact steps taken during this part of the post-processing can be found in Appendix A.1.

Surface finishing

Accurate micrographs require thorough surface preparation to ensure high-quality results. Out of the mould, the surface to be analysed is still rough. Furthermore, a release agent put in the moulds also left streaky marks on the surface of interest. Therefore, these samples require proper surface finishing. To obtain the desired surface finish, the samples were put through a thermoplastic-specific grinding and polishing process. The equipment used for this operation is the Tegramin-20 by Struers [58]. This equipment is manufactured by the same company that makes the moulds and the vacuum chamber. That is why the surface finishing machine has cutouts that match the dimensions of the moulds to hold the moulds during the process. These cutouts can be observed in figure 4.17.

Figure 4.17: Tegramin-20 surface finishing machine by Struers [58]

During the process, both the sample holder and the plate below rotate to ensure optimal surface finishing. Firstly, the moulds had to be ground after which they could be polished. The exact surface finishing steps can be found in the appendix chapter A.3.
The last steps used specific diamond suspensions to further polish the surface. After completing each step, the holder and the samples were cleaned properly to ensure minimal cross-contamination between steps and therefore minimal scratches in the final polished sample. One can get an idea of the resulting surface finish from figure 4.18.

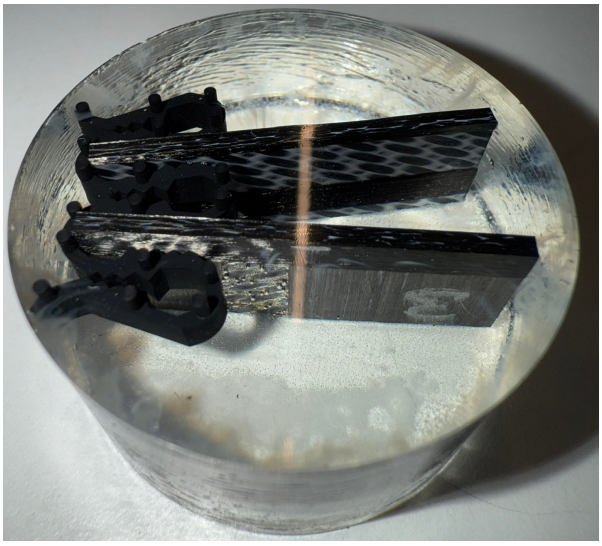

Figure 4.18: Resulting surface finish

Polishing losses for Trial One

Finally, as mentioned before, the 0 mm gap sample was first put through this process and had a polishing loss of 1.8 mm. This loss was taken into account for the cutting process of the following samples. However, the losses for these samples were also measured to precisely log the exact location of the final surface reached with respect to the layup. Samples one and two were placed in the same mould, and the same holds for samples three and four. The polishing losses for these two moulds were as follows:

- Polishing loss samples one and two: 1.68 mm
- Polishing loss samples three and four: 1.58 mm

This concludes the post-processing steps taken for both experiments in which samples were cut from the laminate, then moulded and polished. This ensured that the samples were optimally prepared for taking high-quality micrographs that are shown in the analyses steps in the next section.

5

Sample Analyses

5.1. Sample analysis Trial One

5.1.1. Polishing correction

To start the analysis, the exact location of the plane that was reached after polishing must first be determined with respect to the layup. This allows for the gap later determined by the micrographs to be compared to the gap sizes measured by the LLS and analytically determined gap sizes at the same locations. To do this, the polishing losses must be applied to the sample heights seen in figure 4.15 and compared to the locations of the plane of interest indicators spotted in figure 4.14. For sample one, considering the location of the indicator and the polishing loss, the reached plane is located as follows:

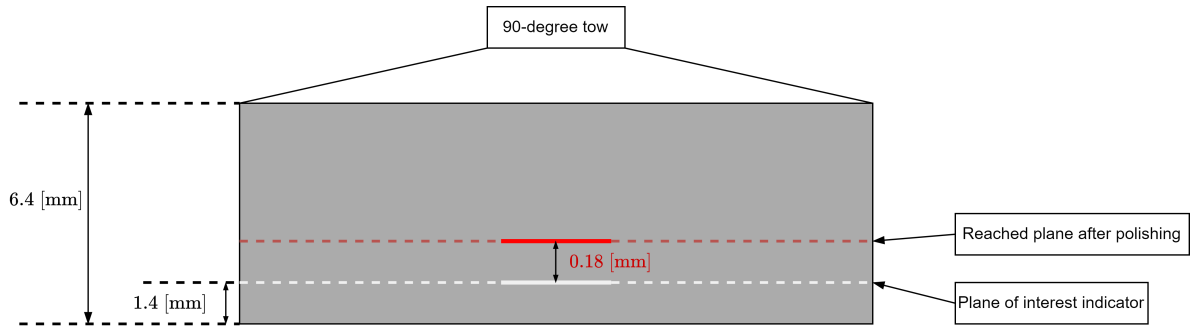

Figure 5.1: The reached plane relative to the reference marker for sample one

Applying the same methodology to the remaining samples, their positions relative to the plane of interest indicator could be determined. Resulting in the following relative positions for all samples:

- sample 1: -0.18 mm
- sample 2: -1.98 mm
- sample 3: +0.13 mm
- sample 4: +0.12 mm

From these values, one can again identify that during the cutting process, a manufacturing error occurred during the cutting of sample 2, where the polishing loss of 1.8 mm was not applied correctly. The other deviations are relatively small and do not exert a large gap size change compared to the intended gap sizes.
These relative positions can be converted to the gap locations in the complete layup by subtracting them from the original intended locations:

$$\text{Old gap locations in } mm = [50, 100, 150, 200]$$

$$\text{New gap locations in } mm = [50 - -0.18; 100 - -1.98; 150 - +0.13; 200 - +0.12]$$

$$\text{New gap locations in } mm = [50.18; 101.98; 149.87; 199.88] \tag{5.1}$$

Now using again equation 3.4 can be used to analytically determine the gap sizes at the new locations after polishing:

$$\begin{bmatrix} w_4 \\ w_3 \\ w_2 \\ w_1 \end{bmatrix}_{\text{after polishing}} = \begin{bmatrix} 199.88 \\ 149.87 \\ 101.98 \\ 50.18 \end{bmatrix} * \tan(\alpha) = \begin{bmatrix} 6.346 \\ 4.758 \\ 3.238 \\ 1.593 \end{bmatrix} mm \tag{5.2}$$

To better understand the comparison between the intended locations and respective sizes, they can both be plotted next to each other. This visualisation can be seen in figure 5.2.

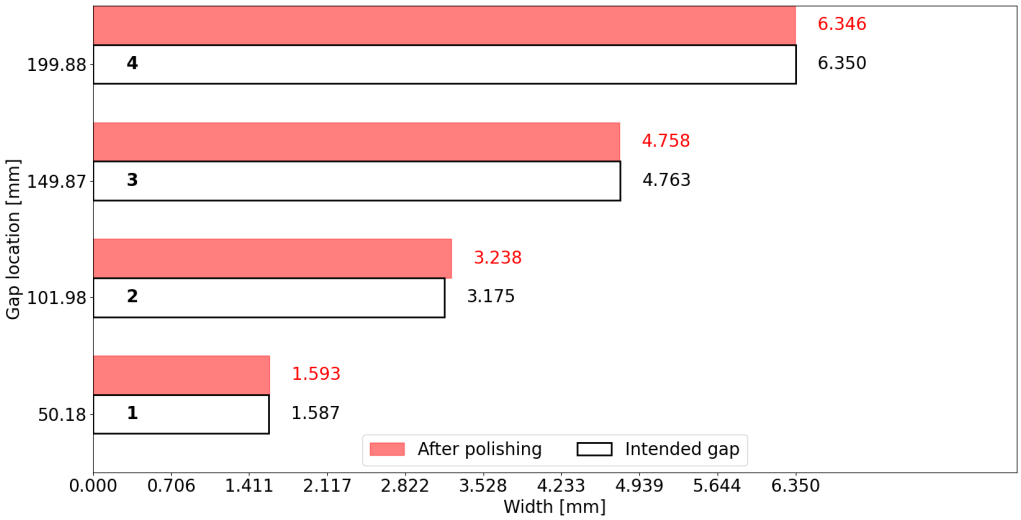

Figure 5.2: Analytical gap sizes and locations before and after polishing

5.1.2. LLS gap sizes

Section 4.1.1 already explained the use and the working principle of the LLS. After placing the 0-degree layer it was positioned at the intended gap locations of [50, 100, 150, 200] mm along the length of the layup. At these positions, it measured the gaps, and the corresponding frames could be backtracked. The gaps were determined by measuring the width of the gap from the absolute edges of the 0-degree layer. The method is shown in figure 5.3. This method was chosen as spotting the same locations in the micrographs later would be straightforward, providing a good comparison between the two methods. The lower schematic in figure 5.3 is a visual aid and does not represent the actual proportions of the compressed 0-degree layer.

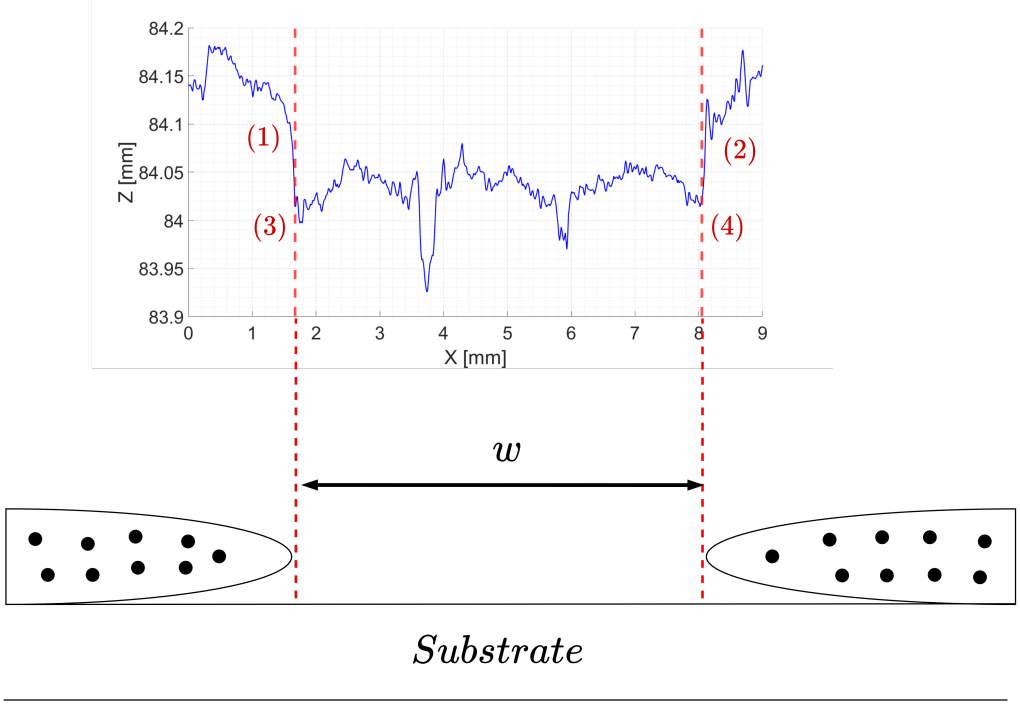

Figure 5.3: LLS width methodology

The lower schematic in figure 5.3 illustrates that the gap width is measured from the absolute edges of the 0-degree tows. This approach is supported by the real LLS scan shown above the schematic in figure 5.3, which depicts a sloped region near the tow edges at points (1) and (2). This slope results from increased compression at the tow boundaries and does not yet indicate the start of the actual gap. Therefore, in the LLS scans, the gap width was measured from the point where the surface profile exhibits a clear directional change beyond this initial sloped region, indicated by points (3) and (4).

The measured widths following this methodology are the following:

$$\begin{bmatrix} w_4 \\ w_3 \\ w_2 \\ w_1 \end{bmatrix}_{\text{LLS}} = \begin{bmatrix} 6.377 \\ 4.731 \\ 3.386 \\ 1.455 \end{bmatrix} mm, \text{ corresponding to: } \begin{bmatrix} 3121 \\ 2636 \\ 2258 \\ 1709 \end{bmatrix} \text{ Frame Numbers} \tag{5.3}$$

However, these dimensions were measured at the exact intended locations for the gaps but these locations differ from the real locations as the polishing losses were not yet known. Therefore, to properly compare gap sizes between the analytical approach, the LLS, and later the micrographs, one should correct for these losses. To correct for this in the LLS profile that was made for the entire length of the layup, the assumption is made that between every data point, the distance is the same such that the speed is constant. With this assumption, the distance per frame could be computed. The scan speed was 20 mm/s and the exposure time was 5 ms. This dictates that every frame is $20 * 0.005 = 0.1\ mm$. This could then be taken into account to adjust the frames for the polishing losses as the following:

$$\begin{bmatrix} +0.12 \\ +0.13 \\ -1.98 \\ -0.18 \end{bmatrix} mm = \begin{bmatrix} +1 \\ +1 \\ -20 \\ -2 \end{bmatrix} \text{ Frame Numbers, New Frames: } \begin{bmatrix} 3121 - +1 \\ 2636 - +1 \\ 2258 - -20 \\ 1709 - -2 \end{bmatrix} = \begin{bmatrix} 3120 \\ 2635 \\ 2278 \\ 1711 \end{bmatrix} \text{ Frame Numbers} \tag{5.4}$$

Finally, the frame shifts and the methodology shown in figure 5.3 could be taken into account. The LLS recorded gap sizes including polishing losses were determined and are displayed below.

$$\begin{bmatrix} w_4 \\ w_3 \\ w_2 \\ w_1 \end{bmatrix}_{\text{LLS incl. polishing loss}} = \begin{bmatrix} 6.376 \\ 4.755 \\ 3.244 \\ 1.433 \end{bmatrix} mm, \text{ corresponding to: } \begin{bmatrix} 3120 \\ 2635 \\ 2278 \\ 1711 \end{bmatrix} \text{ Frame Numbers} \tag{5.5}$$

5.1.3. Micrograph gap sizes

With polishing completed the samples were ready to be analysed with a microscope. The microscope used for making the micrographs is the Keyence VR 5000 digital microscope [59]. The micrographs were taken at 40-times zoom at a resolution of 2048x1536. Six micrographs were made, one of the ply drop, and then five ranging from a 0 mm gap to around a 6.35 mm gap.

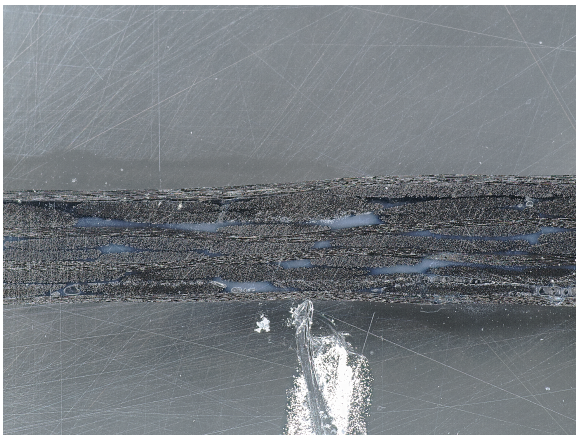

(a) Ply drop sample

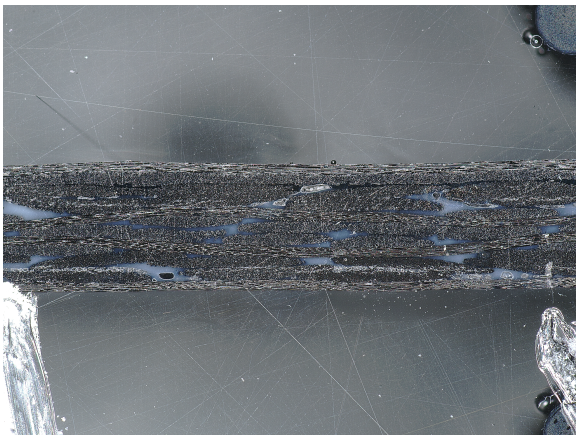

(b) 0 mm gap sample

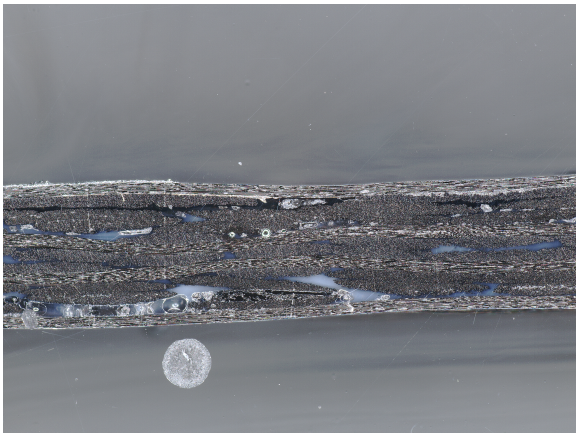

(c) Sample 1

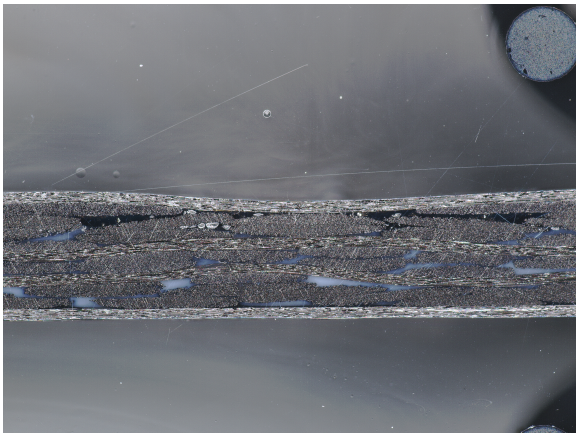

(d) Sample 2

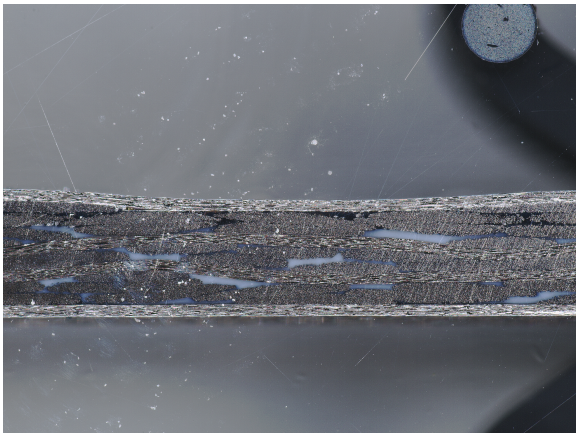

(e) Sample 3

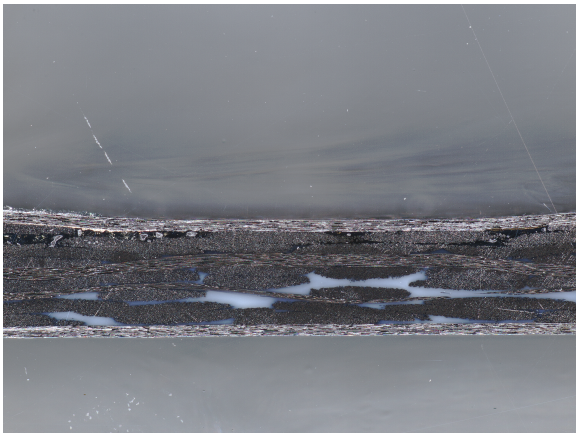

(f) Sample 4

Figure 5.4: Micrographs of all samples

The micrographs in figure 5.4 could then be further analysed. The micrographs are quite convoluted as the substrate turned out to be more irregular than previously thought. Therefore, an overlay is made to better illustrate the boundaries between the 90-degree layer, the 0-degree layer, and the substrate. This overlay can be observed in figure 5.5.

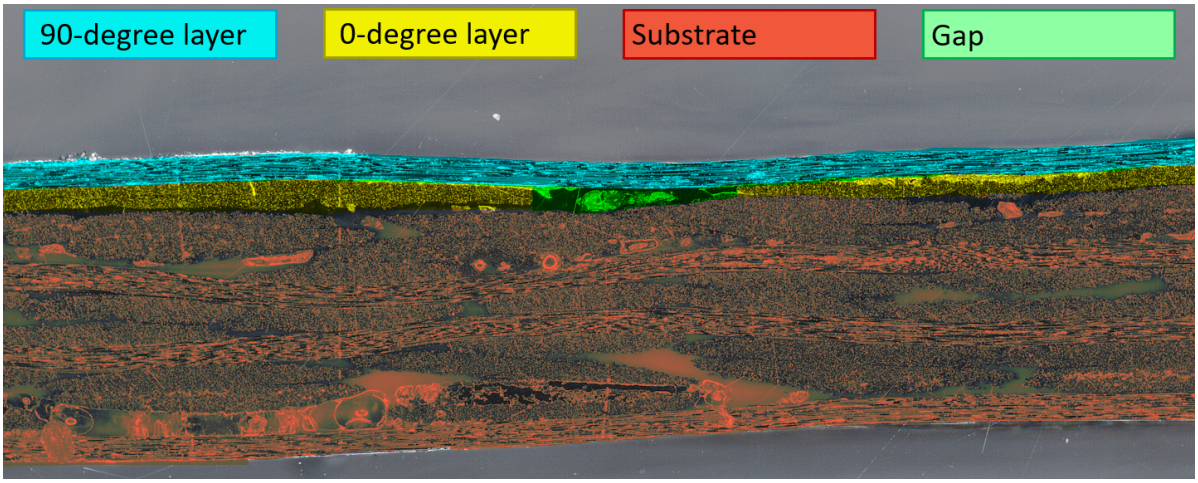

Figure 5.5: Layers and substrate distinction overview example using sample 1

Similarly, the layer distinction could be done for the 0 mm sample. However, this sample presented quite a challenge with regard to the distinction between the 0-degree tows. This result makes sense as hence a truly 0 mm gap was achieved, but it simultaneously meant that it was difficult to draw conclusions from this. The conclusion that can be drawn from this is that when placed with the right spacing, the tow compaction ensures good consolidation of the sides of the tape. This effect can be seen in figure 5.6.

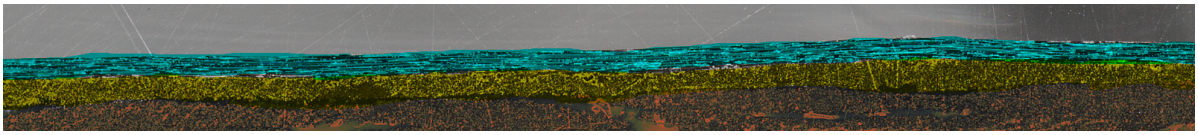

Figure 5.6: Layer distinction 0 mm sample

As the distinction between the edges of the tows was not able to be made, no further data could be extracted from this. Therefore, this sample will be excluded from the following analysis steps.

Additionally, after the manufacturing process, it was decided to include the ply drop sample, as it did not require additional steps but could provide additional valuable data. Figure 5.4 shows the micrograph for the ply drop sample, but this work will not further investigate this. Hence, the focus will be on the different sizes of gaps for this work.

Using the same methodology illustrated in figure 5.3, the micrographs in figure 5.4 could be used to determine the gap widths after placing the 90-degree layer on top of it. Figure 5.7 shows this approach applied to the micrograph of sample 1.

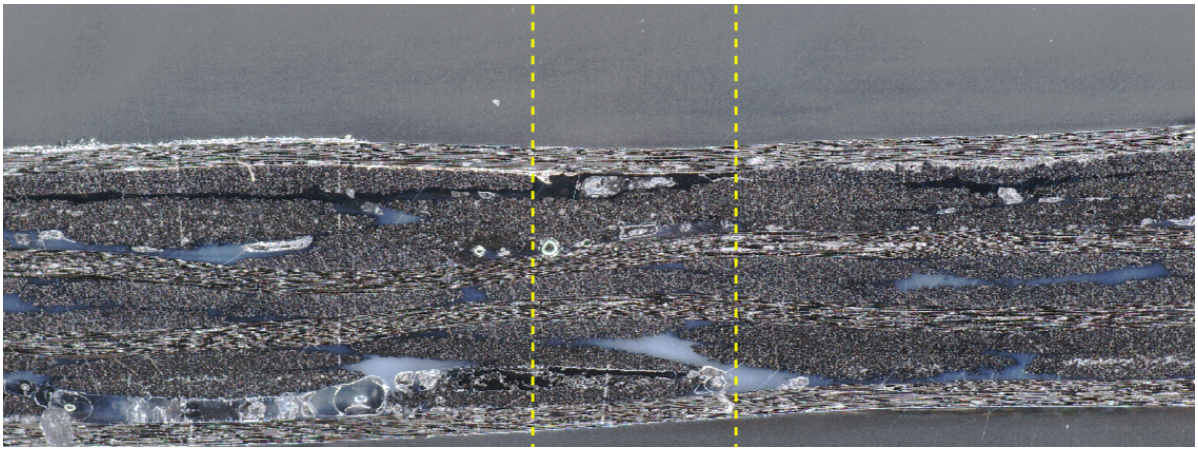

Figure 5.7: Micrograph gap width for sample 1

This was done for every micrograph and the obtained widths for all samples can be seen below:

$$\begin{bmatrix} w_4 \\ w_3 \\ w_2 \\ w_1 \end{bmatrix}_{\text{micro}} = \begin{bmatrix} 6.266 \\ 4.625 \\ 3.101 \\ 1.297 \end{bmatrix} mm \tag{5.6}$$

With the gap widths of the micrographs, comparisons can be made between the LLS gap widths (5.5), the micrograph gap widths (5.6), and the intended gap widths (5.2). The differences between the intended gap width and the gap widths measured by the micrographs and the LLS data were best summarised in a bar chart. This can be seen in figure 5.8.

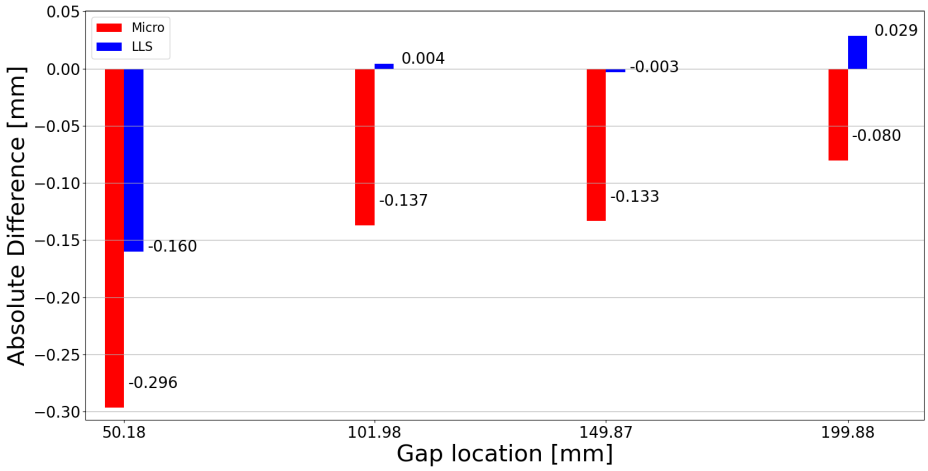

Figure 5.8: Absolute Difference between Intended and Measured Widths

Figure 5.8 allows for further investigation of the behaviour of the gaps. Firstly, it can be seen that the microscope width is consistently smaller than the intended gap width. Furthermore, both the LLS gap width and the microscope widths are considerably smaller than the intended gap width at the first gap position compared to the other positions.
That the microscope gap widths are consistently smaller than the intended gap widths makes sense. It makes sense as the intended embedded gap in the 0-degree layer was designed to be a perfect triangle. However, the micrographs are made from the finished layup. This includes the 90-degree

layer. This meant that the gaps were reheated and re-compacted when the 90-degree layer was being placed, resulting in even more tow-width expansion. This expansion meant that the gap decreased in size. Therefore, placing the 90-degree layer resulted in a gap width decrease which can be seen in figure 5.8. Furthermore, considering the same reasoning it makes sense that the difference of the intended gap widths compared to the gap widths measured with the LLS is much less.

The gap widths from the LLS were obtained after only placing the 0-degree layer. Therefore, it was already expected to show less of a difference with the intended gap widths than the widths from the micrographs. Although it was not expected for the LLS widths to be so close to the intended gap widths, as can be seen in figure 5.8. Moreover, the LLS gap widths also show positive differences at the second and fourth gap locations. This means that at those locations, the gaps by the LLS are larger than the intended gaps. Nevertheless, the differences are sufficiently small to attribute this to either process variations or geometric variations of the tape.
Additionally, as mentioned before, at the first gap location both the LLS gap width and the micrograph gap width are considerably smaller than the intended gap width. This is most likely due to how the layup path was computed. To be able to manufacture the embedded gap, the third tow on the right in figure 3.7 had to undergo tow steering. This steered path was obtained by following two straight paths connected by a region that allowed the robot to make the turn. This region had a height of 10 mm. In this distance, the robot had to rotate to the desired angle computed in figure 3.5. Nevertheless, 10 mm is still sufficiently far away from the first gap to not influence the gap width. However, this statement only holds if the tow is completely steered in the 10 mm. However, the suspicion is that the tow resisted this steering significantly more than expected. Therefore, even though the programmed path was straight again after 10 mm, the tow was most likely not steered to this straight part yet and had shifted on the surface of the roller. The suspected tow shift on the roller due to the steered path is believed to be the cause of the considerably smaller gap widths measured by the LLS and the micrograph for the first gap compared to the intended gap width.

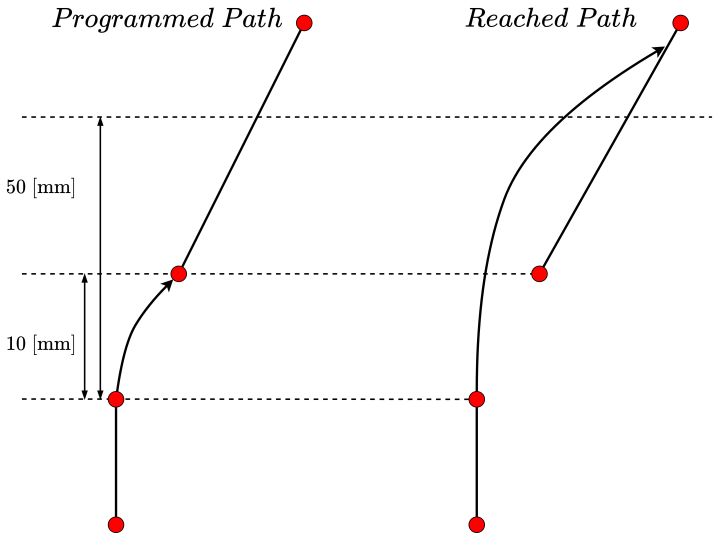

Figure 5.9: Programmed vs hypothesised obtained steered path of the tow

The deviation from the programmed path can be observed in figure 5.9. This figure shows why at the first gap location at 50 mm the gap is suspected to be smaller than was intended, as the right edge of the gap has moved inwards.

5.1.4. Comparison between LLS and micrograph gap widths

As previously explained, it made sense that the gap widths measured from the micrographs were consistently smaller than those of the LLS as they experienced the processing heat and pressure once more than the gaps from the LLS scan. This effect became clear in figure 5.8. However, this chart shows the absolute difference to the intended gap sizes. The relative difference between the two dif-

ferent measuring methods has not yet been shown. Figure 5.10 shows the difference in gap widths between the two measuring methods.

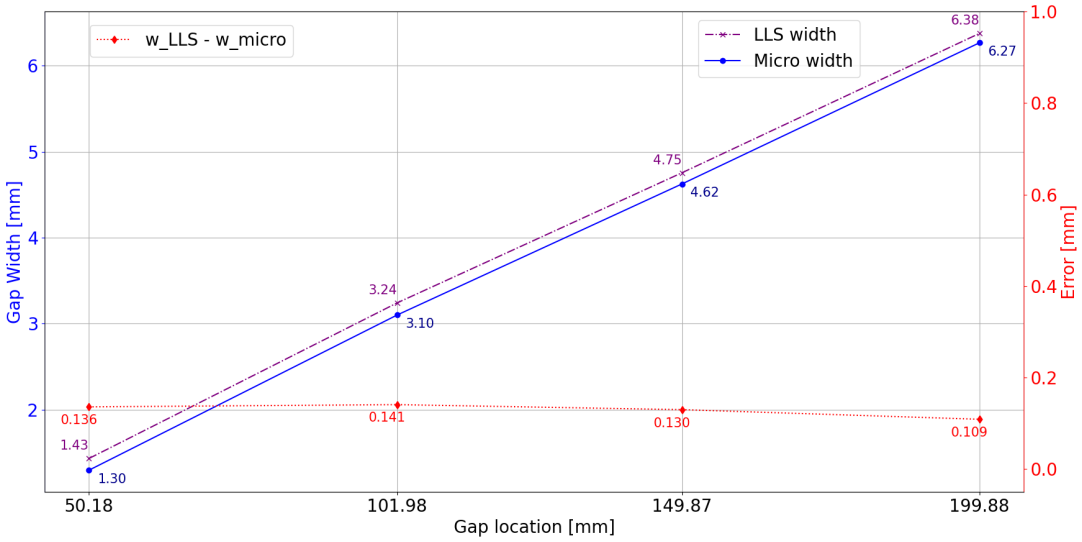

Figure 5.10: Difference in gap width between the micrographs and the LLS scan

Figure 5.10 again clearly illustrates that the LLS gap widths are consistently larger than those of the micrographs. Furthermore, it shows a quite constant difference. Figure 5.10 indicates that the gaps measured in the micrographs are consistently between 0.11 mm and 0.14 mm smaller than those of the LLS. Therefore, it shows a relatively constant compaction due to reheating and reapplying the consolidation force.

Superimposition of LLS data on micrographs

The difference between the LLS measured gaps and the gap dimensions obtained from the micrographs can also be visualised by overlaying the LLS data on top of the micrographs. This provides an intuitive overview of how both measurements compare, and why their differences make sense. To be able to superimpose the LLS data on top of the samples' micrographs it is crucial to match both coordinate systems such that the LLS data indeed correlates to the same position on the micrograph. As the LLS gap widths are different from the gap widths from the micrographs one must know their relative positions. To achieve this, an assumption was made. It was assumed that the gap width increase or decrease was symmetrical around the midline of the gap determined on the micrograph. This ensures a shared x-axis of the LLS data and the micrographs. With the gap widths from the micrographs determined in expression 5.6 and the resolution, it allows for a scale factor calculation, to obtain the distance per mm. The resolution of the micrographs was 2048 by 1536 pixels. The amount of mm per pixel should be the same for all micrographs, but for the sake of robustness, they were all calculated.

Superimposition of LLS data on sample one

The gap width for sample one determined by the micrograph was obtained in expression 5.6. Additionally, from figure 5.11, the number of pixels between the two yellow dotted lines, and thus the gap, was determined. Combining this width with the amount of pixels allows for the following scale factor calculation:

$$\begin{aligned}
\text{Left edge position}: &\quad x_{\text{left}} = 911 \text{ pixels} \\
\text{Right edge position}: &\quad x_{\text{right}} = 1260 \text{ pixels} \\
\text{Middle of gap}: &\quad x_{\text{middle}} = \frac{(x_{\text{left}} + x_{\text{right}})}{2} \text{ pixels} = 1085 \text{ pixels} \\
\text{Gap width}: &\quad w_{\text{gap}} = x_{\text{right}} - x_{\text{left}} = 1260 - 911 = 349 \text{ pixels} \\
\text{Scale factor}: &\quad s = \frac{1.297\ mm}{349 \text{ pixels}} \approx 0.0037\ mm/\text{pixel}
\end{aligned} \tag{5.7}$$

With the scale factor known and the LLS width for sample one from 5.5, the LLS gap and its edges can be appropriately scaled to the micrograph:

$$\begin{aligned} \text{LLS Gap width in pixels :} \quad & w_{\text{LLS}} = \frac{w_{LLS}\ mm}{s\ mm/\text{pixel}} = \frac{1.433\ mm}{0.0037\ mm/\text{pixel}} = 385.63 \text{ pixels} \\ \text{LLS left edge position :} \quad & x_{\text{LLS,left}} = x_{\text{middle}} \text{ pixels} - 0.5 \cdot w_{\text{LLS}} \text{ pixels} = 892.18 \text{ pixels} \\ \text{LLS right edge position :} \quad & x_{\text{LLS,rigtht}} = x_{\text{middle}} \text{ pixels} + 0.5 \cdot w_{\text{LLS}} \text{ pixels} = 1227.81 \text{ pixels} \end{aligned} \tag{5.8}$$

The middle of the LLS gap is then matched to the previously determined gap from the micrograph. This ensured that the edges of the gap measured by the LLS were at the right position. The LLS gap edges are indicated in figure 5.11 as cyan dotted lines. The next step was scaling the LLS data such that the edges in the data matched with the cyan lines. To do this the same edges of the gap had to be identified in the raw LLS data in the corresponding frame previously determined in expression 5.5. The profile for this frame including the edges of the gaps defined according to the philosophy illustrated in figure 5.3, can be seen in figure 5.12.

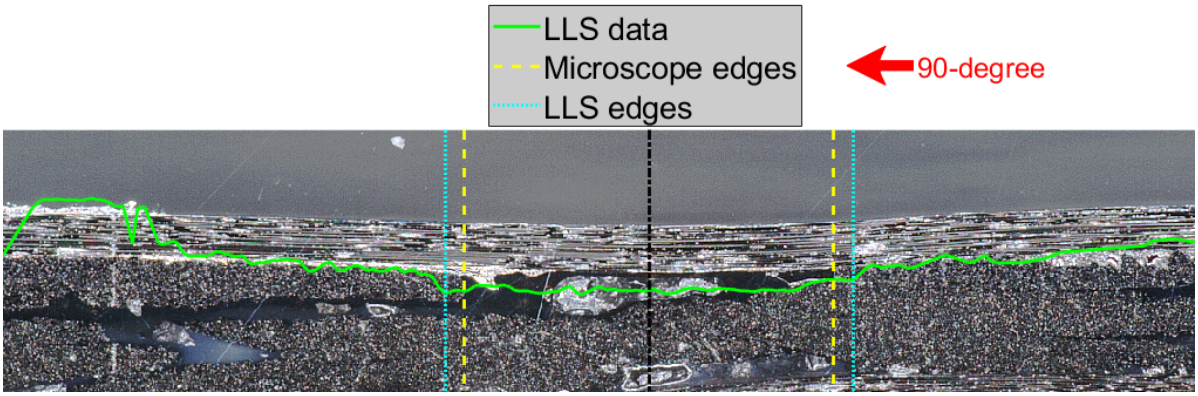

Figure 5.11: Superimposition of LLS data on micrograph.

To map the data correctly on the micrograph, it had to be appropriately scaled to the micrograph. To do this, the previously determined scale factor from expression 5.7 could be used to transform the X and Y data from the LLS from pixels to mm. This ensured the conversion of the complete data set to pixels.
The next challenge was the alignment of the LLS data with the corresponding micrograph. To achieve this, at least one fixed reference point had to be identified. For the X-direction, the right cyan line in figure 5.11 was selected as the reference, as it had previously been established as the right edge of the LLS-measured gap. Although the left cyan line could also have been used, a single reference point was sufficient for alignment. The alignment process involved locating the data point in the X-coordinate data set that corresponded to the right edge of the gap. The value for this data point could then be extracted, which resulted in the exact right side edge for the LLS scan, illustrated in figure 5.12 by the right dotted line. This physical dimension was then converted to pixels and compared to the pixel position of the right cyan line in the micrograph. The difference between these two pixel values yielded the required X-direction offset.
For clarity, the right edge position at 3.25 mm will be referred to as the variable R.

$$X_{\text{offset}} = x_{\text{LLS,right}} \text{ pixels} - \frac{R\ mm}{s\ mm/\text{pixels}} = 402.22 \text{ pixels} \tag{5.9}$$

This ensured that in the X-direction, the data was scaled and positioned correctly. The same had to be done for the Y-axis. The Y data was already scaled, as mentioned before, by the conversion of the complete data set to pixels. The positioning of the data in the Y-direction turned out to be slightly more challenging. In the Y-direction, there were no consistent landmarks on the micrograph to anchor the LLS data to. Therefore, the scaled y data was manually positioned on the micrograph as good as possible.

Finally, with the correct scaling and positioning, the superimposition of the LLS data on the micrograph could be visualised. This visualisation can be seen in figure 5.11. In this figure, the green line is the scaled and positioned LLS data, the yellow dashed lines are the gap edges determined from the micrograph, the black line is the midline of the gap, the cyan dotted lines are the edges determined from the LLS data, and the red annotated arrow is the layup direction of the 90-degree layer.

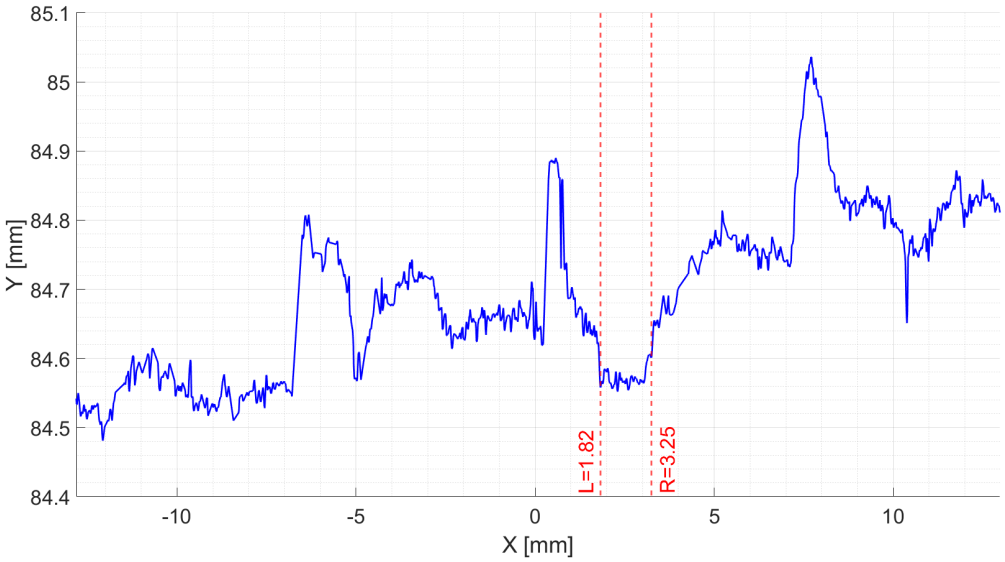

Figure 5.12: LLS profile for frame 1711 (5.5) including identified gap edges

From figure 5.11 one can observe that the edges of the LLS measurement are further away from the midline than the edges of the micrograph-determined gap. This is a logical result as after the LLS measurement the 90-degree layer was placed and therefore the laminate was heated up again in combination with pressure from the roller. This effect was already discussed previously in section 5.1.3. Figure 5.11 therefore strengthens this hypothesis by displaying both gap geometries on top of each other which makes the difference clearer. Re-compaction and reheating cause the gap width to decrease by squishing the edges of the gap causing it to expand more inwards the gap, which can be seen in the figure.

Another observation can be made. The right edge of the gap seems to be more squished than the left one. A possible cause for this can be the layup direction of the 90-degree layer. As the left edge could create a shadow, and could therefore be less affected than the right edge. To more clearly illustrate this effect, a schematic is shown below in figure 5.13. Although the right side would also create some shadow below the rounded edge of the gap, the reflections from the bottom layer would still result in full heating of this edge.

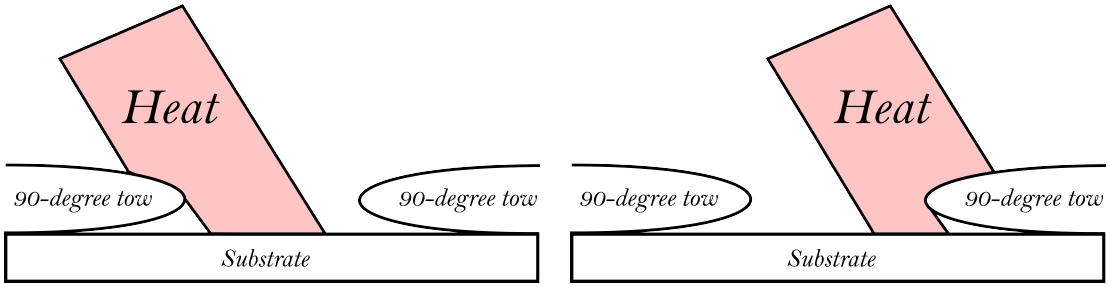

Figure 5.13: Heating of left and right edges of gap

Additionally, the white artefact seen in figure 5.11 is suspected to be a combination of the resin from the moulding process and moisture left behind by the cutting process. A more enhanced micrograph was made by making use of a more powerful microscope. This micrograph showed that the gap had indeed filled with resin, but at the location of the white artefact, the surface was quite rough, indicating the presence of an additional effect. This can be seen in figure 5.14.

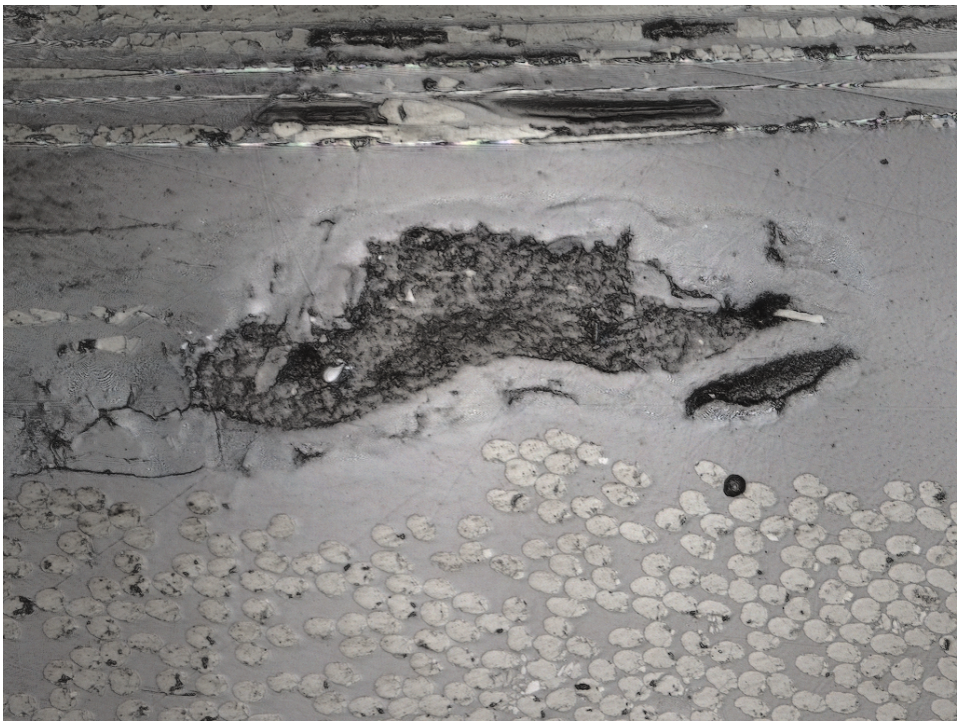

Figure 5.14: Laser microscopy image of the gap in sample 1

This micrograph also shows a faint white ring around the artefact. This could be residual stresses surrounding it due to uneven shrinkage of the poured resin in the gap caused by the combination of moisture and resin.

Superimposition of LLS data on sample two

The data extracted from the LLS scan at the frame for sample two can be observed below in figure 5.15. The main challenge for the data in this frame was identifying the right edge of the gap. The right edge was positioned at the location shown in Figure 5.15. This specific point was chosen because, to its right, the slope leading up to the top surface of the tow appeared relatively consistent and smooth. In contrast, to the left of this point, the surface of the underlying substrate was noticeably rough and uneven. Supporting this claim is the micrograph seen in figure 5.4(d), which shows three distinct features in the substrate along the gap width. These three features correlate to the three peaks in between the two red dotted lines in figure 5.15.

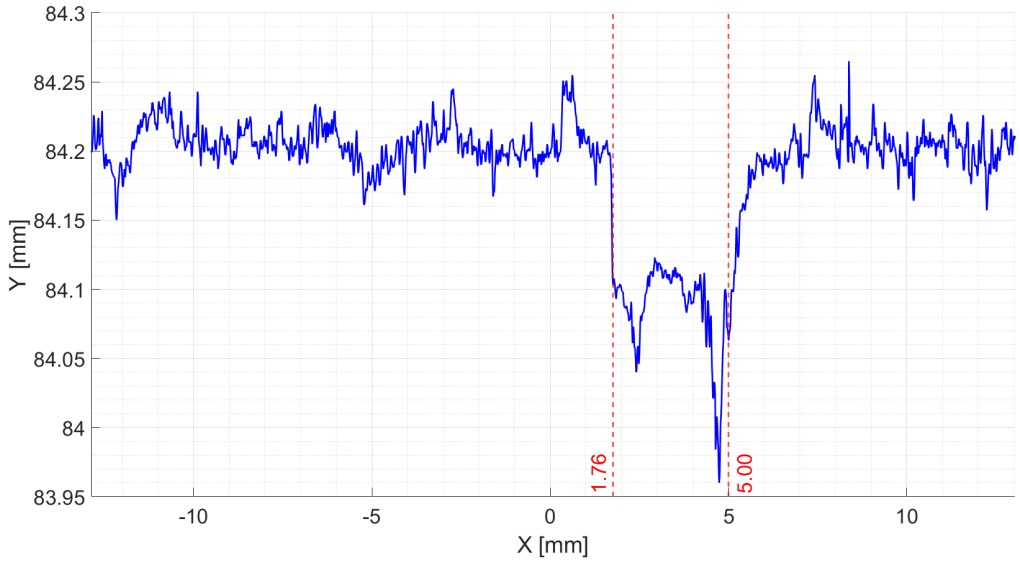

Figure 5.15: LLS profile for frame 2278 (5.5) including identified gap edges

This data could then be superimposed on the micrograph for sample two. To do this, the same procedure was followed as shown in the superimposition for the data of sample one in expressions 5.7, and 5.8. Additionally, the same MATLAB program was used to scale and position the LLS data appropriately on the micrograph. This resulted in the following micrograph, including the superimposition of the LLS data of sample two in figure 5.16.

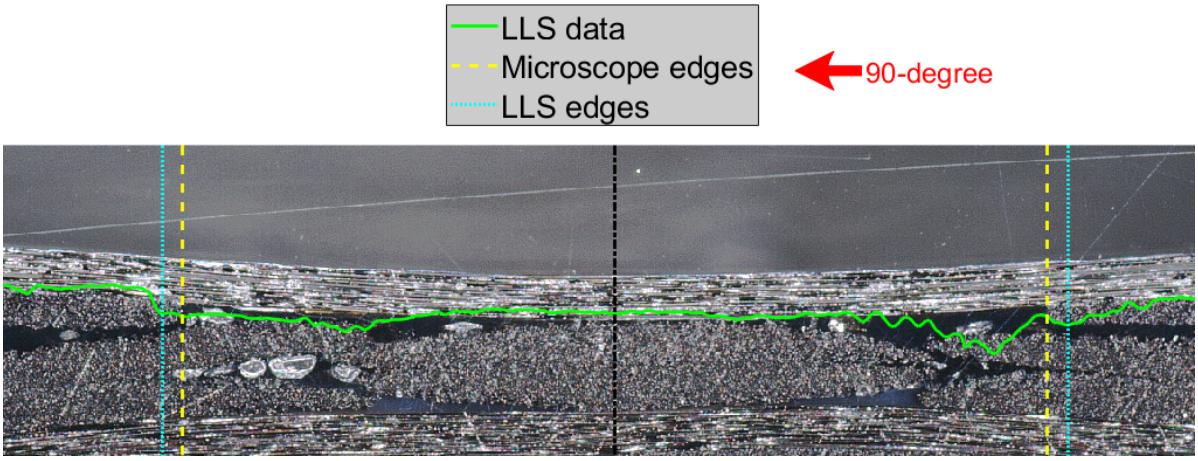

Figure 5.16: Superimposition of LLS data on a micrograph of sample two

Figure 5.16 shows the correlation between the LLS data and the micrograph. This correlation also indicates that the tow in the middle of the gap has been compressed from all sides. This is an interesting result as the layup direction of the top 90-degree layer is from right to left. This could mean that the material was pressed and directed in the same direction. Nevertheless, the material seems to be pressed in both directions. Different effects could have played a role in this behaviour. The most likely effect is considered the effects of the trailing edge of the roller. During the placement of the top layer, first the right side of the bottom layer is again indirectly compressed because the layup direction is from right to left. Then, the left side of the bottom is indirectly compressed through the top 90-degree layer by the trailing edge of the roller. Hence, the contour of the bottom layer in the LLS (the green line) is compressed in all directions, resulting in an overall smaller corresponding feature in the micrograph.

Superimposition of LLS data on sample three

In a similar fashion the LLS data from the third sample could be scaled and positioned on its respective micrograph. To reduce repetitiveness the elaboration can be found in Appendix B. From this the figure 5.17 followed which shows the superimposition of the LLS data gathered for the third sample on its micrograph.

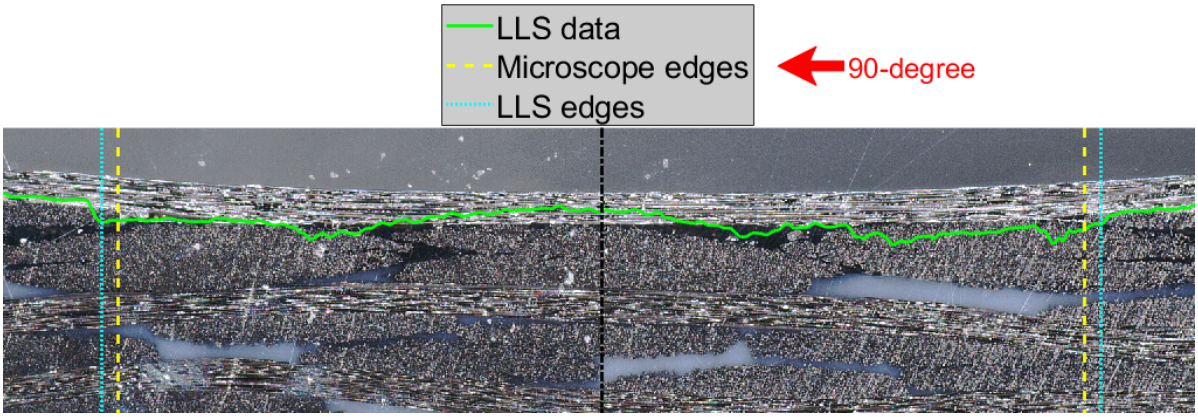

Figure 5.17: Superimposition of LLS data on a micrograph of sample three

Superimposition of LLS data on sample four

Similarly to the previous superimposition methods the superimposition of sample four could be achieved. The same program written in MATLAB was used to achieve the right scaling and positioning. This then resulted in the superimposition of the LLS data on the micrograph for the fourth sample which can be seen in figure 5.18. The LLS data and a slight elaboration can be found in Appendix B.

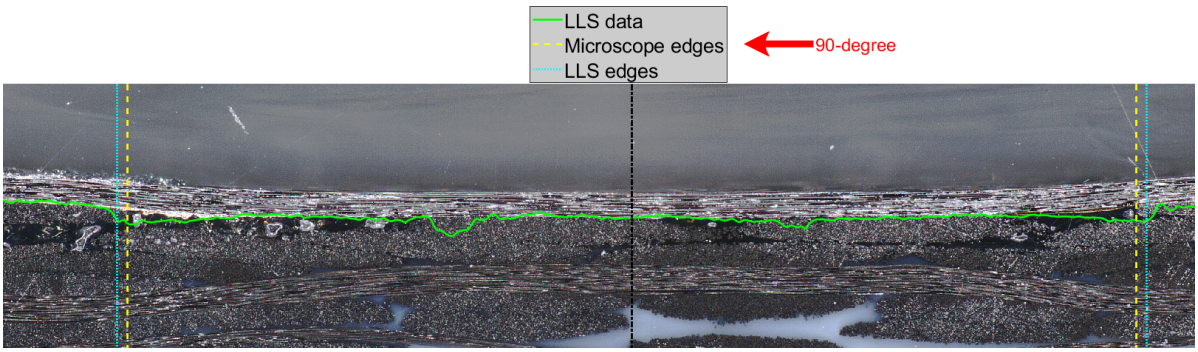

Figure 5.18: Superimposition of LLS data on a micrograph of sample four

5.1.5. Parametrisation of the gaps

From the previous analysis, the size and behaviour of the gaps were examined at different steps in the manufacturing process. Based on this, three different types of gap morphologies were identified. In the first type, the top 90-degree layer does not touch the substrate and instead fully bridges the gap. In the second type, the top 90-degree layer just about touches the substrate, effectively closing the gap at a single point. In the third and fourth types, the top 90-degree layer touches the substrate and closes the gap over a certain distance. Therefore, the first type includes a completely bridging top layer, the second only closes the gap at a single point, and the third type closes it over a finite length.

From earlier results, it became clear that the substrate is significantly rough. However, since the substrate was primarily used to facilitate the manufacturing process, its effect on gap morphology was neglected in the analysis. As a result, the bottom surface of the gap was parametrised as a straight line, rather than reflecting the rough surface observed in the earlier micrographs.

Parametrisation of type 1 gap

The introduction shortly introduced the morphology of the first type of gap encountered during the analysis. This section will explore this type of gap further.

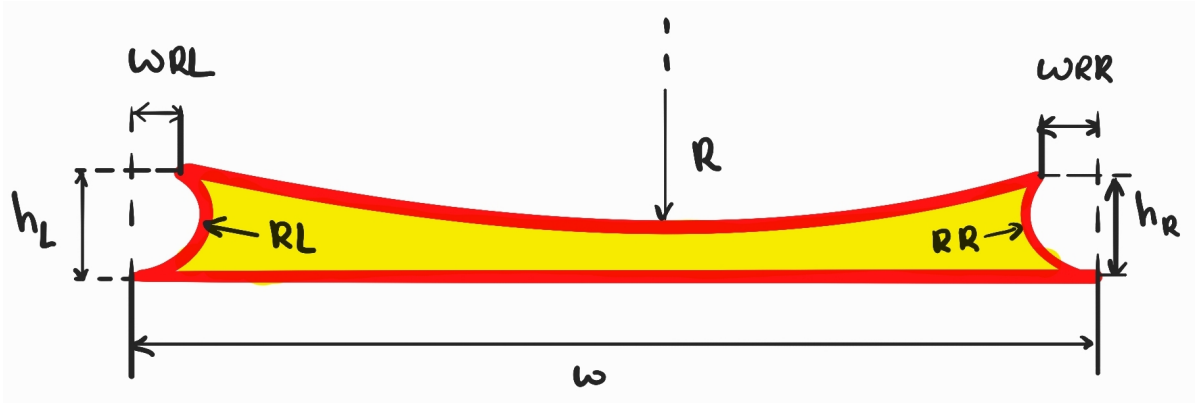

Figure 5.19: Parametrisation of the type 1 gap

Figure 5.19 shows the parametrisation of the first gap type. This gap type requires eight dimensions to fully describe the geometry. Furthermore, from the previous analysis it became evident that the gap edges could be well parametrised by circular arcs. The same holds for the top edge of the gap. Hence the gap could be parametrised by the following dimensions: the radii of the left, right, and top circular segments, the overall gap width, and the x and y position of where the circular arcs intersect. Parametrising these edges by circular arcs provided an optimal combination between accuracy and repeatability. Following these assumptions, the edge and top radii and the other dimensions could be measured from the micrographs through the software of the microscope. These dimensions could then be used to construct the parametrised morphology for gap one. The dimensions shown in figure 5.19 for the first gap are shown below in table 5.1:

Table 5.1: Variables and their dimensions for gap one

	Value	Unit
w	1.362	mm
R_L	0.053	mm
R_R	0.025	mm
h_L	0.101	mm
h_R	0.047	mm
w_{RL}	0.020	mm
w_{RR}	0.013	mm
R	26.205	mm

A keen eye might have noticed that the gap width mentioned in table 5.1 is not the same as previously mentioned in 5.6. This is because in 5.6 the gap width was measured as the smallest distance between the gap edges, and in figure 5.19 the gap width is parametrised as the distance between where the arcs of the edges close the gap at the bottom. Therefore, it makes sense that the gap width used for the parametrisation is slightly larger than the one shown previously in 5.6.

Combining the morphology parametrisation illustrated in figure 5.19, the measured dimensions shown in table 5.1, and the micrograph for gap one 5.4. This allows for the following parametrisation of gap one seen in figure 5.20.

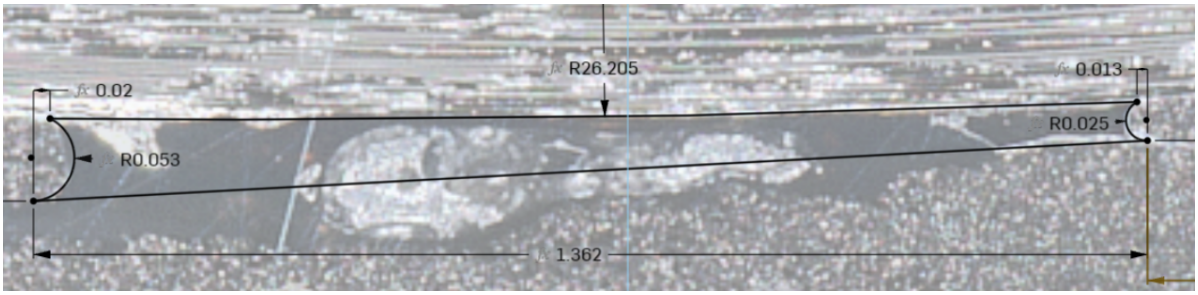

Figure 5.20: Parametrisation of gap one

The software used to produce this parametrisation could also be used to obtain a comparison between areas of the parametrisation and the exact traced circumference of the gap (including the assumed straight bottom line). The parametrised gap has a surface area of 0.088 mm^2 while the exactly traced shape has a surface area of 0.091 mm^2, as can be seen in Appendix C.1. Therefore, the accuracy of the assumptions can be computed as the following:

$$\text{Parametrisation error void} = 1 - \frac{\text{Parametrised area } mm^2}{\text{Traced area } mm^2} = 1 - \frac{0.08799}{0.09140} = 3.8\% \tag{5.10}$$

This is an error of 3.8 $\%$ which is small enough to consider the parametrised morphology for gap one an accurate one.

Parametrisation of type 2 gap - Cross-over point

The second type of gap morphology is a gap for which the top layer just touches the bottom layer of the gap at a single point. This creates two voids at the left and right sides of the gap. From the previous micrographs in 5.4 it became evident that a circular arc would again be a good approximation of the top and edge boundaries of the gap. However, the top surface does not have to conform to one radius. The top layer of the left void can, and probably will, have a different radius than the right void. To account for this, two separate circular arcs were modelled for this gap type. Additionally, it is good to mention that a condition is applied that cannot be seen. This condition is that the circular top arc must curve into the void. This fully constrains the shape of the voids. The parametrisation for this gap type can be seen in figure 5.21.

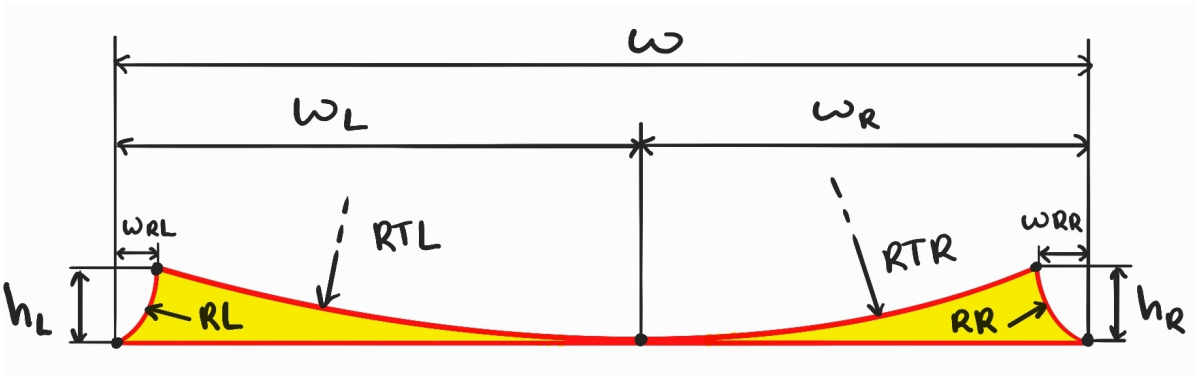

Figure 5.21: Parametrisation of the type 2 gap

As both arcs from the top 90-degree layer always meet in a single point, the inclusion of both w_R and w_L is not necessary, and either one of them could be excluded. All the other variables are required to fully dimension this gap type. From figure 5.4 it can be seen that the second gap already remains closed for a short distance and therefore just falls outside this gap type.

The fact that the circular arcs must meet in a singular point is morphologically fine but unlikely to occur in reality. As probably most gaps either stay open or if they close, they remain closed for a distance, even if this distance is minute. Hence, this gap type is more seen as a cross-over point between the two main gap types: type one and type three.

Parametrisation of type 3 gap

The morphology for the third gap type looks similar to the second. However, for this type, the two arcs of the top surface do not need to meet at the same point. Both arcs reach the bottom surface of the gap at different points, creating a distance where the gap is completely closed in addition to the two voids at the edges. Therefore, now the inclusion of both w_R and w_L is necessary, in contrast to the second gap type. Apart from that, the morphological parametrisation is similar to the second gap type. Therefore, this also refutes the first hypothesis suspecting that if the gaps closed for a set distance, that the top edges of the voids would be more linear. The parametrisation for the morphology of the third gap type can be seen in figure 5.22.

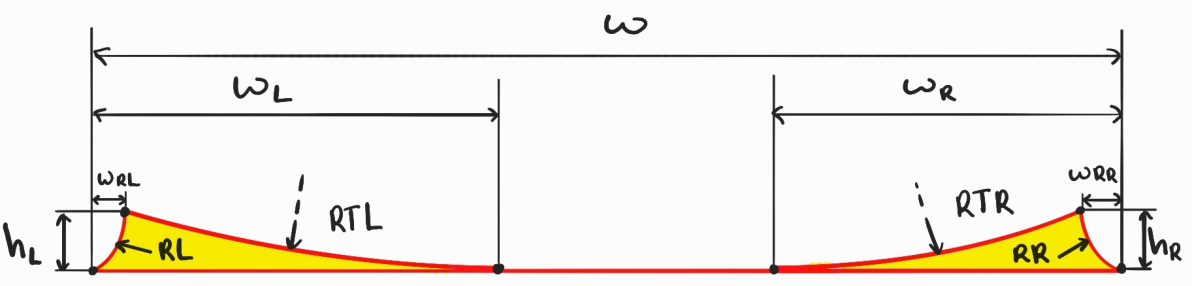

Figure 5.22: Parametrisation of the type 3 gap

Gaps two, three, and four all complied with the gap morphology shown in figure 5.22.

From the micrograph, the following dimensions for the second gap were found:

	Value	Unit
w	3.185	mm
W_L	1.389	mm
w_R	1.387	mm
R_{TL}	39.904	mm
R_{TR}	23.516	mm
w_{RL}	0.027	mm
w_{RR}	0.052	mm
h_L	0.083	mm
h_R	0.072	mm
R_L	0.058	mm
R_R	0.057	mm

Table 5.2: Variables and their dimensions for gap two

These dimensions could then be used to complete the parametrisation for the second gap. This parametrisation can be seen in figure 5.23. Again, the width is slightly larger than found in 5.6 as a result of the reasons already discussed for the previous parametrisation.

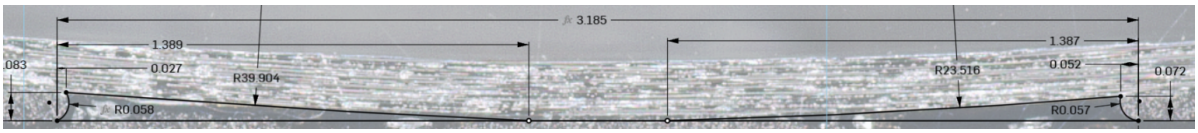

Figure 5.23: Parametrisation of gap two

Again, the error due to the circular arc assumptions and parametrisation model can be calculated in terms of a difference in traced and parametrised areas. A maximum error was found for the left void of 2.9% which is considered small, confirming the parametrisation to be accurate. The traced area and the computations can be found in Appendix C.2.

For the third gap, the following dimensions were found in the micrograph:

	Value	Unit
w	4.641	mm
w_L	0.811	mm
w_R	0.474	mm
R_{TL}	24.506	mm
R_{TR}	3.774	mm
w_{RL}	-0.008	mm
w_{RR}	-0.015	mm
h_L	0.079	mm
h_R	0.033	mm
R_L	0.040	mm
R_R	0.022	mm

Table 5.3: Variables and their dimensions for gap three

The reason that the values for w_{RL} and w_{RR} are negative is because they are both in the opposite direction as initially indicated for this morphology parametrisation in figure 5.22. The voids at the edges of gap three will be viewed in separate figures. Otherwise, the width of the image would result in unclear dimensions. Figures 5.24 and 5.24 show the parametrisation for both voids of gap three according to the dimensions of table 5.3.

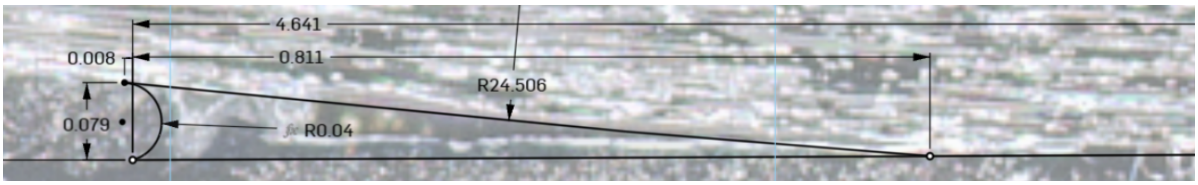

Figure 5.24: Parametrisation of gap three, left void

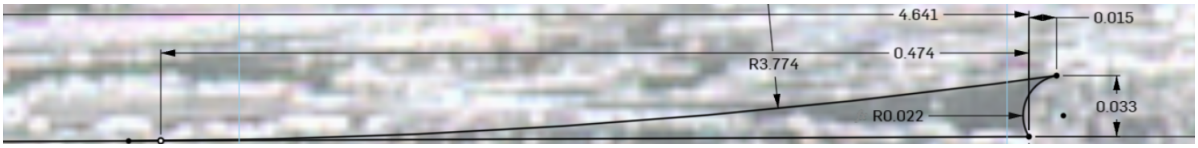

Figure 5.25: Parametrisation of gap three, right void

The largest error between the two voids of the third gap is the error of the parametrised model of the left void, which has an error of 6.9%. This error can still be considered small enough to deem the parametrisation as accurate. The computation for this can be found in Appendix C.3

For the fourth gap, the following dimensions were found in the micrograph:

	Value	Unit
w	6.332	mm
w_L	0.781	mm
w_R	0.801	mm
R_{TL}	16.732	mm
R_{TR}	6.873	mm
w_{RL}	0.028	mm
w_{RR}	0.031	mm
h_L	0.078	mm
h_R	0.062	mm
R_L	0.044	mm
R_R	0.039	mm

Table 5.4: Variables and their dimensions for gap three

These dimensions could then be applied to the parametrisation of the fourth gap. Figure 5.26 shows the parametrisation of the left void of the fourth gap

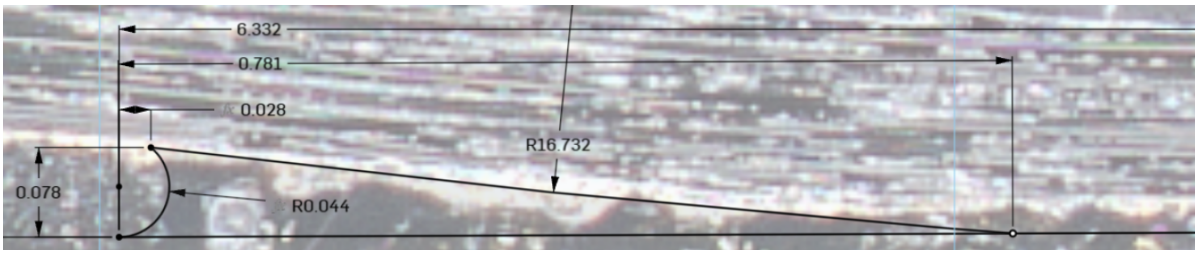

Figure 5.26: Parametrisation of gap four, left void

Figure 5.27 shows the parametrised right void of gap four including the applied dimensions from 5.4.

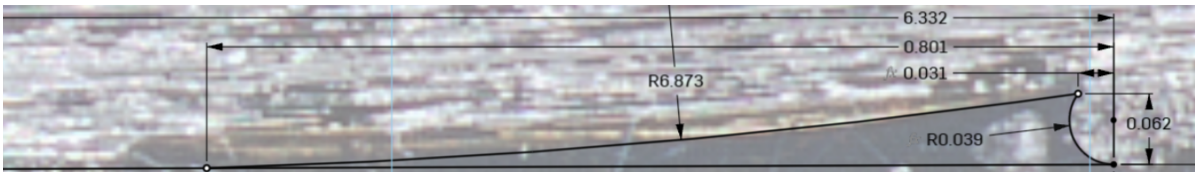

Figure 5.27: Parametrisation of gap four, right void

The largest error of 6.9% was found for the right hand void and deemed small enough to consider the parametrisation an accurate one. The computation as well as the traced areas can be found in Appendix C.4.

All gaps have now been parametrised and compared to the traced areas, from which it could be concluded that the parametrised areas come quite close to the traced areas. This means that the gaps could be well parametrised by the predefined metrics. With this in mind the next experiment could be analysed, in which the metrics defined in this analysis can be used to parametrise the gaps found in for the next trial.

5.2. Sample analysis Trial Two

This section will discuss the results of the second experiment and evaluate the effects of the force and the velocity on the morphology of the gaps. The five different combinations discussed in section 3.2.2 for the negative 90-degree layup direction will be discussed; these are tows 11/13/14/15/17.

5.2.1. LLS data

From all of the above mentioned tows, three samples are to be extracted, each of the same size gap. These gaps have been mapped along the complete length of the layup. Along this length, markers were placed at the location of tows 6, 12, and 18. By placing markers at equally spaced intervals of 150 mm, the difference in frames could be used to determine the distance per frame. Therefore, allowing to accurately determine the location of all the tow locations in between and their respective gap sizes. This computation can be seen in Appendix D. From this computation, it became evident that between tows there are 42 frames, which allowed for an accurate determination of all tow locations in the LLS scans and hence their respective gap widths.

Gap widths determined by LLS

As the distance in frames between tows is now known, the gap widths for the tows for all three repetitions can be determined. Doing this results in the following gap sizes:

Table 5.5: Gap widths across the three scans in mm

Tows	Scan 1	Scan 2	Scan 3
17	3.0908	2.8938	3.0152
15	3.1494	2.9300	3.0724
14	3.1138	2.8862	3.0407
13	3.1675	2.9576	3.0942
11	3.1603	2.9513	3.0597

From this, it can already be seen that the values from the first scan are the closest to the designed gap of 3.175 mm. The second scan is consistently smaller than the first scan, and the third scan is in between the first and the second scan. These measurements can later be used to compare them to the widths measured from the micrographs.
To more clearly illustrate this, the mean of each scan can be taken and compared to the designed value of 3.175 mm.

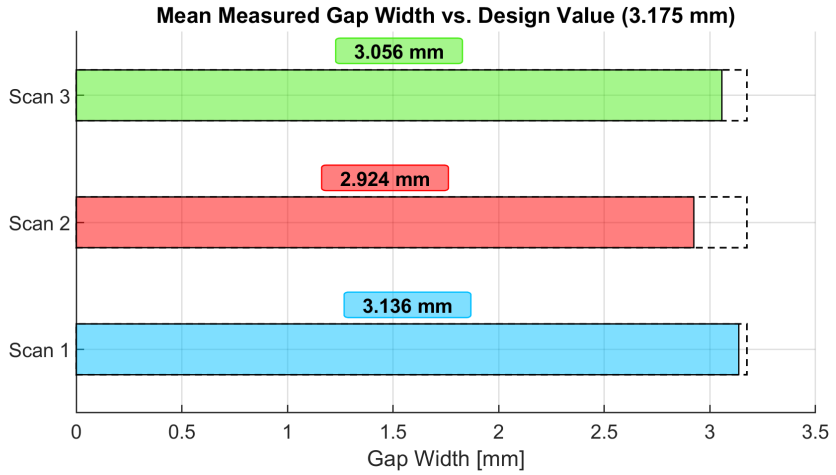

Figure 5.28: Mean deviation scans compared to the designed value

Figure 5.28 confirms the previous suspicion and shows the deviation from the mean to the designed gap. It can also be seen that not only does the mean value remain lower than the designed gap size,

but also all entries in table 5.5 do not exceed this value. This makes sense, as during the process, the tows are heated and pressed, causing them to expand in the width direction, resulting in a smaller gap than designed.

5.2.2. Force Torque Sensor data

The previous section presented all data obtained from the LLS. This section focuses on the data collected from the FTS. Unlike the LLS measurements, which were taken after placement of the 0-degree layer and before the 90-degree layer, the FTS data was recorded during the placement of all 18 tows in the 90-degree layer. The forces to be applied during the placement of 90-degree tows had previously been determined in section 3.2.2. However, the FTS data was collected to monitor if the forces during the placement of the tows were similar to their designed values.

An example of a FTS scan was shown in section 4.11. Section 3.2.2 already discussed the different features of the FTS data such as when the robot arm is moving, when it is initially pressed, and when it loses contact with the substrate. The bottom part of the FTS data can be used to calculate a mean pressure exerted on the substrate. Doing this for all minus 90-degree tows resulted in the following force values illustrated in table 5.6:

Table 5.6: Mean forces across different tows in N

Tows	Force (N)
T10	345
T11	360
T12	375
T13	298
T14	356
T15	380
T16	297
T17	343
T18	385

These values can then be used to compare the designed forces to the forces reached during the process.

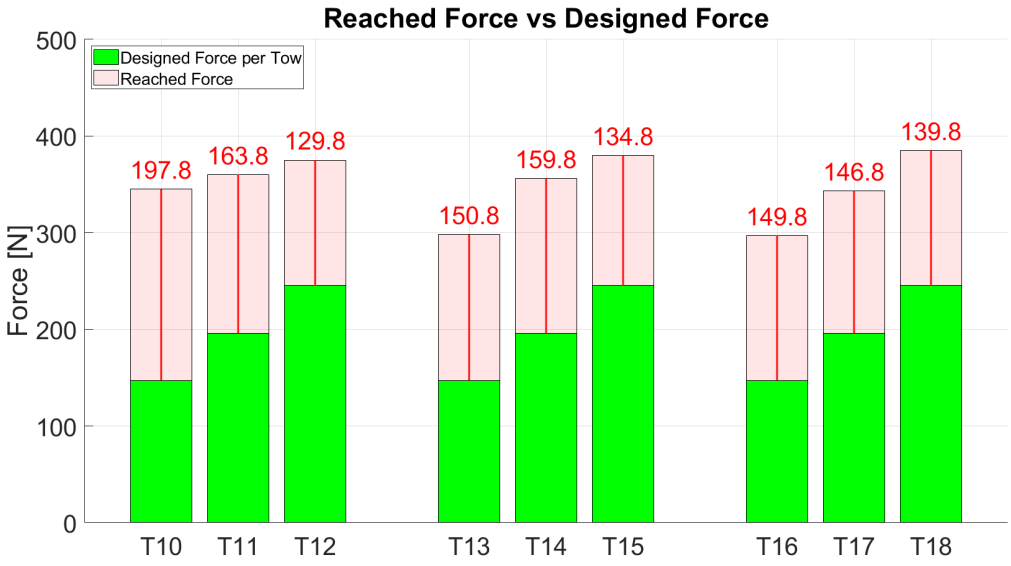

Figure 5.29: Measured forces per tow vs the designed forces in N

Figure 5.29 indicates the forces measured during the process compared to the forces that were intended for the process. The red lines between the designed force bars and the reached force bars indicate the difference of force in N.The measured forces are consistently higher than the intended forces. Not only are they consistently higher than the intended forces, they are significantly higher. Sometimes even twice as high as their intended values. The purpose of this experiment was to investigate the influence of different process parameters on the morphology of the gaps. Applying this much excess force could have an influence on the results of the experiment. This will be discussed later.

5.2.3. Infrared camera data

While the FTS data was being recorded, the IR simultaneously captured the temperature throughout the entire layup of the 90-degree tows. An example of this data can be seen in section 4.2.1. Figure 4.9 also shows the areas from which the temperatures were extracted. The area from which the temperature of the tape is extracted has been tuned to only contain the hottest area of the tape and avoids also reading temperature data from the roller. The area constructed for the temperature extraction of the substrate is placed directly below the Humm3 flashlamp at the hottest part of the substrate. Taking the mean values for both of these areas during the placement of the 90-degree tows resulted in the following temperatures:

Table 5.7: Tape and Substrate Temperatures across different tows in C°

Tows	Tape Temperature	Substrate Temperature
T10	317.5	407.5
T11	317.6	411.2
T12	321.2	411.9
T13	302.3	412.1
T14	309.7	414.8
T15	314.0	407.7
T16	304.5	427.1
T17	315.9	433.4
T18	319.1	423.7

As mentioned previously in the design for the second trial, the Humm3 input voltage was set to result in a temperature of around 350 C°. From table 5.7 it is evident that the tape reached lower temperatures while the substrate reached higher temperatures. Hence, the tape temperature was slightly lower than aimed for and the substrate temperature higher. This is probably the cause of the fact that two different materials were used for the substrate and tape with different thermal properties, causing different thermal behaviour.

This data concludes all the data recorded during the second experiment. The analysis can now move on to inspecting the morphology of the samples with the microscope to investigate the influence these parameters had on the shape and size of the gaps.

5.2.4. Gap morphology

Tow 11 (v_1F_2)

Tow 11 was designed to be the combination between the lowest layup velocity, 20 mm/s, and the intermediate consolidation force with a mass equivalent of 20 kg. Similarly to the results of experiment one, the LLS data could be superimposed onto the micrographs to observe the differences between the gap measured by the LLS and the gap dimensions obtained from the micrographs. The superimposition of the first repetition of the 11th tow can be seen below in figure 5.30:

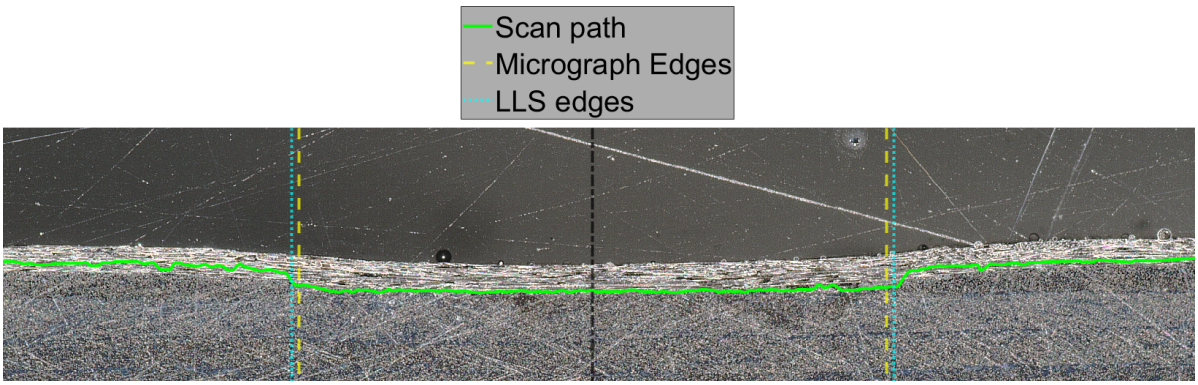

Figure 5.30: Superimposition of the LLS data of the 11th tow, first repetition

Similarly to the results for experiment one, it makes sense that the gap obtained from the micrograph is smaller than the gap determined from LLS, as the LLS data was obtained after placing the 0-degree layer and the micrograph after placing the 90-degree layer.

Furthermore, as mentioned previously, the force was measured during the placement of each tow. For this tow, the average force experienced during placement turned out higher than expected and reached 360 N, or 36.7 kg. Additionally, the substrate showed an average temperature of around 411 C° during the placement of the tow. As previously discussed, the PPS substrate had a working temperature of around 220-260 C°. This primarily affected the 0-degree layer since it was consistently in direct contact with the substrate. The 90-degree tows only encountered the substrate across the gaps in the 0-degree layer. Therefore, it did not cause any burning; however, at the locations where the 90-degree tows encountered the gaps and therefore the PPS, it could mean that the material could have melted and influenced the gap morphology.

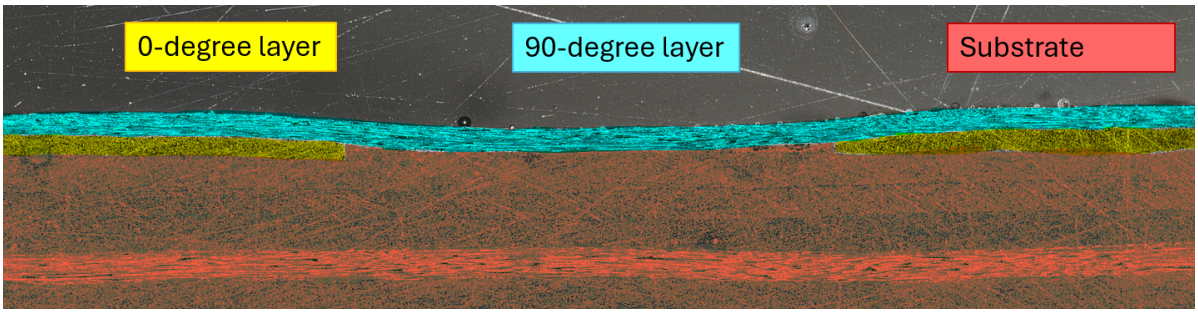

Figure 5.31: Layer identification tow 11 repetition 1

Figure 5.31 shows the micrograph of tow 11 for the first repetition. It confirms the suspicion that the large difference in working temperatures between PPS and LM/PAEK, in combination with a significantly higher than expected consolidation force, indeed has had an influence on the morphology of the gap. In contrast, the layer identification of the micrograph for the first experiment (5.5) showed a clear void as a result of the embedded gap in the 0-degree layer. From figure 5.31 the PPS substrate seems to have flowed into the voids at the edges of the gaps. Additionally, it is also likely that during the placement of the 0-degree that the top layer of the PPS had melted. This phenomenon could be attributed to the relative solidity of the LM/PAEK tows compared to the PPS substrate during placement, facilitating their integration into the molten matrix. Hence, the filling of the voids is most likely a result of the large temperature difference between the two layers, causing the tows to be pressed into the substrate, and the substrate to have flowed into the voids. The other repetitions for tow 11 showed the same behaviour and can be found in the Appendix chapter F.

To parametrise the gaps, an assumption had to be made regarding the filling of the voids by the substrate material. The assumption is the same as the one used for the parametrisation of the first trial. The bottom edge of the gap is formed by connecting the bottom edges of the left and right 0-degree tows. The 90-degree layer seemed to follow the same behaviour as for the first experiment. Moreover, the sides of the 0-degree layers, which form the edges of the gap, again follow a circular arc profile. The combination of the assumption with the same behaviour for the 90-degree layer and the 0-degree layer gap edges, the parametrisation types defined for the first trial can again be used to parametrise the gaps for the second experiment.

The parametrisation for the first repetition for tow 11 showed interesting results and can be seen in figure 5.32.

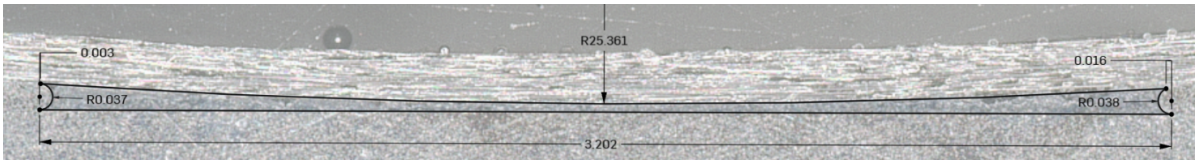

Figure 5.32: Parametrisation of tow 11, first repetition

Adhering to the previous assumptions, the first repetition for the gap of tow 11 falls under the first type of gap defined in section 5.1.5. This is particularly interesting as tow 11 was designed to be placed with the lowest layup velocity of 20 mm/s. A lower layup velocity was expected to give the material more time to be pressed while simultaneously being heated. Therefore, it was expected for the gap to fully close; however, connecting both bottom edges of the gap with a straight line and adhering to the other conditions, this gap could be well parametrised by the first gap type.

Nevertheless, this turned out to be a discrepancy regarding the other two repetitions for tow 11. These repetitions showed the behaviour of the third gap type where there are two voids created at the edges of the gap. In this case; however, the gaps had been filled with PPS substrate material. This behaviour can be seen in figure 5.33.

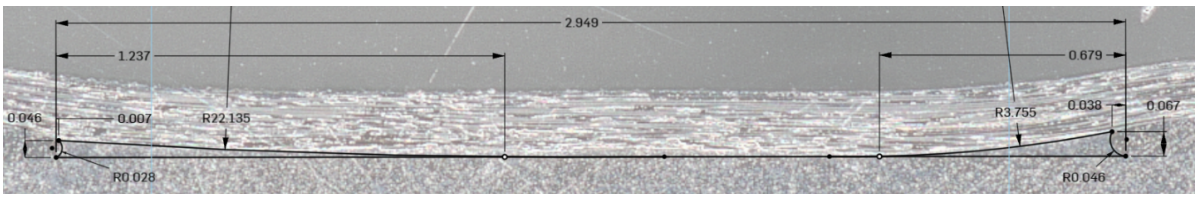

Figure 5.33: Parametrisation of gap for tow 11, second repetition

Similarly to the parametrisation of the gaps for the first trial, the area of the parametrised voids can be compared to the actual traced surface of the voids. This resulted in 97.0$\%$ match for the left void and a 105.9$\%$ for the right void. Therefore, the maximum deviation from the actual shape compared to the parametrised one is around 6$\%$. This is considered to be a good match.

Tow 13 (v_2F_1)
This tow was designed to be placed with the intermediate layup velocity of 30 mm/s, and the lowest force of around 150 N. The results of this combination could be interesting, as it is the only tow looked at during this work that was placed with the lowest force settings. This could mean that the gap closes less compared to a higher force setting due to it being pressed less. A micrograph for this tow can be seen below in figure 5.34.

Figure 5.34: Micrograph of the 13th tow, first repetition

Nevertheless, this tow was also placed with double the amount of force than it was designed to be placed with at 298 N. This could override the effect of using the least amount of force, which has to be seen in the parametrisation. The temperature reached during the placement of the 13th tow was consistent with the other temperatures; therefore, remaining much higher than the working temperature of PPS.

The features of this gap again allow for it to be parametrised according to the third gap type defined in section 5.1.5. Furthermore, the influence of the exceedingly large consolidation force in combination with the mismatch in working temperatures caused the voids of the gap to fill with the substrate material for all repetitions. Again, adhering to the same assumptions made for the previous parametrisations, the gap for the 13th tow could be parametrised.

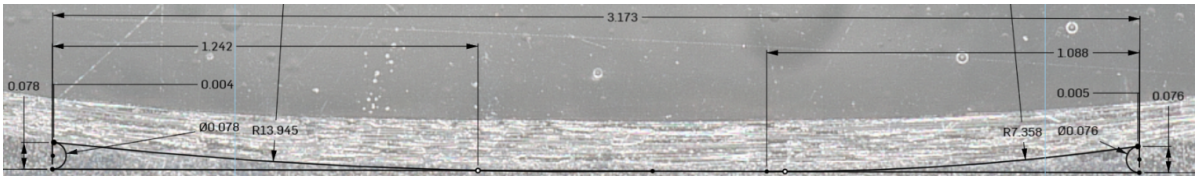

Figure 5.35: Parametrisation for the gap of tow 13, first repetition

Figure 5.35 shows the parametrisation of the 13th tow for the first repetition. The maximum deviation by the parametrised area to the traced area was 4.2 $\%$ for the right void, therefore confirming that the void is well parametrised. This tow was placed using the least amount of consolidation force of the experiment. However, this did not result in an immediate effect on the morphology of the gap. It was hypothesised that a decrease in force would result in a gap that remained more open and perhaps even in a gap that did not close. Nevertheless, this gap still fully closed and its dimensions, for all three repetitions, did not show a different behaviour to the other gaps. Again, this is likely to be a result of the mismatch in working temperatures and the excessive force reached compared to the force that was designed to be used.

Tow 14 (v_2F_2)
This tow was placed using the intermediate settings for both layup velocity and consolidation force, specifically 30 mm/s and approximately 200 N, respectively. Nevertheless, the consolidation force that was actually obtained during the placement of the tow was 356 N which is around 180 $\%$ of the designed force. This, in combination with a temperature much above the working temperature for the PPS substrate, again meant that the 0-degree layer was pressed into the substrate and that the voids at the edges of the gap had been filled with substrate material.

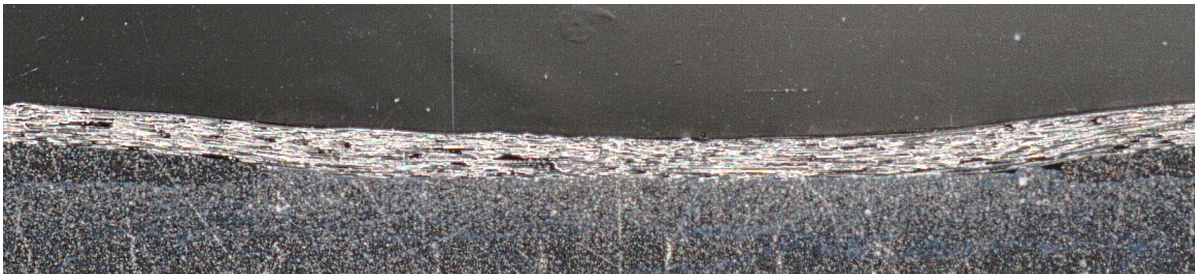

Figure 5.36: Micrograph of the 14th tow, third repetition

The micrographs from all three repetitions of the gaps showed the same behaviour, and no obvious outliers were identified. The gaps closed fully for all repetitions for this particular combination. Then adhering to the assumptions made previously, it was possible to parametrise the gaps according to the third gap identified in section 5.1.5. This parametrisation can be seen below in figure 5.37:

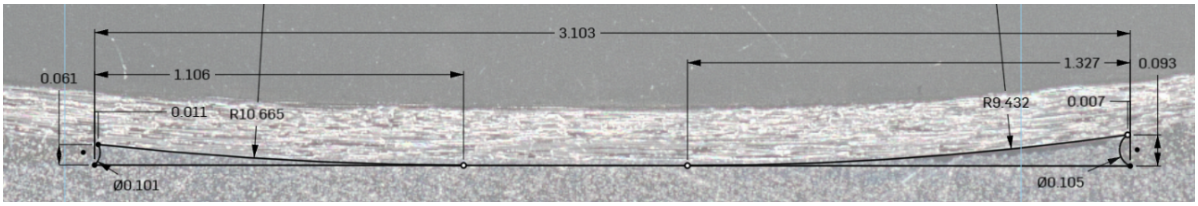

Figure 5.37: Parametrisation for the gap of tow 14, third repetition

Comparing the parametrised area to the traced area of the voids, the maximum parametrisation error was 8.1 $\%$ for the right hand void.

Tow 15 (v_2F_3)
This tow was again placed using the intermediate setting for the layup velocity but used the highest consolidation force of around 245 N. However, the force measured during the placement of the tow showed an average force of 380 N. Interestingly, the voids at the edges of the gap for this combination of processing parameter settings seemed to have been less filled by the PPS substrate material. This is an interesting result as this combination was expected to have the smallest voids. It was expected to have the smallest voids as the consolidation force was the highest, resulting in the tape being more severely pressed during the placement of the tow. This behaviour can be seen in figure 5.38:

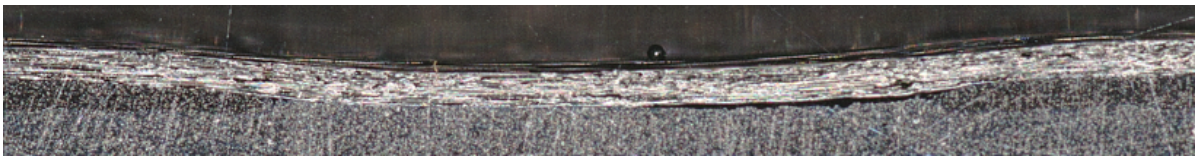

Figure 5.38: Micrograph of the 15th tow, third repetition

The dark spots at the edges of the gap in the figure clearly indicate the voids. The third repetition was displayed as this showed the largest void, but the other two repetitions also showed clear voids. In previous tows, slight voids could also be identified. However, for this tow, the voids are significantly larger. Additionally, the third repetition was particularly interesting. As after applying the assumptions to be able to parametrise the gaps, this repetition for the 15th tow does not close and has a different morphology than the other two repetitions.

As for this gap, the 90-degree top layer did not close the gap. This repetition could best be parametrised using the first gap type described in 5.1.5.

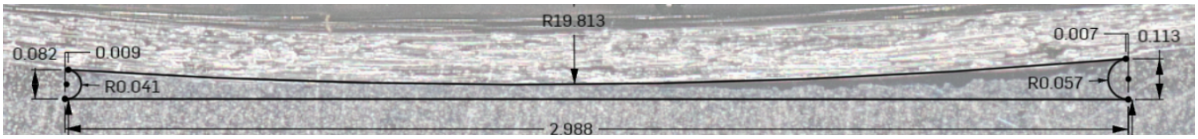

Figure 5.39: Parametrisation for the gap of tow 15, third repetition

Figure 5.39 shows the parametrisation of the third repetition for the 15th tow according to the first gap type. The other two repetitions (1 and 2); however, did show different behaviour. Even though they both also showed significant voids, they could best be parametrised by the third gap type, as both repetitions exhibited complete closure over a defined segment. For the other two repetitions again a maximum deviation to the parametrised area to the traced area was computed to be less than 10 $\%$ which indicated a good parametrisation.

Tow 17 (v_3F_2)
This tow is placed with the highest layup velocity for this trial of 40 mm/s. The consolidation force was set to the intermediate value of the range at around 200 N. Although the actual force reached for the placement of this tow also reached much higher values than intended. Figure 5.29 indicates an excess of 146.8 N which is significantly larger than the 200 N with which the process parameter setting combination was designed. This, combined with the mismatch in processing temperatures between the substrate and the laid-up tape, is again likely to influence the morphology of the resulting gap. However, these discrepancies are already known from the previous combinations. For this tow it is most interesting to see if the highest value for the layup velocity has had an influence on the morphology of the gap. The first and third repetitions for this gap showed some voids at the edges of the gaps, similar to the voids that were seen for the 15th tow but slightly smaller. However, this tow appears to be less well consolidated to the bottom of the gap compared to the others, as the distinction between the 90-degree and 0-degree tows seems still very pronounced. Nevertheless, for now this is only a suspicion. Figure 5.40 shows the third repetition for the 17th tow.

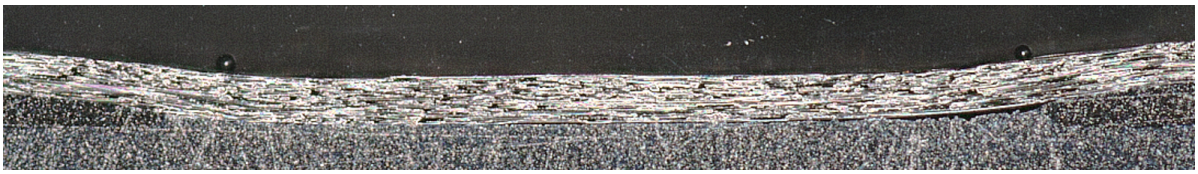

Figure 5.40: Micrograph of the 17th tow, third repetition

Even though the suspicion is that for this combination the top and bottom tows of the gap are less consolidated, it did not have an influence on the general morphology of the gap. All three repetitions, when adhering to the assumptions, could all be well parametrised by the third gap type identified in section 5.1.5. An example of this could be seen in figure 5.41 which shows the parametrisation of the third repetition for the gap of tow 17.

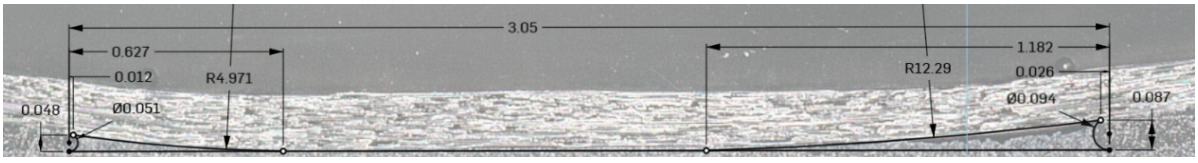

Figure 5.41: Parametrisation for the gap of tow 17, third repetition

The voids seen in figure 5.41 could be particularly well parametrised by a type three gap as both parametrised areas of the voids remained within 2 $\%$ difference from the actual traced areas.

5.2.5. Interpretation of parametrisation data

From the previous section 5.2.4 it became evident that the difference in working temperatures between the PPS substrate and the LM/PAEK tape alongside the unintended elevation in applied force had a large influence on the gap morphology. This made it significantly difficult to draw conclusions from the gaps concerning the effects of the variations in the severity of the applied process parameters. Nevertheless, all gaps, including repetitions, were parametrised and all dimensions were documented. This facilitates the identification of trends in the data that may not be discernible to the naked eye. Hence, an analysis method was found to further investigate if there are any trends in the gathered bulk data from the parametrisation of the gaps. Firstly, an analytical analysis of variables will be performed (ANOVA) to be able to determine which dimensions were most influenced by the difference in combination between process parameter settings or by which repetition they belong to. With this information in mind, these parameters can be investigated further.

Analysis of Variables (ANOVA)

An ANOVA works by comparing the means of two or more groups to see if they are significantly different from each other. In this case it works for example by taking the average value of a parameter like the gap width for different tows and checking if those means differ more than expected from random variation. It checks this by measuring how much each tow's average differs from the overall average and comparing that to how much the individual values for the gap width vary within each tow. Then if the tow averages are more spread out than the variation within each tow, the analysis will return a so-called high F-value. This value can be converted into a so-called p-value which can be used to identify if the observed difference between group means is unlikely to have occurred by chance. If this p-value is below 0.05 it indicates that the influence of the group has been large on the result, therefore indicating a clear correlation. If this value is high than the variation is likely due to random noise.

To illustrate how this works in this case, a short example will be given for the gap width, parameter w from the third gap type defined in section 5.1.5. The gap width measured for every combination of parameters and every repetition can be seen below in table 5.8.

Table 5.8: Parametrised gap width for tows and repetitions

Tow	Rep	w
Tow 11	1	3.202
Tow 11	2	2.949
Tow 11	3	3.199
Tow 13	1	3.173
Tow 13	2	2.915
Tow 13	3	3.060
Tow 14	1	3.166
Tow 14	2	2.928
Tow 14	3	3.103
Tow 15	1	3.095
Tow 15	2	2.882
Tow 15	3	2.988
Tow 17	1	3.101
Tow 17	2	2.866
Tow 17	3	3.050

From this data, the mean for every tow group could be taken as well as the mean for every repetition. So for example, the mean gap width of tow 11 can be taken and the mean gap width for all 1st repetitions. This results in the following two tables for the mean gap widths for the tow and repetition groups.

Table 5.9: Mean gap widths for tow groups

Tow	w
Tow 11	3.117
Tow 13	3.049
Tow 14	3.066
Tow 15	2.988
Tow 17	3.006

Table 5.10: Mean gap widths for repetition groups

Repetition	w
1	3.147
2	2.908
3	3.080

From these averages eventually the F-values can be computed following a series of statistical calculations. These calculations are lengthy and can be found in the Appendix chapter E. The same calculations have been performed for every dimension of the parametrised gaps. Only a few parameters yielded high F-values, resulting in p-values below 0.05. Since p-values are plotted as $-\log_{10}(p)$, taller bars indicate stronger significance. Bars above the threshold line at $-\log_{10}(0.05) \approx 1.3$ are statistically significant. This indicated that those dimensions had been significantly influenced by either the repetition or the specific combination of process parameter settings. The dimensions for which this was the case were the gap width w, the width of the right-hand void w_R, the height of the right-hand void h_R, and finally the radius of the top edge of the right-hand void R_{TR}. The corresponding values can be viewed below in figure 5.42.

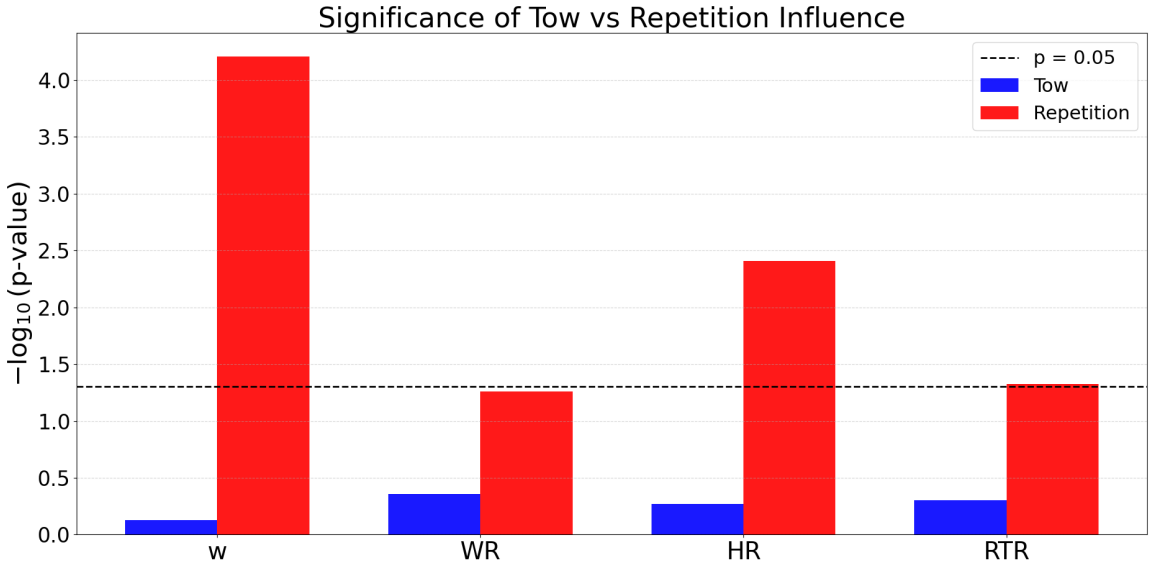

Figure 5.42: Significance of parameter combination vs repetition influence

From this graph, it can be concluded that the difference in repetition had the most influence on the magnitude of the dimensions, as only the red bars (influence of repetition) seem to approach the black dotted line.

The gap width w shows to be extremely dependent on the repetition and almost shows no influence of the combination of process parameters. Firstly, this illustrates that a variation in the combination of processing parameters had little influence on the actual width of the gap. Additionally, this further strengthens the gap width determination by the LLS, as from table 5.5 and figure 5.28 it became evident that deviation from the designed gap size was quite constant per scan. Hence, a strong influence of the repetition on the gap width makes sense.

Figure 5.42 also illustrates a strong dependence on the repetition by the dimensions w_R, h_R, and R_{TR}.

The dimensions of the left-hand void showed almost no influence and are hence not illustrated in figure 5.42. This means that the height, width, and radius of the top edge of the right-hand void depended more on the repetition than on the combination of process parameters. This is an interesting result, as it indicates that the overall dimensions of the right-hand void are dependent on the repetition. This raises the question of whether reversing the layup direction for the 90-degree layer would cause this effect to re-occur, but for the dimensions of the left-hand void.

The ANOVA was done to investigate if there would be any relations between the morphology of the gaps and the processing parameters that had not been spotted. The ANOVA, however, confirms that only a few dimensions of the gaps showed any dependency on either the repetition or process parameter combination. Furthermore, the ANOVA shows that no morphological features of the gap had been significantly influenced by the process parameter settings (tow).

To further analyse the results, plots could be made to investigate the mean, maximum, and minimum values of all force and velocity combinations on the significant parameters from the ANOVA plot. Firstly, the gap widths recorded with the LLS and microscope will be compared to further investigate the influence of repetition on w.

LLS vs Micrograph width: repetition 1

The first repetition for indicates a relatively stable difference between the gaps recorded by both methods, as can be seen in figure 5.43. No clear conclusions can be drawn on the basis of different setting combinations.

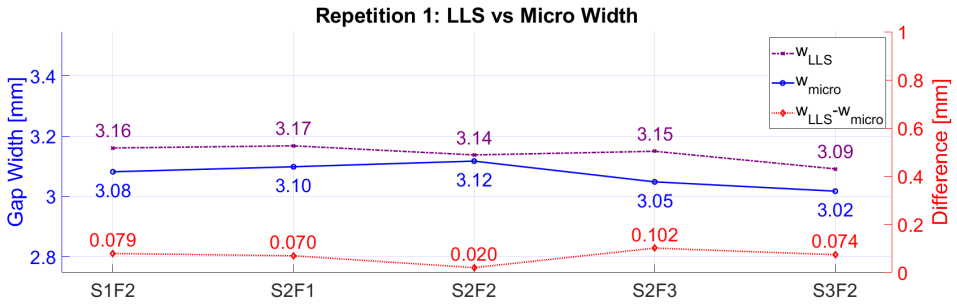

Figure 5.43: LLS vs micrograph gap widths, including error, repetition 1

LLS vs Micrograph width: repetition 2

Figure 5.44 indicates a very consistent gap size recorded from the micrographs, and does not show a dependence on the parameter setting combinations. Nevertheless, combination S2F2 does show a clear reduction in gap size by the LLS data, but the following combination does not follow up on this reduction, which is reason to believe this has not been influenced by the setting combination.

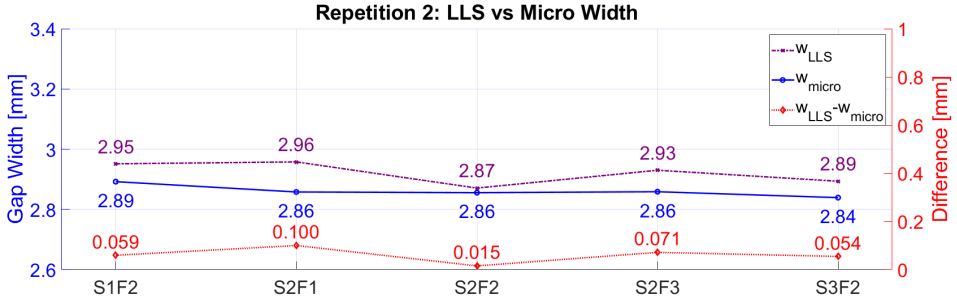

Figure 5.44: LLS vs micrograph gap widths, including error, repetition 2

LLS vs Micrograph width: repetition 3

The data in figure 5.45 fluctuates relatively much compared to the previous repetitions. Additionally, the gap widths recorded by both methods show a significant drop in gap width for the highest force setting

compared to the other combinations using the same speed. Hence, this does show some correlation between the process parameter setting force and the resulting gap width.

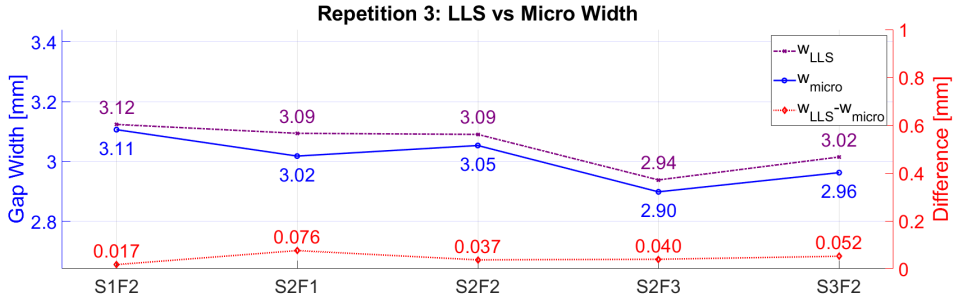

Figure 5.45: LLS vs micrograph gap widths, including error, repetition 3

From figures 5.43, 5.44 and 5.45 the claim that the gap width is significantly dependent on the repetition has been strengthened as it can clearly be seen that the gap widths remain quite constant within the repetition groups and that the influence of the combinations displayed in every figure is minimal.

Right-hand void metrics plotted per subgroup

This section shows plots that indicate the values obtained for the dimensions of the right-hand void for the force levels with subgroups for the different speeds and vice versa.

The plot below in figure 5.46 shows the deviation in w_R across different force levels, including the different speed subsets. This plot shows large overlaps between the w_R bars for different force levels. This overlap entails that the influence of the force level on the magnitude of w_R is difficult to distinguish. Nevertheless, it is quite evident from figure 5.46 that F3 results in a significantly smaller w_R.

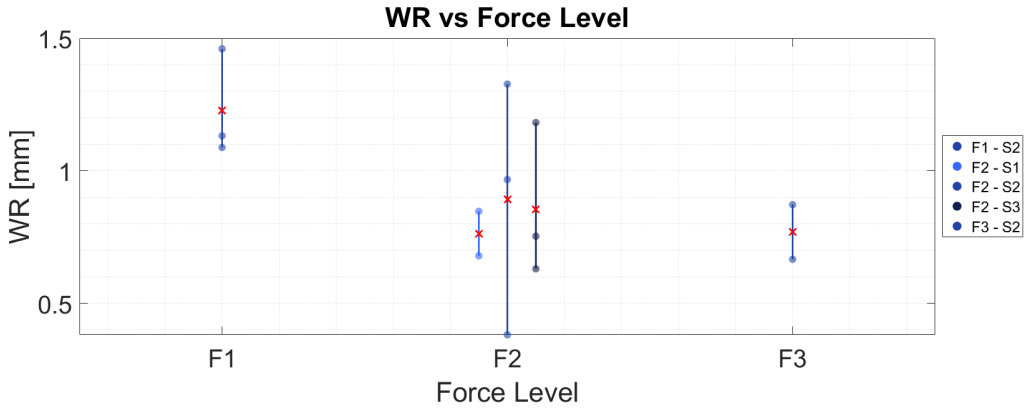

Figure 5.46: w_R for different force levels, including speed level subsets

Figure 5.46 shows all values obtained for the different combinations between speed and force on w_R. It connects the maximum and minimum values by a line and plots the average as a red cross. Figure 5.47 plots w_R to the different speed levels, also indicating a significant amount of overlapping between the bars. The bar for the combination S2-F2 seems to be overlapping almost completely with every other bar. Making it hard to draw conclusions from this graph. Although, the mean for the combination S2-F1 does seem to be significantly higher than the other means, possibly suggesting that a lower force could result in a larger right-hand void.

Figure 5.47: w_R for different speed levels, including force level subsets

Figure 5.48 shows the plot for h_R, the height of the right-hand void, for the different force levels. This plot indicates that there is no large difference in mean h_R values for different force levels. Additionally, relatively large portions of the bars are overlapping, which makes it difficult to draw conclusions on the effect of the force on the h_R values. However, h_R does seem significantly lower for F3 than for F1.

Figure 5.48: h_R for different force levels, including speed level subsets

Figure 5.49 shows similar effects as figure 5.48. The means differ only slightly between speed levels. This, in combination with the bars overlapping largely makes it difficult to draw meaningful conclusions from the plot.

Figure 5.49: h_R for different speed levels, including force level subsets

Figure 5.50 shows the plot for R_{TR}, the radius of the top edge of the right-hand void, for the different

force levels including speed subsets. R_{TR} seems to decrease from F1 to F2. Additionally, within F2 the value for R_{TR} changes significantly with regard to the different speed subsets, making it more difficult to identify a trend. The bar for F3 is very small, indicating that the recorded R_{TR} for this combination of parameters was quite consistent across repetitions.

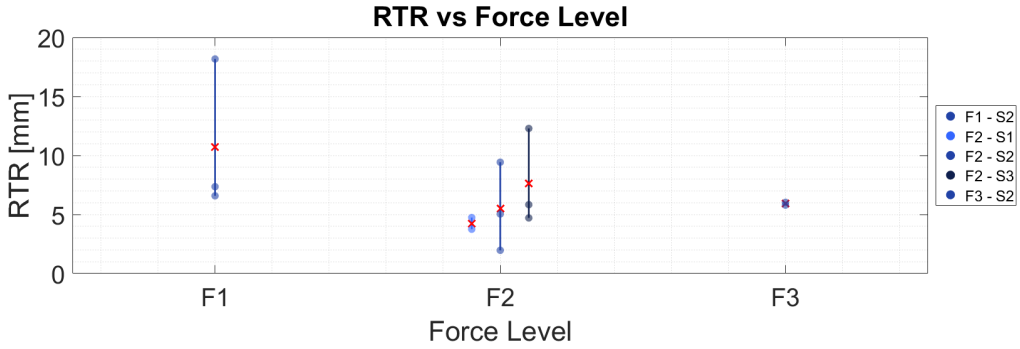

Figure 5.50: R_{TR} for different force levels, including speed level subsets

In figure 5.51 it can be seen that again in general there is a notable overlap between the bars for different speed levels. This makes it difficult to draw any conclusions on the effect of speed on R_{TR}. The variability at the first speed level appears relatively low, whereas the second speed level exhibits a much wider spread due to the inclusion of samples from multiple force levels, suggesting that the observed differences in R_{TR} may be more strongly influenced by the interaction between speed and force or by repetition effects rather than by speed alone.

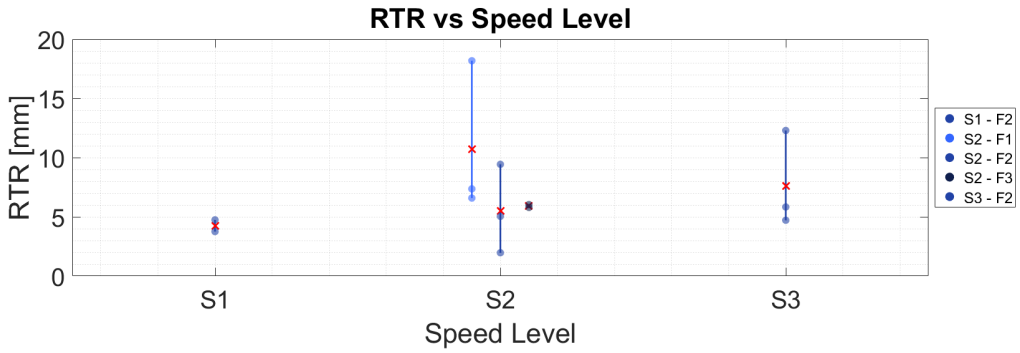

Figure 5.51: R_{TR} for different speed levels, including force level subsets

These plots conclude the analysis for the second trial. Hence, completing the analysis. After the analysis, the results can be discussed in the following section.

5.3. Discussion

This section provides a detailed summary of the results achieved from both trials. It provides an interpretation and discussion of these results. Sections 5.3.1 and 5.3.2 will discuss the results from trials one and two respectively.

5.3.1. Results Trial One

Trial One revealed a strong correlation between the nominal gap size and the resulting gap morphology after the in-situ consolidation during the AFP process. By varying the initial gap width from 0 mm to 6.35 mm, two main morphological categories were observed with one cross-over point. These included entirely open gaps (Type 1), single-point closure cross-over point (Type 2), and a gap that closed over a distance (Type 3). This clear progression shows that gap width governs whether a gap closes under thermal and mechanical load, with a threshold near half a tow width, the cross-over point (Type 2).

This was shown, however, for constant processing parameters in Trial One which was different for the second Trial.

The defined metrics for each type, such as arc radii, void widths, and void heights, provided a meaningful quantitative framework for describing the geometry of these defects. Type 1 gaps required the fewest parameters to fully describe them, as their top edge could be parametrised by a single circular arc segment. In contrast, the closed gap types (Type 2 and Type 3) necessitated separate measurements for the left-hand and right-hand voids. This illustrates that those gap types are slightly more complex and require additional descriptors.

An insightful observation came from comparing the Laser Line Scanner (LLS) data with the micrograph measurements. The LLS data, that was captured after the first 0-degree layer, consistently reported narrower gaps than those programmed. This indicates that the tape indeed adhered to the previous findings stating that the tape would be compressed during the production from 6.35 mm to somewhere around 7 mm. Hence, the gap edges moved slightly inwards from the initial design, creating slightly smaller gap widths. Additionally, after placing the 90-degree layer, the gaps narrowed further. This demonstrates that the second application of heat and pressure has a compounding effect, reinforcing gap closure. Thus, the additional compaction from the top layer not only influences bonding but also contributes to gap closure.

These findings support the hypothesis that the edges of the gap adhere to some sort of curved geometries under consolidation. Even in closed gap cases, the top does not flatten completely to a linear geometry but retains an arced shape, hence refuting the hypothesis that closed gaps would have linear top edges for the voids. The data gathered from the first trial indicates that gap width is a crucial parameter for its morphology as it influences which category can be used to parametrise its shape.

In summary, Trial One successfully established a repeatable classification scheme and metric set for describing gap morphology. These results now provide a baseline for evaluating how variations in processing parameters can drive similar changes, which were investigated in Trial Two.

5.3.2. Results Trial Two

This trial, Trial Two, investigated whether a change in the processing conditions layup velocity and consolidation force could induce changes to a gap's morphology, specifically if it could mean a shift in a gap's morphological type. For example, if a type 1 gap could shift to a type 3 gap. This was done by holding the nominal gap width fixed at 3.175 (a suspected tipping point between gap types 1 and 3) and applying three different settings for the layup velocity and consolidation force.

The findings showed a large influence of the force used during the production of the laminate on the gap morphology. Due to an overshoot in applied force, the actual compaction levels were considerably higher than intended. As a result, most of the gaps in all conditions were nearly or entirely closed, falling into the type 3 gap category. This also applied to the combination with the highest speed, which was initially expected to give a gap that remained more open than closed. Although the near or complete closure of all gaps indicates that consolidation force is likely a dominant factor in the AFP process, the use of a different material for the substrate complicates this conclusion, as it prevents isolating the effects of force alone.

The substrate that was used for this trial was made of a material called PPS. This material has a considerably lower working temperature than the tape material. This caused the substrate material to be in a more molten state during the production than the tape, allowing for the substrate material to flow into the voids. Additionally, due to its increased molten state, the tape material was likely pressed further into the substrate, contributing to even more extensive filling of the voids. Consequently, the differences between the gap morphologies across different combinations of process parameter settings

were masked by the substrate's contribution to void filling. This result illustrates the importance of considering material thermal compatibility as it can influence the evaluation process.

Despite the narrowing of differences across samples, the morphological classification method from Trial One remained applicable by making the same assumption for the linear bottom edge of the gap. With this assumption, all gaps could still be parametrised using either a type 1 or type 3 gap. Again, no cases were found that matched an exact type 2 gap, demonstrating its behaviour as a cross-over point. Hence, proving the system's robustness. However, it has to be noted that only two gaps adhered to a type 1 gap.

A more subtle insight emerged from the asymmetrical behaviour of the gap voids. The right-hand void's dimensions varied consistently between repetitions but not between different combinations, while the left-hand void's dimensions did not show a dependence on either. This repeatable asymmetry suggests an influence of layup direction, where a change in layup direction may cause one side of the gap to receive different thermal exposure. This observation supports the hypothesis from Trial One that layup direction affects gap morphology, even when geometry is held constant.

Taken together, the results of Trial Two reinforce the notion that both geometry and process parameter settings can govern gap closure. In fact, the excessive compaction and heat observed in the second trial had an effect comparable to an increase in gap width for the first trial. This parallel highlights that both process parameters and initial gap geometry can govern the type with which the gap can be classified.

Therefore, coming back to the research question about what processing parameters would have the greatest influence on the morphological features of gaps. This work suggests that the consolidation force has had more of an influence on the quantitative metrics describing the gaps than the layup velocity. Although, due to the combination of too high consolidation force and mismatch in working temperatures between the substrate and tapes, the effect of processing parameters could have been different if these discrepancies would have had less of an effect.

6

Conclusion

The manufacturing process of in-situ consolidated thermoplastic automated fibre placement (ISC-TP AFP) can induce defects into the resulting laminate. One of the most common defects encountered when producing laminates with this process are gaps. These defects occur when there is a space in between placed tows, either due to geometrical variations in the tows or due to process variations. These gaps play a significant role in the quality and mechanical properties of the produced laminate. This makes it important to understand these gaps thoroughly. Therefore, it is necessary to investigate the formation of gaps rigorously. The ISC-TP AFP process involves several process parameters that can influence gap formation, including layup velocity, nip-point temperature, and consolidation force. These parameters not only play a role in gap formation but also in gap shape and size, or in other words, on the gap's morphology. Quantifying a gap's morphology could provide current research with a better understanding of gaps and allow for a unified method of identifying certain morphological features. Currently, there is no research focused on gap morphology in thermoplastic composites, making it challenging to ensure consistency and clarity when discussing or comparing findings across studies. This work aimed to address this gap by establishing a clear and consistent method for defining gap morphology in thermoplastic composites. In addition, the influence of key process parameters on gap morphology was systematically investigated to identify potential trends between processing conditions and morphological characteristics.

The experimental study presented in this thesis demonstrated that gaps formed during the ISC-TP AFP process could be categorised with three types of morphology. The necessary substrates used for this study caused effects not considered to be representative of a laminate where the bottom edge of the gap is of the same material as the sides and top. Therefore, the bottom of both gap edges were connected by a straight line. Nevertheless, with this in mind, all gaps produced showed behaviour in line with one of the three gap types. For the top and side edges of the gap, fitting circular arcs proved to be an accurate parametrisation of their shape, offering an optimal balance between geometric precision and repeatability.

This confirms the initial hypothesis that the gap edges would follow a curved geometry. While other curved geometries such as parabolas were considered, the circular arc edge geometry was preferred for its high accuracy in combination with its repeatability. Furthermore, as hypothesised, the top edge of the gap also showed a curved profile in open gaps. However, the same behaviour was found for when the gap completely closed, hence refuting the hypothesis that when the gap closes the top edges would become linear. Lastly, the hypothesis that the actual width of the gap would influence the morphology was also confirmed, which directly resulted in three different types of gaps dependent on their width.

For the first gap type, the complete top edge of the gap can be well parametrised by a singular circular

arc connecting the left and right arcs of the edges. The second and third gap types closed completely, resulting in two voids. The left-hand and right-hand voids. Both top edges of these voids could be well parametrised by circular arcs. The second gap type requires that these arcs must meet at their intersection with the bottom linear gap edge. This does not mean their radii must be the same, as this intersection does not have to be in the middle of the gap. For the third gap type, both top edge circular arcs intersect the bottom edge at a different location, resulting in a gap that remains closed for a set distance. In summary, the parametrisation procedure begins by identifying the applicable gap type, followed by fitting a linear bottom edge and circular arcs to the top and side boundaries. This results in a table with quantitative dimensional metrics that accurately describes the gap morphology. The parametrisation described above offers a clear and concise approach to capturing gap morphology, allowing for more consistent gap mapping and enabling effective comparison across different processes, thereby improving clarity and communication within the field concerning ISC-TP AFP produced laminates. This allows further research on different aspects of ISC-TP AFP produced laminates with gaps to refer back to this study and relate their results to different morphological features of their specific gaps.

The second part of this experimental study demonstrated the effect of several processing parameters on the previously determined quantitative metrics of the gap morphology. This study investigated the effect of the layup velocity and consolidation force during the placement of the top tow of the gap on the dimensions of the gaps while keeping the nip-point temperature constant. For this part of the study, a fixed gap width of 3.175 mm (1/2”) was chosen, as from the first part of this study this width turned out to be close to the point where the gap type could switch from a type one gap to a type two gap. The results of the experiment turned out to be inconclusive. A significant mismatch between the working temperatures of the substrate and the tows caused the substrate material to flow into the voids. In addition, excessive force during placement pressed down the top boundary, consistently closing the gap across all combinations of process parameters tested. The combination of both effects made it difficult to spot meaningful relations between process parameter settings and the quantitative metrics regarding gap morphology.

As a result, the hypothesis that the process parameter combinations would show a clear influence on the morphological features of the gaps could not be conclusively confirmed. The expectation that an increased layup velocity would result in gaps with less closure could not be validated because all gaps closed regardless of the velocity setting. Similarly, while higher pressures were expected to increase closure and filling, the excessive consolidation force applied uniformly across tests obscured more subtle effects. Temperature influence, while hypothesised to reduce viscosity and promote filling, was not isolated due to the temperature mismatch between substrate and tows. Still, the fact that all gaps closed under every condition suggests that the combination of excessive pressure and the temperature mismatch was enough to cause full closure.

This study therefore highlights the importance of providing a robust and accurate system for determining the consolidation force during the process. Furthermore, the choice of substrate material was shown to have a significant influence on the manner gaps could be perceived. Nevertheless, the results from this study are still valuable for future work. The fact that the voids consistently filled with PPS substrate material is not necessarily problematic. A laminate with overall less void volume could prove to have improved mechanical properties to a laminate with the same sized voids but less filled with substrate material.

Lastly, the final sub-research question and hence its hypothesis could not be answered due to time limitations. However, from the analysis of the second trial, it became evident that only the right-hand void’s morphological metrics had been significantly influenced by the process. This prompts the question of whether a different layup direction would have influenced other metrics, but the hypothesis could not be confirmed nor refuted.

Hence, this study provides a detailed procedure to characterise gap morphology enabling effective gap

comparison for future work regarding ISC-TP AFP produced laminates. Furthermore, the second part of the study highlights the importance of a robust consolidation force monitoring system and the effects of the substrate on gap morphology.

7

Recommendations

Throughout the experimental and analytical phases of this research, several aspects were encountered that could be valuable for future work related to the topic of this thesis.

Substrate choice
Both experiments were initially designed to be placed onto an aluminium tool directly. This stacking sequence would have resulted in a straight bottom edge for the gap. The main challenge with this is that thermoplastic material is not sticky before and after being exposed to heat. This means that the tows do not stick to the tool before and after placement. This was a known fact, and a solution was devised. The solution entailed placing horizontal tows at the top and bottom underneath the first layer. These tows were tensioned and then fixed to the tool by taping them onto it. This allowed the first layer to stick to these horizontal tows at the beginning and end of its tow path. However, most likely due to play in the horizontal tows when placing a tow next to a previously placed tow, the previously placed tow would bulge up. This caused this tow to come too close to the Humm3 and burn. Therefore, both experiments were forced to use pre-manufactured substrates.

The substrate used in the first batch of samples was of the same material as the tows (LM/PAEK). This substrate; however, had a woven structure. This resulted in convoluted micrographs, which could be hard to interpret at first. Moreover, this woven structure caused a noisy bottom edge of the gap, requiring the need for the flat bottom line assumption to be able to define the morphology. The substrate used in the second batch of samples was chosen because of its clear stacking sequence, including an already manufactured 0-degree top layer. Although this did result in less convoluted micrographs, the fact that the substrate material was not the same as the tow material caused a mismatch in working temperatures. The working temperature of the substrate was around 100 C° lower than that of the tow. This caused the voids at the gap edges to consistently almost completely fill with substrate. Moreover, the tows had also likely been pressed into the substrate.

Therefore, the recommendations for future work it would be interesting to investigate the effect of the substrate on the gap morphology even further. This study often neglected the effect of the substrate as the main focus was on the gap. However, the substrates used for both trials showed distinctly different behaviour, hence making the investigation in the effects of this substrate an interesting topic.

Asymmetric gap edge morphology
This work investigated gaps created by the AFP process for two trials. Both trials made use of a similar stacking sequence, [Substrate/0/90]. Where the layup direction for the 90-degree layers in both trials was the same, from right to left. The results for the first trial already indicated asymmetric behaviour for the gap edges, raising the question of whether the layup direction for the top layer could have influenced the gap morphology. The right edge of the gap consistently exhibited smaller radii, which was further

supported by the Laser Line Scanner data, as the slope of the captured profile was consistently less steep on the right side compared to the left. It was hypothesised that this phenomenon could have occurred due to a shadow created by the 90-degree layup direction below the left gap edge, which was significantly less at the right edge due to this directionality. Hence, more of the right edge was heated and therefore its viscosity lowered, making it more susceptible to the consolidation pressure and thus flattening this gap edge more.
The results for the second trial again showed interesting results for the dimensions of the right-hand void of the gap. Although trends were not immediately apparent through visual inspection, analysis of the bulk data revealed a consistent effect of the process parameters on the dimensions of the right-hand void. The dimensions showed a significant dependence on the repetition of the sample. This could indicate that again the morphology of the right edge of the gap has been significantly influenced by the layup direction of the 90-degree tow. Therefore, these findings provide additional support to the hypothesis made previously for this phenomenon.
From these findings and the hypothesis, a recommendation for future work can be made. This work suggests a strong correlation between the layup direction of the top tow of a gap and the morphology of the edges. During AFP production, it is not uncommon for the robotic arm to rotate 180 degrees after placing the first 90-degree tow to place the second in the opposite direction, as this minimises production time.

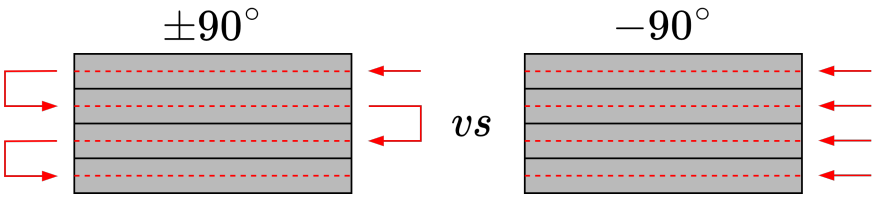

Figure 7.1: Layup direction 90-degree layer schematic, practice (left) this work (right)

Figure 7.1 illustrates the manner in which the 90-degree layer was programmed in this study, compared to an alternating layup direction (±90°), which could be used in practice to reduce production time by avoiding repeated head rotations. This highlights the importance of being aware of the effect the directionality of the layup can have on the morphology of the gaps that can be introduced during manufacturing.
Therefore, it is recommended that future research systematically investigates the influence of layup directionality on gap edge morphology. This could involve controlled experiments where the layup direction of the top tow is intentionally varied while keeping all other parameters constant, allowing for a clearer isolation of its effect. Such work could not only confirm the hypothesis made in this study but could also provide valuable guidance for optimising AFP layup strategies to minimise undesirable defects.

Stacking sequence variations
This work presents a detailed approach for describing a gap's morphology. This was done for two trials utilising the same stacking sequence, although the substrate material was different. The metrics defined for the first trial were also able to be applied to the gaps of the second trial. The fact that both trials shared a similar stacking sequence will probably have contributed to this. Therefore, this raises the question of whether a change in stacking sequence of the laminate would also result in fundamentally different gap morphologies. For example, this work used a stacking sequence of [Substrate/0/90] but it would be interesting to see the effect of a stacking sequence like [Substrate/0/45]. This could mean that the circular edge geometries no longer present an accurate contour parametrisation. Hence, for future work, it could be interesting to perform a similar analysis to this work but for a different stacking sequence, as the morphology of the gap is likely to be influenced by the used stacking sequence. This is illustrated below in figure 7.2 on the right.

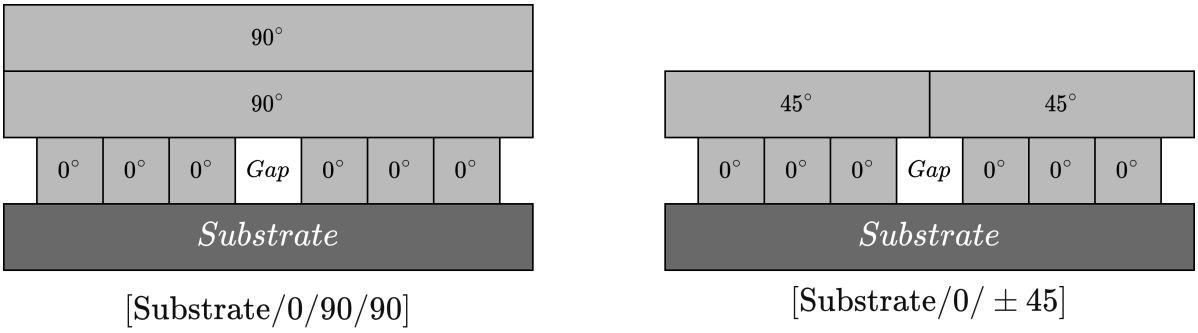

Figure 7.2: Multi-ply variation (left), stacking sequence variation (right)

Not only would it be interesting to investigate the stacking sequence, but also to explore how morphological behaviour evolves when a second 90-degree ply is placed on top of an existing one. As indicated on the left of figure 7.2. This would simulate a situation in which a gap undergoes a second round of consolidation due to the additional heating and pressing from subsequent layers. It could offer valuable insights by observing how the morphology of the gap changes if it is heated and pressed one more time compared to this research. If it closes considerably more, for example, this could be beneficial for the mechanical properties of the final laminate. Hence, such research could further clarify whether gap characteristics observed after a single ply remain stable or evolve through the layup sequence.

Influence of morphological metrics on mechanical properties

Based on the analysis conducted in this study, the morphological features of gaps were successfully parametrised, resulting in a set of metrics that quantitatively describe their dimensions. This was the main goal for trial one, which was again used to parametrise the gaps found for the second trial. As the presented study is solely focused on the morphology of the gaps, it did not investigate or discuss the possible consequences the gaps can have on a laminate's mechanical properties. However, with the metrics found in this work, it becomes possible to explore how specific morphological features influence performance. For example, it would be insightful to examine how variations in the radius of the top edge of a type one gap affect the mechanical behaviour of the laminate. It is therefore recommended for future investigations to use this study as a foundation for investigating the relationship between gap morphology and mechanical performance in ISC-TP AFP laminates.

References

[1] dictionary.com. “Morphology definition.” Accessed: 2025-01-16. (2025), [Online]. Available: https://www.dictionary.com/browse/morphology.

[2] OYLA Magazine. “A combination of properties.” Accessed: 2025-07-03. (2021), [Online]. Available: https://oyla.us/2021/03/a-combination-of-properties/.

[3] J. Guo and S. Wang, “Multiphase flow coupling behavior of bubbles based on computational fluid dynamics during afp process: The behavior characteristics of bubbles during afp process,” *Advances in Materials Science and Engineering*, vol. 2021, p. 12, 2021, Open Access; accessed 2025-07-03. DOI: 10.1155/2021/3237713. [Online]. Available: https://doi.org/10.1155/2021/3237713.

[4] F. Diemar, J. Holmes, S. Sommacal, *et al.*, “X-ray micro-computed tomography for mechanical behaviour analysis of automated fiber placement (AFP) laminates with integrated gaps and overlaps,” *Composite Structures*, vol. 351, p. 118 601, Jan. 2025, ISSN: 02638223. DOI: 10.1016/j.compstruct.2024.118601. [Online]. Available: https://linkinghub.elsevier.com/retrieve/pii/S0263822324007293 (visited on 11/26/2024).

[5] D. Del Rossi, V. Cadran, P. Thakur, M. Palardy-Sim, M. Lapalme, and L. Lessard, “Experimental investigation of the effect of half gap/half overlap defects on the strength of composite structures fabricated using automated fibre placement (AFP),” *Composites Part A: Applied Science and Manufacturing*, vol. 150, p. 106 610, Nov. 2021, ISSN: 1359835X. DOI: 10.1016/j.compositesa.2021.106610. [Online]. Available: https://linkinghub.elsevier.com/retrieve/pii/S1359835X21003286 (visited on 02/12/2025).

[6] M. A. Khan, P. Mitschang, and R. Schledjewski, “Parametric study on processing parameters and resulting part quality through thermoplastic tape placement process,” *Journal of Composite Materials*, vol. 47, no. 4, pp. 485–499, Feb. 1, 2013, Publisher: SAGE Publications Ltd STM, ISSN: 0021-9983. DOI: 10.1177/0021998312441810. [Online]. Available: https://doi.org/10.1177/0021998312441810 (visited on 11/21/2024).

[7] E. Oromiehie, A. K. Gain, and B. G. Prusty, “Processing parameter optimisation for automated fibre placement (AFP) manufactured thermoplastic composites,” *Composite Structures*, vol. 272, p. 114 223, Sep. 2021, ISSN: 02638223. DOI: 10.1016/j.compstruct.2021.114223. [Online]. Available: https://linkinghub.elsevier.com/retrieve/pii/S0263822321006851 (visited on 12/04/2024).

[8] Y. D. Boon, S. C. Joshi, S. K. Bhudolia, and G. Gohel, “Recent advances on the design automation for performance-optimized fiber reinforced polymer composite components,” *Journal of Composites Science*, vol. 4, no. 2, p. 61, 2020. DOI: 10.3390/jcs4020061. [Online]. Available: https://www.mdpi.com/2504-477X/4/2/61.

[9] S. Ranganathan, S. G. Advani, and M. A. Lamontia, “A non-isothermal process model for consolidation and void reduction during in-situ tow placement of thermoplastic composites,” *Journal of Composite Materials*, vol. 29, no. 8, pp. 1040–1062, May 1, 1995, Publisher: SAGE Publications Ltd STM, ISSN: 0021-9983. DOI: 10.1177/002199839502900803. [Online]. Available: https://doi.org/10.1177/002199839502900803 (visited on 01/23/2025).

[10] N. Dong, C. Luan, X. Yao, *et al.*, “Influence of process parameters on the interlaminar shear strength of CF/PEEK composites in-situ consolidated by laser-assisted automated fiber placement,” *Composites Science and Technology*, vol. 258, p. 110 902, Nov. 2024, ISSN: 02663538. DOI: 10.1016/j.compscitech.2024.110902. [Online]. Available: https://linkinghub.elsevier.com/retrieve/pii/S026635382400472X (visited on 12/04/2024).

[11] M. Di Francesco, L. Veldenz, G. Dell'Anno, and K. Potter, "Heater power control for multi-material, variable speed automated fibre placement," *Composites Part A: Applied Science and Manufacturing*, vol. 101, pp. 408–421, Oct. 2017, ISSN: 1359835X. DOI: 10.1016/j.compositesa.2017.06.015. [Online]. Available: https://linkinghub.elsevier.com/retrieve/pii/S1359835X17302427 (visited on 01/07/2025).

[12] T. A. Sebaey, M. Bouhrara, and N. O'dowd, "Fibre alignment and void assessment in thermoplastic carbon fibre reinforced polymers manufactured by automated tape placement," *Polymers 2021, Vol. 13, Page 473*, vol. 13, no. 3, p. 473, Feb. 2021, Publisher: Multidisciplinary Digital Publishing Institute, ISSN: 2073-4360. DOI: 10.3390/POLYM13030473. [Online]. Available: https://www.mdpi.com/2073-4360/13/3/473/htm%20https://www.mdpi.com/2073-4360/13/3/473.

[13] H. Pérez-Martín, S. Buchalik-Bopp, B. E. Guettler, *et al.*, "Effect of crystallinity and morphology on the mechanical properties of CF/PEKK composites manufactured under compression moulding and automated tape placement," *Materials Today Communications*, vol. 36, p. 106 442, Aug. 2023, ISSN: 23524928. DOI: 10.1016/j.mtcomm.2023.106442.

[14] W. Grouve, L. Warnet, B. Rietman, H. Visser, and R. Akkerman, "Optimization of the tape placement process parameters for carbon–PPS composites," *Composites Part A: Applied Science and Manufacturing*, vol. 50, pp. 44–53, Jul. 2013, ISSN: 1359835X. DOI: 10.1016/j.compositesa.2013.03.003. [Online]. Available: https://linkinghub.elsevier.com/retrieve/pii/S1359835X13000742 (visited on 12/17/2024).

[15] E. Oromiehie, B. G. Prusty, P. Compston, and G. Rajan, "Automated fibre placement based composite structures: Review on the defects, impacts and inspections techniques," *Composite Structures*, vol. 224, p. 110 987, Sep. 2019, ISSN: 02638223. DOI: 10.1016/j.compstruct.2019.110987. [Online]. Available: https://linkinghub.elsevier.com/retrieve/pii/S0263822319308281 (visited on 01/23/2025).

[16] S. C. Mantell and G. S. Springer, "Manufacturing process models for thermoplastic composites," *Journal of Composite Materials*, vol. 26, no. 16, pp. 2348–2377, Jan. 1, 1992, Publisher: SAGE Publications Ltd STM, ISSN: 0021-9983. DOI: 10.1177/002199839202601602. [Online]. Available: https://doi.org/10.1177/002199839202601602 (visited on 11/21/2024).

[17] Z. Qureshi, T. Swait, R. Scaife, and H. El-Dessouky, "In situ consolidation of thermoplastic prepreg tape using automated tape placement technology: Potential and possibilities," *Composites Part B: Engineering*, vol. 66, pp. 255–267, Nov. 2014, ISSN: 13598368. DOI: 10.1016/j.compositesb.2014.05.025. [Online]. Available: https://linkinghub.elsevier.com/retrieve/pii/S1359836814002388 (visited on 12/12/2024).

[18] O. Aghababaei Tafreshi, S. Van Hoa, F. Shadmehri, D. M. Hoang, and D. Rosca, "Determination of convective heat transfer coefficient for automated fiber placement (AFP) for thermoplastic composites using hot gas torch," *Advanced Manufacturing: Polymer & Composites Science*, vol. 6, no. 2, pp. 86–100, Apr. 2, 2020, Publisher: Taylor & Francis, see DOI link for e-print, ISSN: 2055-0340. DOI: 10.1080/20550340.2020.1764236. [Online]. Available: https://doi.org/10.1080/20550340.2020.1764236 (visited on 01/07/2025).

[19] R. Funck and M. Neitzel, "Improved thermoplastic tape winding using laser or direct-flame heating," *Composites Manufacturing*, vol. 6, no. 3, pp. 189–192, Jan. 1995, ISSN: 09567143. DOI: 10.1016/0956-7143(95)95010-V. [Online]. Available: https://linkinghub.elsevier.com/retrieve/pii/095671439595010V (visited on 01/07/2025).

[20] K. Yassin and M. Hojjati, "Processing of thermoplastic matrix composites through automated fiber placement and tape laying methods: A review," *Journal of Thermoplastic Composite Materials*, vol. 31, no. 12, pp. 1676–1725, Dec. 1, 2018, Publisher: SAGE Publications Ltd STM, ISSN: 0892-7057. DOI: 10.1177/0892705717738305. [Online]. Available: https://doi.org/10.1177/0892705717738305 (visited on 01/07/2025).

[21] V. Agarwal, R. L. Mccullough, and J. M. Schultz, "The thermoplastic laser-assisted consolidation process-mechanical and microstructure characterization," *Journal of Thermoplastic Composite Materials*, vol. 9, no. 4, pp. 365–380, Oct. 1, 1996, Publisher: SAGE Publications Ltd STM, ISSN: 0892-7057. DOI: 10.1177/089270579600900405. [Online]. Available: https://doi.org/10.1177/089270579600900405 (visited on 01/08/2025).

[22] B. Lauke and K. Friedrich, “Evaluation of processing parameters of thermoplastic composites fabricated by filament winding,” *Composites Manufacturing*, vol. 4, no. 2, pp. 93–101, Jun. 1993, ISSN: 09567143. DOI: 10.1016/0956-7143(93)90076-K. [Online]. Available: https://linkinghub.elsevier.com/retrieve/pii/095671439390076K (visited on 01/08/2025).

[23] D. W. Good, D. P. Johnston, R. A. Buscaglia, and J. A. Johnston, “Ir heating system for automated thermoplastic tape placement process,” in *SAE Technical Paper Series*, SAE International, 2007. DOI: 10.4271/2007-01-3842. [Online]. Available: https://doi.org/10.4271/2007-01-3842.

[24] J. Romagna, G. Ziegmann, and M. Flemming, “Thermoplastic filament winding—an experimental investigation of the on-line consolidation of poly(ether imide) fit preforms,” *Composites Manufacturing*, vol. 6, no. 3, pp. 205–210, Jan. 1995, ISSN: 09567143. DOI: 10.1016/0956-7143(95)95013-O. [Online]. Available: https://linkinghub.elsevier.com/retrieve/pii/0956714395950130 (visited on 01/08/2025).

[25] *Humm3: High-performance light source for industrial applications*, Available: https://www.noblelight.com/media/media/hng/doc_hng/products_and_solutions_1/arc_and_flash_lamps_1/Humm3_ebook_EN.pdf [Accessed Jan. 8, 2025].

[26] D. Tavkari, V. V. Ganesan, S. Amgai, A. Jain, and P. Davidson, “Thermal characterization of xenon-arc flash lamp heating system for automated fiber placement (AFP) of thermoplastic composites,” *Composites Part A: Applied Science and Manufacturing*, vol. 190, p. 108 568, Mar. 2025, ISSN: 1359835X. DOI: 10.1016/j.compositesa.2024.108568. [Online]. Available: https://linkinghub.elsevier.com/retrieve/pii/S1359835X24005669 (visited on 12/17/2024).

[27] L. Brandt, D. Deden, F. J. C. Fischer, *et al.*, “XENON FLASHLAMP BASED IN-SITU AUTOMATED FIBER PLACEMENT OF THERMOPLASTIC COMPOSITES,”

[28] A. Legenstein and E. Fauster, “Effect of flashlamp heating system parameters on the wedge peel strength of thermoplastic carbon fiber tape in the automated tape placement process,” *Journal of Manufacturing and Materials Processing*, vol. 8, no. 3, p. 91, Jun. 2024, Number: 3 Publisher: Multidisciplinary Digital Publishing Institute, ISSN: 2504-4494. DOI: 10.3390/jmmp8030091. [Online]. Available: https://www.mdpi.com/2504-4494/8/3/91 (visited on 12/03/2024).

[29] M. I. Okereke, “Prediction of finite deformation of thermoplastic matrix composites,”

[30] M. Mehdikhani, L. Gorbatikh, I. Verpoest, and S. V. Lomov, “Voids in fiber-reinforced polymer composites: A review on their formation, characteristics, and effects on mechanical performance,” *Journal of Composite Materials*, vol. 53, no. 12, pp. 1579–1669, May 1, 2019, Publisher: SAGE Publications Ltd STM, ISSN: 0021-9983. DOI: 10.1177/0021998318772152. [Online]. Available: https://doi.org/10.1177/0021998318772152 (visited on 11/26/2024).

[31] S. Krishnappa and S. Gururaja, “Numerical investigation of intrinsic competing damage mechanisms in unidirectional fiber reinforced polymer composites under compression,” *Mechanics of Advanced Materials and Structures*, vol. 31, no. 27, pp. 9468–9485, Dec. 2, 2024, Publisher: Taylor & Francis _eprint: https://doi.org/10.1080/15376494.2023.2274140, ISSN: 1537-6494. DOI: 10.1080/15376494.2023.2274140. [Online]. Available: https://doi.org/10.1080/15376494.2023.2274140 (visited on 02/18/2025).

[32] F. Heinecke and C. Willberg, “Manufacturing-induced imperfections in composite parts manufactured via automated fiber placement,” *Journal of Composites Science*, vol. 3, no. 2, p. 56, Jun. 2, 2019, ISSN: 2504-477X. DOI: 10.3390/jcs3020056. [Online]. Available: https://www.mdpi.com/2504-477X/3/2/56 (visited on 11/27/2024).

[33] A. Rajasekaran and F. Shadmehri, “Steering of carbon fiber/PEEK tapes using hot gas torch-assisted automated fiber placement,” *Journal of Thermoplastic Composite Materials*, vol. 36, no. 4, pp. 1651–1679, Apr. 1, 2023, Publisher: SAGE Publications Ltd STM, ISSN: 0892-7057. DOI: 10.1177/08927057211067962. [Online]. Available: https://doi.org/10.1177/08927057211067962 (visited on 01/23/2025).

[34] G. Rousseau, R. Wehbe, J. Halbritter, and R. Harik, “Automated fiber placement path planning: A state-of-the-art review,” *Computer-Aided Design and Applications*, vol. 16, no. 2, pp. 172–203, Aug. 13, 2018, ISSN: 16864360. DOI: 10.14733/cadaps.2019.172-203. [Online]. Available: http://cad-journal.net/files/vol_16/Vol16No2.html (visited on 01/23/2025).

[35] R. Harik, C. Saidy, S. J. Williams, Z. Gurdal, and B. Grimsley, “AUTOMATED FIBER PLACEMENT DEFECT IDENTITY CARDS: CAUSE, ANTICIPATION, EXISTENCE, SIGNIFICANCE, AND PROGRESSION,”

[36] B. Böckl, A. Wedel, A. Misik, and K. Drechsler, “Effects of defects in automated fiber placement laminates and its correlation to automated optical inspection results,” *Journal of Reinforced Plastics and Composites*, vol. 42, no. 1, pp. 3–16, Jan. 1, 2023, Publisher: SAGE Publications Ltd STM, ISSN: 0731-6844. DOI: 10.1177/07316844221093273. [Online]. Available: https://doi.org/10.1177/07316844221093273 (visited on 01/23/2025).

[37] Lopes, C.S., *Damage and failure of non-conventional composite laminates*, PhD Thesis, Delft University of Technology, Delft, The Netherlands, 2009.

[38] S. Pantoji, C. Kassapoglou, and D. Peeters, “Predicting gaps and overlaps in automated fiber placement composites by measuring sources of manufacturing process variations,” *Composites Part B: Engineering*, vol. 291, p. 111 891, Feb. 2025, ISSN: 13598368. DOI: 10.1016/j.compositesb.2024.111891. [Online]. Available: https://linkinghub.elsevier.com/retrieve/pii/S1359836824007030 (visited on 12/04/2024).

[39] N. Yadav and R. Schledjewski, “Inline tape width control for thermoplastic automated tape layup,” *Composites Part A: Applied Science and Manufacturing*, vol. 163, p. 107 267, Dec. 2022, ISSN: 1359835X. DOI: 10.1016/j.compositesa.2022.107267. [Online]. Available: https://linkinghub.elsevier.com/retrieve/pii/S1359835X22004481 (visited on 02/17/2025).

[40] X. Ju, J. Xiao, D. Wang, C. Zhao, T. Gao, and X. Wang, “Effect of gaps/overlaps induced waviness on the mechanical properties of automated fiber placement (AFP)-manufactured composite laminate,” *Materials Research Express*, vol. 9, no. 4, p. 045 305, Apr. 1, 2022, ISSN: 2053-1591. DOI: 10.1088/2053-1591/ac6858. [Online]. Available: https://iopscience.iop.org/article/10.1088/2053-1591/ac6858 (visited on 12/02/2024).

[41] M. Lan, D. Cartié, P. Davies, and C. Baley, “Influence of embedded gap and overlap fiber placement defects on the microstructure and shear and compression properties of carbon–epoxy laminates,” *Composites Part A: Applied Science and Manufacturing*, vol. 82, pp. 198–207, Mar. 2016, ISSN: 1359835X. DOI: 10.1016/j.compositesa.2015.12.007. [Online]. Available: https://linkinghub.elsevier.com/retrieve/pii/S1359835X15004716 (visited on 11/26/2024).

[42] D. Cartié, M. Lan, P. Davies, and C. Baley, “Influence of embedded gap and overlap fiber placement defects on interlaminar properties of high performance composites,” *Materials*, vol. 14, no. 18, p. 5332, Sep. 15, 2021, ISSN: 1996-1944. DOI: 10.3390/ma14185332. [Online]. Available: https://www.mdpi.com/1996-1944/14/18/5332 (visited on 12/02/2024).

[43] A. Sawicki and P. Minguett, “The effect of intraply overlaps and gaps upon the compression strength of composite laminates,” in *39th AIAA/ASME/ASCE/AHS/ASC Structures, Structural Dynamics, and Materials Conference and Exhibit*, Long Beach,CA,U.S.A.: American Institute of Aeronautics and Astronautics, Apr. 20, 1998. DOI: 10.2514/6.1998-1786. [Online]. Available: https://arc.aiaa.org/doi/10.2514/6.1998-1786 (visited on 01/23/2025).

[44] K. Croft, L. Lessard, D. Pasini, M. Hojjati, J. Chen, and A. Yousefpour, “Experimental study of the effect of automated fiber placement induced defects on performance of composite laminates,” *Composites Part A: Applied Science and Manufacturing*, vol. 42, no. 5, pp. 484–491, May 2011, ISSN: 1359835X. DOI: 10.1016/j.compositesa.2011.01.007. [Online]. Available: https://linkinghub.elsevier.com/retrieve/pii/S1359835X11000224 (visited on 12/02/2024).

[45] G. Chahine, U. Marathe, L. Collins, *et al.*, “Effect of plasma treatment on LMPAEK/CF tape and composites manufactured by automated tape placement (ATP),” *Composites Part A: Applied Science and Manufacturing*, vol. 188, Jan. 2025, Publisher: Elsevier Ltd, ISSN: 1359835X. DOI: 10.1016/j.compositesa.2024.108540.

[46] A. Ravangard, V. C. Jamora, J. D. Bhagatji, and O. Kravchenko, “ORIGIN AND SIGNIFICANCE OF NON-UNIFORM MORPHOLOGY IN AFP COMPOSITES,” in *American Society for Composites 2023*, Destech Publications, Inc., Sep. 18, 2023, ISBN: 978-1-60595-691-6. DOI: 10.12783/asc38/36629. [Online]. Available: https://www.dpi-proceedings.com/index.php/asc38/article/view/36629 (visited on 12/18/2024).

[47] D. Peeters, M. Deane, R. O'Higgins, and P. M. Weaver, "Morphology of ply drops in thermoplastic composite materials manufactured using laser-assisted tape placement," *Composite Structures*, vol. 251, p. 112 638, Nov. 2020, ISSN: 02638223. DOI: 10.1016/j.compstruct.2020.112638. [Online]. Available: https://linkinghub.elsevier.com/retrieve/pii/S0263822320309302 (visited on 11/28/2024).

[48] S. Sun, Z. Han, H. Fu, H. Jin, J. S. Dhupia, and Y. Wang, "Defect characteristics and online detection techniques during manufacturing of FRPs using automated fiber placement: A review," *Polymers*, vol. 12, no. 6, p. 1337, Jun. 12, 2020, ISSN: 2073-4360. DOI: 10.3390/polym12061337. [Online]. Available: https://www.mdpi.com/2073-4360/12/6/1337 (visited on 12/03/2024).

[49] T. Yap, N. Heathman, B. Shirani Bidabadi, *et al.*, "In-plane properties of an in-situ consolidated automated fiber placement thermoplastic composite," *Composites Part A: Applied Science and Manufacturing*, vol. 188, p. 108 525, Jan. 2025, ISSN: 1359835X. DOI: 10.1016/j.compositesa.2024.108525. [Online]. Available: https://linkinghub.elsevier.com/retrieve/pii/S1359835X24005232 (visited on 12/16/2024).

[50] N. Heathman, P. Koirala, T. Yap, A. Emami, and M. Tehrani, "In situ consolidation of carbon fiber PAEK via laser-assisted automated fiber placement," *Composites Part B: Engineering*, vol. 249, p. 110 405, Jan. 2023, ISSN: 13598368. DOI: 10.1016/j.compositesb.2022.110405. [Online]. Available: https://linkinghub.elsevier.com/retrieve/pii/S1359836822007788 (visited on 12/16/2024).

[51] Heraeus Noblelight GmbH, *humm3 – High-Power IR Heating Technology*, https://www.noblelight.com/en/etc/products_and_solutions/arc_and_flash_lamps/humm3/humm3_1/humm3.html, Accessed: 2025-04-15, n.d.

[52] A. Danezis, D. Williams, M. Edwards, and A. A. Skordos, "Heat transfer modelling of flashlamp heating for automated tape placement of thermoplastic composites," *Composites Part A: Applied Science and Manufacturing*, vol. 145, p. 106 381, Jun. 1, 2021, ISSN: 1359-835X. DOI: 10.1016/j.compositesa.2021.106381. [Online]. Available: https://www.sciencedirect.com/science/article/pii/S1359835X21001056 (visited on 11/25/2024).

[53] E. GmbH, *TECATEC PPS CF50 T200 CP/IP/OS – Carbon Fibre Reinforced PPS*, https://www.ensingerplastics.com, Continuous service up to 230 °C, short-term to 260 °C, 2025.

[54] Addcomposites. "AFP-XS - All Products." Accessed: 2025-06-23. (2025), [Online]. Available: https://www.addcomposites.com/all-products/afp-xs.

[55] KUKA Deutschland GmbH, "KR 210 R2700□2 Technical Data," KUKA Deutschland GmbH, Augsburg, Germany, Technical Report 0000□325□858 / V11.1, May 2022, Accessed: 2025□06□23. [Online]. Available: https://www.kuka.com/-/media/kuka-downloads/imported/8350ff3ca11642998dbdc81dcc2ed44c/0000325858_en.pdf.

[56] Micro–Epsilon Messtechnik GmbH & Co. KG, *Scancontrol: 2d/3d laser profile sensors – more precision*, Product catalog / manual, 2025.

[57] Struers ApS, *Secotom□60: Instruction Manual (English version)*, Manual No. 16857025□04, Revision B, Released on 18 January 2022, Struers ApS, Ballerup, Denmark, Jan. 2022.

[58] Struers ApS, *Tegramin-20 Technical Data Sheet*, https://www.struers.com, Doc. no.: 16017750_D_en, Release date: 2024-10-07, 2024.

[59] Keyence Corporation, *VR-5000 Wide-Area 3D Measurement System Data Sheet*, https://www.keyence.com, Includes specifications for VR□5000 controller and VR□5200 head; PDF retrieved via Keyence and Covalent Metrology listings, 2019.

[60] Struers ApS, *Cold Mounting Systems for All Materialographic Applications*, https://www.struers.com, Includes product details on CitoVac, EpoFix, ClaroCit, and other mounting resins, 2018.

[61] Struers ApS, *CitoVac Technical Data Sheet*, https://www.struers.com/-/media/Library/Technical-Data-Sheets/English/15927750_A-en_CitoVac_TDS.pdf, Doc. no.: 15927750_A_en, Release date: 2023-06-20, 2023.

A

Post processing programs

A.1. Resin moulds

This step is the same for both trials. The grinding and polishing equipment requires the samples to be embedded in a resin cylinder mould to work properly. The moulds came in three different diameters, 20, 30, and 40 mm. The choice was made to go for the 40 mm as this allowed for the largest samples. A larger width meant that the cutting plane was as far as possible from the embedded gap. Therefore, minimising the influence of the cutting process on the gap morphology. Furthermore, the height of the 40 mm diameter mould was 30 mm. The manual dictated that the height of the resin poured in the mould should remain below 80$\%$ of the mould height. With a height of 30 mm it means that the height of the poured resin and thus the height of the sample must not exceed 24 mm, which is why the height of the samples in figure 4.15 remains below this. However, for the same reason as for maximising the widths, the heights were also optimised. This is why the heights remain below 24 mm but do come quite close. Furthermore, to be able to reach the planes of interest containing the designed gaps for the first trial, it had to be ensured that the samples were mounted perfectly vertical in the moulds. This was achieved by mounting the samples with metal or plastic support clips which ensured their perfect verticality. The resin that was used to embed the samples was a slow-curing resin. This was done because fast-curing resins can generate significant amounts of heat. This heat could alter the morphology of the gaps. Therefore, a resin mix called EpoFix [60] was used. This resin has low shrinkage properties, can be used for all types of specimens, and has an extremely low curing temperature with a maximum of 40 degrees Celsius. The resin takes 12 hours to cure, and this was often done overnight. The clear mixture has a weight-based mixing ratio of 25 parts resin to 3 parts hardener, which had to be mixed for at least two minutes to ensure a properly mixed epoxy.

Additionally, to increase the quality of the poured moulds, they were put into a vacuum chamber to extract most of the bubbles from the epoxy caused by pouring and mixing. The vacuum chamber in question was a CitoVac by Struers [61]. The vacuum allowed for easy placing of the moulds. The exact vacuum program used can be found in the appendix chapter A.2.
Following this procedure ensures high-quality samples with minimal air pockets. Though, one has to be aware of a side effect of this procedure. Applying a vacuum to the epoxy could also cause the epoxy to be pulled into the gaps. Although it probably will not alter the morphology of the gaps much, it can show up in the micrographs.

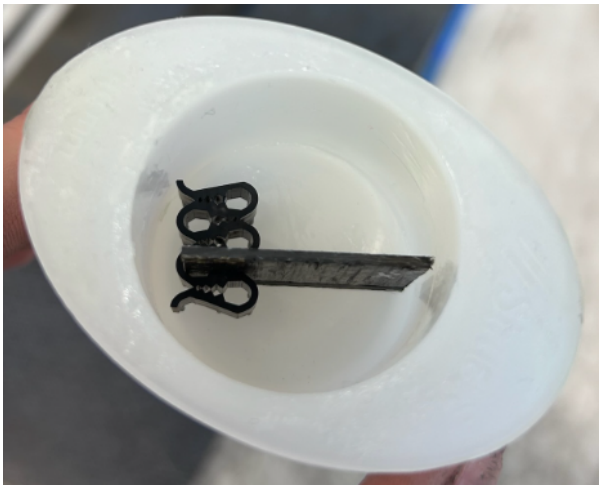

Figure A.1: Sample held up vertically in moulding cup by plastic clip

A.2. Vacuum program

1. Placing the clamped samples in the moulds, see figure A.1
2. Placing the moulds in the vacuum chamber
3. Applying 0.9 bar for 40 minutes
4. After 1 minute pour epoxy into the moulds
5. Let the remainder of the timer pass
6. Leave the samples overnight

A.3. Surface finishing program

1. Grinding for 1:00 at 320 grit with water as a lubricant
2. Grinding for 1:00 at 1000 grit with water as lubricant
3. Grinding for 1:00 at 2000 grit with water as a lubricant
4. Polishing for 2:00 on chem-plate with DiaPro dur 3 μm as a lubricant
5. Polishing for 3:00 on chem-plate with DiaPro dur 1 μm as a lubricant

B

Elaboration on superimposition of Trial One

B.1. Superimposition of the third sample

The data extracted from the LLS scan for the corresponding frame for sample three can be observed in figure B.1. This figure shows the raw LLS data out of proportion to aid in spotting the gap location and other features. From this frame, the left and right edges were identified and their corresponding measurements were accounted for in the coming computations. It is again evident by the several peaks and valleys that, after several heating cycles, the substrate had become significantly rough. Although, the edges could still be identified without confusion.

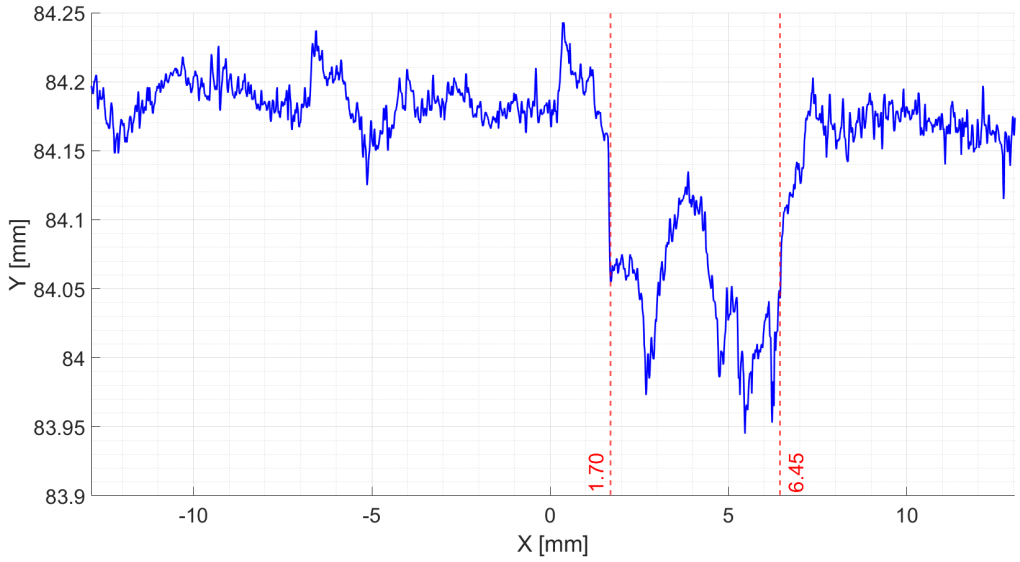

Figure B.1: LLS profile for frame 2635 (5.5) including identified gap edges

The data was then superimposed on the micrograph for sample three. The same procedure as used before, in 5.7 and 5.8 was used. Furthermore, the same MATLAB code was used to appropriately scale and position the data was used as before. This resulted in the following micrograph with the superimposed LLS data properly scaled in 5.17. Figure 5.17 again shows the similarity in the features of the substrate within the gap in both the LLS data and the micrograph.

B.2. Superimposition of the fourth sample

The data extracted from the LLS for the corresponding frame for the fourth gap can be seen in figure B.2. The figure clearly shows the location of the gap and its edges; however, still, red lines were added to aid in the visualisation of the exact location of the edges. Furthermore, as the dimensions are out of proportion it is easier to spot the features in the substrate along the gap width.

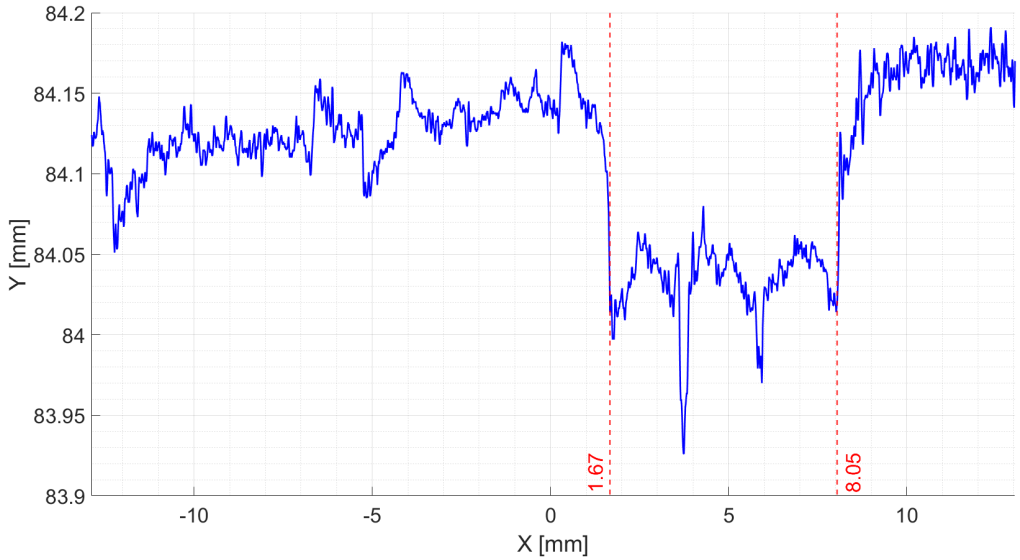

Figure B.2: LLS profile for frame 3120 (5.5) including identified gap edges

The data was then superimposed on the micrograph for sample four. The same procedure as used before was used in 5.7 and 5.8. Furthermore, the same MATLAB code was used to appropriately scale and position the data as before. This resulted in the following micrograph with the superimposed LLS data properly scaled in 5.17. Figure 5.17 again shows the similarity in the features of the substrate within the gap in both the LLS data and the micrograph.

C

Traced areas for Trial One

C.1. Traced area for gap one

Figure C.1: Traced area for gap one

C.2. Traced area for gap two

Figure C.2: Traced area for gap two, left void

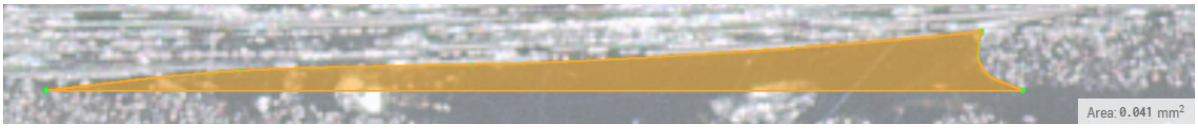

Figure C.3: Traced area for gap two, right void

The area of the left void in figure 5.23 was found to be 0.055 mm^2, and the right void had an area of 0.032 mm^2. Fitting a spline to the exact circumference of the two voids resulted in the areas for the left and right voids of 0.053 mm^2 and 0.041 mm^2 respectively.

$$\begin{aligned} \text{Parametrisation error left void} &= 1 - \frac{\text{Parametrised area } \ mm^2}{\text{Traced area } \ mm^2} = 1 - \frac{0.05460}{0.05307} = -2.9\% \\ \text{Parametrisation error right void} &= 1 - \frac{\text{Parametrised area } \ mm^2}{\text{Traced area } \ mm^2} = 1 - \frac{0.04149}{0.04112} = -0.9\% \end{aligned} \tag{C.1}$$

C.3. Traced area for gap three

Figure C.4: Traced area for gap three, left void

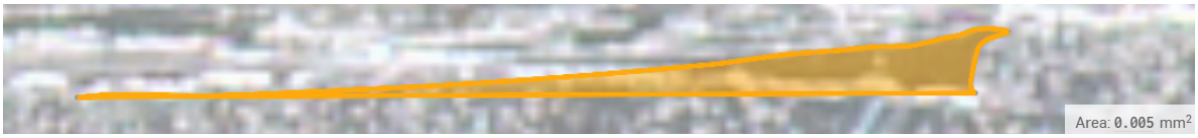

Figure C.5: Traced area for gap three, right void

The parametrised area of the left void of gap three was found to be 0.028 mm^2, while the area of the traced perimeter was found to be 0.030 mm^2. Therefore, resulting in a parametrisation error of:

$$\text{Parametrisation error left void} = 1 - \frac{\text{Parametrised area } mm^2}{\text{Traced area } mm^2} = 1 - \frac{0.02798}{0.03004} = 6.9\% \tag{C.2}$$

Figure 5.25 shows the parametrised right void of gap three including the dimensions from 5.3. The parametrised area of the right void of gap three was found to be 0.0050 mm^2, while the area of the traced perimeter was found to be 0.0051 mm^2. Therefore, resulting in a parametrisation error of:

$$\text{Parametrisation error right void} = 1 - \frac{\text{Parametrised area } mm^2}{\text{Traced area } mm^2} = 1 - \frac{0.00497}{0.00511} = 2.7\% \tag{C.3}$$

C.4. Traced area for gap four

Figure C.6: Traced area for gap four, left void

Figure C.7: Traced area for gap four, right void

The parametrised area of the left void of gap four was found to be 0.028 mm^2, while the area of the traced perimeter was found to be 0.030 mm^2. Therefore, resulting in a parametrisation error of:

$$\text{Parametrisation error left void} = 1 - \frac{\text{Parametrised area } mm^2}{\text{Traced area } mm^2} = 1 - \frac{0.02801}{0.02955} = 5.2\% \tag{C.4}$$

The parametrised area of the left void of gap four was found to be 0.018 mm^2, while the area of the traced perimeter was found to be 0.020 mm^2. Therefore, resulting in a parametrisation error of:

$$\text{Parametrisation error right void} = 1 - \frac{\text{Parametrised area } mm^2}{\text{Traced area } mm^2} = 1 - \frac{0.01832}{0.01967} = 6.9\% \tag{C.5}$$

D

Landmark LLS position computation

The computation below shows how the number of frames between tows was calculated and provides further elaboration on the reasoning behind the decisions made for this.

$$\begin{aligned}\text{Frame 18th gap} &= 749\\ \text{Frame 12th gap} &= 497\\ \text{Frame 6th gap} &= 251\\ \text{Frame difference} &= 250 \text{ frames}\\ \text{Positional difference} &= 25 * 6 = 150\ mm\end{aligned}$$

The resulting displacement per frame is:

$$\frac{150\ mm}{250 \text{ frames}} = 0.6\ mm/\text{frame}$$

These frames are extracted from the scan made for the 9th gap. Other scans showed different frames but the same difference in frames between the markers. The difference between markers shifts slightly in different scans but always remains within 5 frames. As 5 frames is equal to 3 mm, which is less than half a tow width, it was still an accurate representation of the gap that would later be covered by a tow. Therefore, this allowed for rounding the difference of frames between markers to 250. Additionally, the markers were thicker than a single frame resulting in them appearing in multiple frames. The frame locations mentioned above are taken from the middle of this range. For example, the range for the 18th tow was between frame 744 and 754, from which 749 was taken as the middle.

To find the number of frames required to cover a distance of $25\ mm$ (distance between tows):

$$F = \frac{25\ mm}{0.6\ mm/\text{frame}} = 41.7\ mm = \boxed{42 \text{ frames}}$$

This enables precise determination of the frames for all other 90-degree tow locations. The frames for tows 11, 13, 14, and 15 were established using the 12th tow as a reference point, while tow 17 was determined using the marker at the 18th tow.

E

ANOVA calculation gap width

The grand means for the tows and repetitions can now be computed. For every repetition, there are 5 values, and for every tow, there are 3. The grand means can then be computed as the following:

$$\bar{Y}_{reps} = \frac{3.147 + 2.908 + 3.080}{3} = 3.045 \tag{E.1}$$

$$\bar{Y}_{tows} = \frac{3.117 + 3.049 + 3.066 + 2.988 + 3.006}{5} = 3.045 \tag{E.2}$$

Now both between-group the sum of squares (SSG) can be calculated as the following:

$$\begin{aligned} SSG_{reps} &= \sum_{i=1}^{3} n_i(\bar{Y}_i - \bar{Y})^2 \\ &= 5(3.147 - 3.045)^2 + 5(2.908 - 3.045)^2 + 5(3.080 - 3.045)^2 \\ &= 5(0.0104) + 5(0.0187) + 5(0.0012) = 0.0520 + 0.0935 + 0.0060 = 0.1515 \end{aligned} \tag{E.3}$$

$$\begin{aligned} SSG_{tows} &= \sum_{i=1}^{5} n_i(\bar{Y}_i - \bar{Y})^2 \\ &= 3(3.117 - 3.045)^2 + 3(3.049 - 3.045)^2 + 3(3.066 - 3.045)^2 \\ &\quad + 3(2.988 - 3.045)^2 + 3(3.006 - 3.045)^2 \\ &= 3(0.0052) + 3(0.00001) + 3(0.00043) + 3(0.00327) + 3(0.00153) = 0.0313 \end{aligned} \tag{E.4}$$

Similarly the within-group sum of squares (SSR) can both be calculated according to the following equation:

$$SSR = \sum_{i=1}^{k} \sum_{j=1}^{n_i} (Y_{ij} - \bar{Y}_i)^2 \tag{E.5}$$

where Y_{ij} is the individual observation, $\bar{Y}_i$ is the mean of group i, and k is the number of groups. This results in:

$$\begin{aligned} SSR_{reps} &= 0.0262 \\ SSR_{tows} &= 0.0262 \end{aligned} \tag{E.6}$$

Finally, this allows for the total sum of squares (SST):

$$\begin{aligned} SST_{reps} &= SSG_{reps} + SSR_{reps} = 0.1777 \\ SST_{tows} &= SSG_{tows} + SSR_{tows} = 0.0575 \end{aligned} \tag{E.7}$$

The degrees of freedom for the between-group (group) and within-group (residual) components are defined as:

$$\begin{aligned} df_G &= k - 1 \\ df_R &= N - k \end{aligned} \tag{E.8}$$

where k is the number of groups and N is the total number of observations.

This gave the following values for k and N: $k = 3$ and $N = 15$ in the repetition case, and $k = 5$, $N = 15$ in the tow case. This resulted in the following:

$$\begin{aligned} df_{G,\,reps} &= 3 - 1 = 2 \\ df_{R,\,reps} &= 15 - 3 = 12 \\ df_{G,\,tows} &= 5 - 1 = 4 \\ df_{R,\,tows} &= 15 - 5 = 10 \end{aligned} \tag{E.9}$$

Using these degrees of freedom, the mean squares are calculated as:

$$\begin{aligned} MSG_{reps} &= \frac{SSG_{reps}}{df_{G,\,reps}} = \frac{0.1515}{2} = 0.07575 \\ MSR_{reps} &= \frac{SSR_{reps}}{df_{R,\,reps}} = \frac{0.0262}{12} = 0.00218 \\ MSG_{tows} &= \frac{SSG_{tows}}{df_{G,\,tows}} = \frac{0.0313}{4} = 0.00783 \\ MSR_{tows} &= \frac{SSR_{tows}}{df_{R,\,tows}} = \frac{0.0262}{10} = 0.00262 \end{aligned} \tag{E.10}$$

Finally, the F-statistic for each case is obtained as the ratio of the between-group to within-group mean squares:

$$\begin{aligned} F_{reps} &= \frac{MSG_{reps}}{MSR_{reps}} = \frac{0.07575}{0.00218} = 34.75 \\ F_{tows} &= \frac{MSG_{tows}}{MSR_{tows}} = \frac{0.00783}{0.00262} = 2.99 \end{aligned} \tag{E.11}$$

The p-values associated with the computed F-statistics are derived from the F-distribution, using the degrees of freedom corresponding to the group and residual components. Specifically, the p-value represents the probability of observing an F-statistic as large or larger than the computed value under the null hypothesis.

$$\begin{aligned} p_{reps} &= P(F > 34.75;\ df_1 = 2,\ df_2 = 12) \\ p_{tows} &= P(F > 2.99;\ df_1 = 4,\ df_2 = 10) \end{aligned} \tag{E.12}$$

Using the cumulative distribution function (CDF) of the F-distribution, the p-values can be computed as:

$$\begin{aligned} p_{reps} &= 1 - F_{\text{CDF}}(34.75;\ 2,\ 12) \approx 1 - 0.999978 = 2.2 \times 10^{-5} \\ p_{tows} &= 1 - F_{\text{CDF}}(2.99;\ 4,\ 10) \approx 1 - 0.933 = 0.067 \end{aligned} \tag{E.13}$$

F

Micrographs: Trial Two

Figure F.1: Micrograph for tow 11, repetition 1

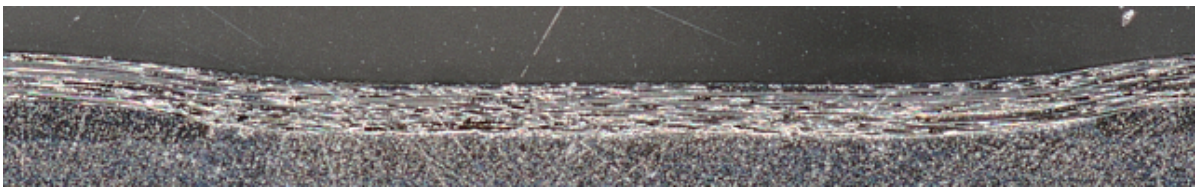

Figure F.2: Micrograph for tow 11, repetition 2

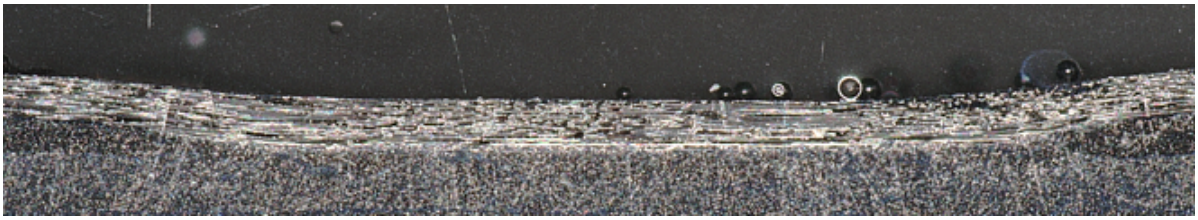

Figure F.3: Micrograph for tow 11, repetition 3

Figure F.4: Micrograph for tow 13, repetition 1

Figure F.5: Micrograph for tow 13, repetition 2

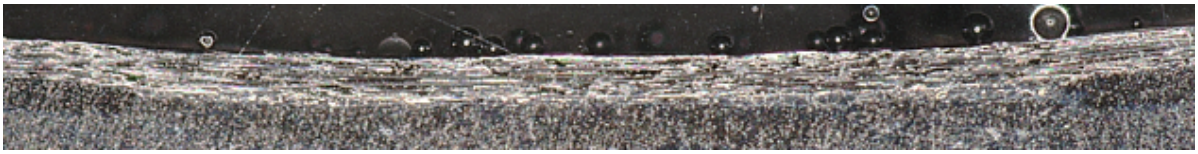

Figure F.6: Micrograph for tow 13, repetition 3

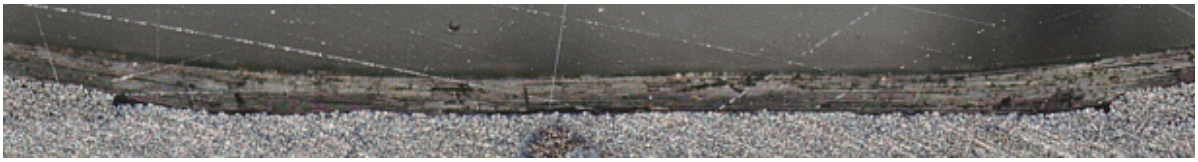

Figure F.7: Micrograph for tow 14, repetition 1

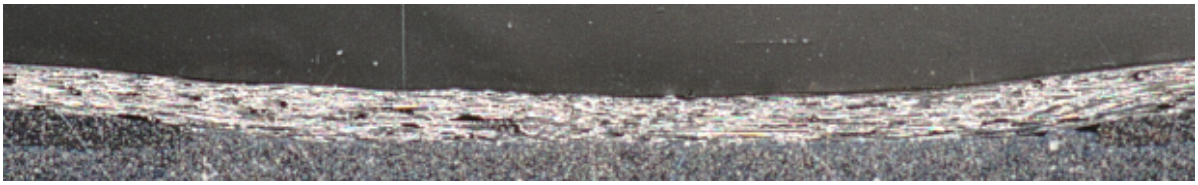

Figure F.8: Micrograph for tow 14, repetition 2

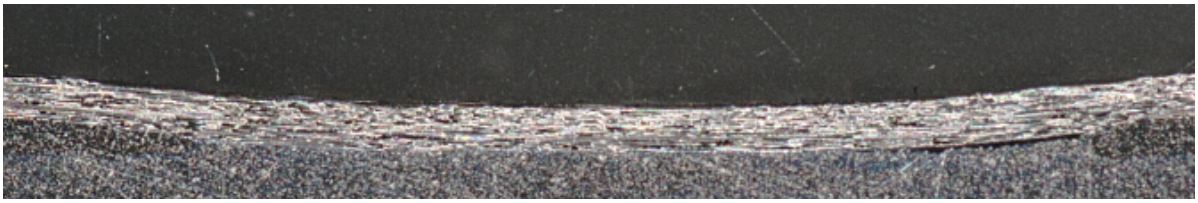

Figure F.9: Micrograph for tow 14, repetition 3

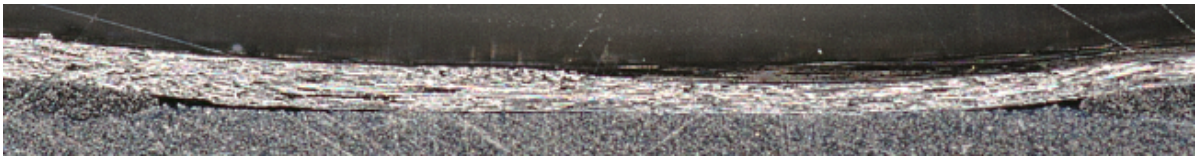

Figure F.10: Micrograph for tow 15, repetition 1

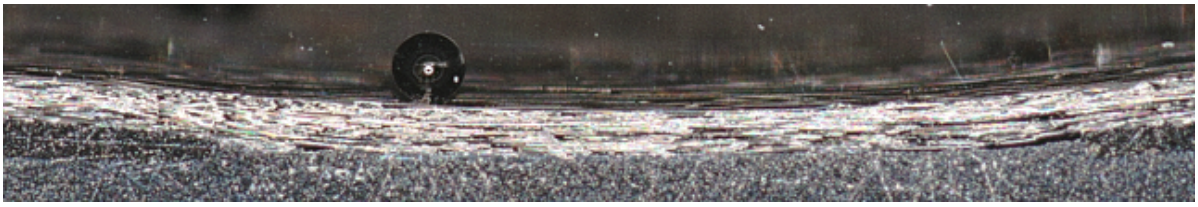

Figure F.11: Micrograph for tow 15, repetition 2

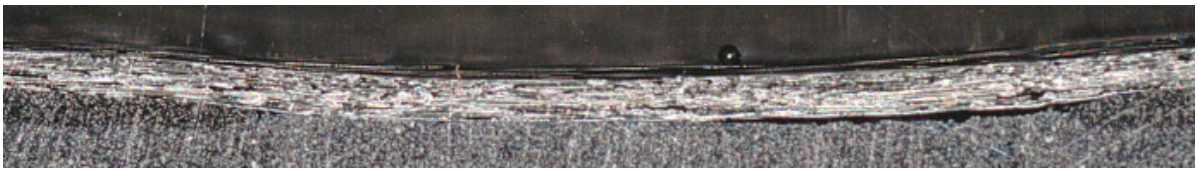

Figure F.12: Micrograph for tow 15, repetition 3

Figure F.13: Micrograph for tow 17, repetition 1

Figure F.14: Micrograph for tow 17, repetition 2

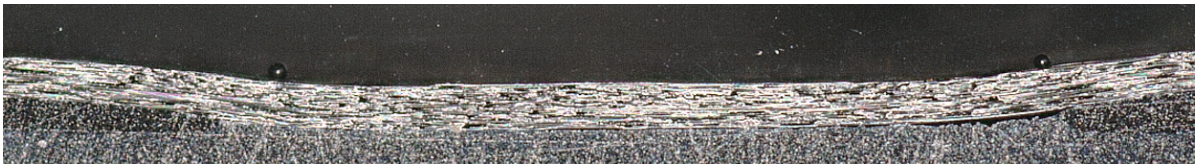

Figure F.15: Micrograph for tow 17, repetition 3